ISTANBUL TECHNICAL UNIVERSITY ★ GRADUATE SCHOOL OF SCIENCE ENGINEERING AND TECHNOLOGY

OPTIMIZATION OF FRAGMENTATION BEHAVIOUR OF BRITTLE PHASE IN A DUCTILE MATRIX DURING MECHANICAL ALLOYING FOR THE PRODUCTION OF NANO COMPOSITE POWDERS AND FINAL PRODUCTS

PhD THESIS

Aydın ŞELTE

Department of Metallurgy and Materials Engineering

Metallurgy and Materials Engineering Programme

JANUARY 2019

ISTANBUL TECHNICAL UNIVERSITY ★ GRADUATE SCHOOL OF SCIENCE ENGINEERING AND TECHNOLOGY

OPTIMIZATION OF FRAGMENTATION BEHAVIOUR OF BRITTLE PHASE IN A DUCTILE MATRIX DURING MECHANICAL ALLOYING FOR THE PRODUCTION OF NANO COMPOSITE POWDERS AND FINAL PRODUCTS

PhD THESIS

Aydın ŞELTE
(506112412)

Department of Metallurgy and Materials Engineering

Metallurgy and Materials Engineering Programme

Thesis Advisor: Prof. Dr. Burak ÖZKAL

JANUARY 2019

İSTANBUL TEKNİK ÜNİVERSİTESİ ★ FEN BİLİMLERİ ENSTİTÜSÜ

MEKANİK ALAŞIMLAMA SIRASINDA GEVREK FAZIN SÜNEK MATRİS İÇERİSİNDEKİ UFALANMA DAVRANIŞLARININ OPTİMİZE EDİLMESİ VE NANO KOMPOZİT TOZU NİHAİ ÜRÜN ÜRETİMİ

DOKTORA TEZİ

Aydın ŞELTE
(506112412)

Metalurji ve Malzeme Mühendisliği Anabilim Dalı

Metalurji ve Malzeme Mühendisliği Programı

Tez Danışmanı: Prof. Dr. Burak ÖZKAL

OCAK 2019

Aydın Şelte, a Ph.D. student of ITU Graduate School of Science Engineering and Technology student ID 506112412, successfully defended the thesis/dissertation entitled "OPTIMIZATION OF FRAGMENTATION BEHAVIOUR OF BRITTLE PHASE IN A DUCTILE MATRIX DURING MECHANICAL ALLOYING FOR THE PRODUCTION OF NANO COMPOSITE POWDERS AND FINAL PRODUCTS", which he prepared after fulfilling the requirements specified in the associated legislations, before the jury whose signatures are below.

Thesis Advisor :	**Prof. Dr. Burak ÖZKAL** İstanbul Technical University	.....
Jury Members :	**Prof. Dr. Sebahattin GÜRMEN** İstanbul Technical University	.....
	Prof. Dr. Müzeyyen MARŞOĞLU Gedik University	.....
	Prof. Dr. M. Lütfi ÖVEÇOĞLU İstanbul Technical University	.....
	Asst. Prof. Hakan YILMAZER Yıldız Technical University	.....

Date of Submission : 12 December 2018
Date of Defense : 10 January 2019

To the scientists who fought for the humanity,

FOREWORD

First and foremost, I would like to extend my best wishes and my deepest gratitude to my Ph.D. adviser and mentor Prof. Dr. Burak ÖZKAL for his leading in this long, rough and difficult path by inspiring me with his knowledge in that deep materials science and for his enlightment to find impetus inside myself to continue and deepen in all my research studies. I would like to give my sincere appreciation to Prof. Dr. M. Lütfi ÖVEÇOĞLU for all his priceless advices during my Ph.D. studies and teaching me many detailed scientific aspects, as well.

I would also like to thank Prof. Dr. Müzeyyen MARŞOĞLU who has always supported and helped me ever since I took a step into this academic world. I would like to acknowledge and give my respects to my committee member Prof. Dr. Sebahattin GÜRMEN for his advises and encouragement during my research and Prof. Dr. İsmail DUMAN for inspiring knowledge of metallurgy, alchemy, chemistry, life and history.

I am particularly thankful to my colleague Şeyma DUMAN (Ph.D.) and my soulmate Duygu YILMAZ (Ph.D.) for helping me in this stressful route. I would like to give my best wishes and desires to Aziz GENÇ (Ph.D.) and Hadi JAHANGIRI (Ph.D.), who led me in this crystallographic world, for many of the scientific discussions. I am especially grateful to all the precious members of the Particulate Materials Laboratories (PML): Ceren İMER (Ph.D.), Didem OVALI (Ph.D.), Duygu AĞAOĞULLARI (Ph.D.), Kübra YUMAKGIL AKBEN (Ph.D.), Özge BALCI (Ph.D.), Umut SÖYLER (Ph.D.), Emre TEKOĞLU (M.Sc.), Merve KÜÇÜK (M.Sc.) and Sıddıka MERTDİNÇ (M.Sc.) for their invaluable support and friendship.

I would also thank to Istanbul Technical University Research Fund (ITU-BAP) under the Project No: 39304 and to The Scientific and Technological Research Council of Turkey (TÜBİTAK) Project 1505 under the Project No: No: 5140011 (2015 – 2017) for the financial support of this study. I am grateful as well to Istanbul Development Agency (İSTKA) under the Project No: BİL-28 for contribution to development of laboratory infrastructure.

In addition, I appreciate Böhler Uddeholm Çelik A.Ş. in Turkey and Uddeholms AB in Sweden for their consistent support and counselling.

A special thanks to my wonderful family for the support, love and continuous encouragement I have gotten over the years. I would like to thank my mother Birsen and my father Selim whose words of encouragement and push for tenacity ring in my ears. My brother Azer, who has never left my side, is very special.

January 2019 Aydın ŞELTE
(Metallurgical and Materials Engineer, M.Sc.)

TABLE OF CONTENTS

Page

FOREWORD ..... **ix**
TABLE OF CONTENTS ..... **xi**
ABBREVIATION ..... **xiii**
SYMBOLS ..... **xv**
LIST OF TABLES ..... **xvii**
LIST OF FIGURES ..... **xix**
SUMMARY ..... **xxiii**
ÖZET ..... **xxvii**
1. INTRODUCTION **1**
2. THEORETICAL BACKGROUND **3**
2.1 Transition Carbides 3
2.1.1 Production techniques of carbides 4
2.1.2 Interstitial carbides, structure, composition and physicochemical properties 6
2.2 Application of Transition Carbides 11
2.2.1 Tools and tool holding 12
2.2.2 Machinery and equipment 13
2.2.3 Automotive and aerospace 13
2.2.4 Transportation and construction 14
2.2.5 Electronic and optical applications 14
2.2.6 Nuclear applications 14
2.3 Composite Powders 15
2.3.1 Nanocomposites and nanocrystalline materials 15
2.3.2 Properties of nanocomposite powders and materials 17
2.3.3 Application of nanocomposites and nanocrystalline materials 22
2.3.3.1 Nanocomposites for structural, electrical, magnetic applications 22
2.3.3.2 Nanocoatings 24
2.3.4 Synthesis of nanocomposite powders 25
2.3.5 Mechanosynthesis 27
2.3.5.1 Mechanism of mechanical alloying 28
2.3.5.2 Systems of mechanical alloying 30
2.3.5.3 The effect of grain size 31
3. EXPERIMENTAL PROCEDURE **33**
3.1 Materials 33
3.2 Powder Processing 34
3.3 Powder Characterisation 35
3.4 Verification 40
4. RESULTS AND DISCUSSION **43**
4.1 Initial Powder Characterisations 43

4.2 Fragmentation Behaviour of Brittle Phase in Cu Matrix 44
4.3 Fragmentation Behaviour of Brittle Phase in Fe Matrix 55
4.4 Fragmentation Behaviour of Brittle Phase in Ni Matrix 65
5. BROAD DISCUSSION 77
6. CONCLUSIONS 87
REFERENCES 89
CURRICULUM VITAE 103

ABBREVIATION

BPR	**:** Ball to Powder Ratio
bcc	**:** Body-Centered Cubic
BEI	**:** Back Scattered Electron Image
BF	**:** Bright Field
CMC	**:** Ceramic Matrix Composite
CNT	**:** Carbon Nano Tubes
CVD	**:** Chemical Vapor Deposition
DF	**:** Dark Field
EDS/EDX	**:** Energy-Dispersive X-ray Spectroscopy
fcc	**:** Face-Centered Cubic
FPA	**:** Fundementals Parameters Approach
FWHM	**:** Full Widht at Half-Maximum
G	**:** Gaussian Function
hcp	**:** Hexagonal Closed-Pack
HEM	**:** High Energy Milling
IB	**:** Integral Breadth
ICDD	**:** International Centre for Diffraction Data
L	**:** Lorentzian Function
MA	**:** Mechanical Alloying
MMC	**:** Metal Matrix Composite
PM	**:** Powder Metallurgy
PMC	**:** Polymer Matrix Composite
PSD	**:** Particle Size and Distribution
pV	**:** pseudo-Voigt Function
PVA	**:** Pseudo-Voigt Approach
PVD	**:** Physical Vapor Deposition
rpm	**:** Rotation per minute
RVE	**:** Representative Volume Element
SEI	**:** Secondary Electron Image
SEM	**:** Scanning Electron Microscope
T/M	**:** Toz Metalurjisi
TCH	**:** Thompson-Cox-Hasting
TEM	**:** Transmission Electron Microscope
T_M	**:** Melting Temperature
TM	**:** Trademark
UV	**:** Ultra Violet
XRD	**:** X-ray Diffraction

SYMBOLS

Å	**:** Angstrom
a, b, c	**:** Lattice parameters
λ	**:** Wavelength
D	**:** Crystallite size
β	**:** Integral breadth (IB) or full width at half maximum (FWHM)
φ	**:** Voigt function
ε	**:** Crystallite strain
d	**:** Grain size
V	**:** Volume fraction

LIST OF TABLES

Page

Table 2.1 : Fabrication process of carbides. **.....4**
Table 2.2 : Transition elements fit the criterias . **.....8**
Table 2.3 : Main compositions and structures of interstitial carbides **.....9**
Table 2.4 : Density of metals and their carbides **.....9**
Table 2.5 : Reviewed physicochemical and mechanical properties of transition metals and their carbides. **.....10**
Table 2.6 : Potential and realistic technical applications of metal matrix composites **.....24**
Table 3.1 : Raw materials used in the experiments. **.....34**
Table 3.2 : Summary of basic assumptions made in line-profile decomposition methods and the type of size and strain data obtained . **.....38**
Table 4.1 : Theoretical and true densities of initial powders. **.....43**
Table 4.2 : Crystallite size and strain rates of Cu25TaC, Cu25VC and Cu25WC powders against MA time. **.....44**
Table 4.3 : Crystallite size and strain rates of Cu25TaC, Cu25VC and Cu25WC powders against MA time. **.....46**
Table 4.4 : Change in position of Cu (111) due to carbide type against MA time. **...48**
Table 4.5 : PSD of nano fractions and zeta potential values against MA time. **.....50**
Table 4.6 : Density values of composite powders against MA time. **.....50**
Table 4.7 : Density values of composite powders against MA time. **.....55**
Table 4.8 : Crystallite size and strain rates of Fe25TaC, Fe25VC and Fe25WC powders against MA time. **.....57**
Table 4.9 : Change in position of Fe (110) due to carbide type against MA time. **...58**
Table 4.10 : PSD of nano fractions and zeta potential values against MA time. **.....61**
Table 4.11 : Density values of composite powders against MA time. **.....66**
Table 4.12 : Crystallite size and strain rates of Ni25TaC, Ni25VC and Ni25WC powders against MA time. **.....68**
Table 4.13 : Change in position of Ni (111) due to carbide type against MA time**...69**
Table 4.14 : PSD of nano fractions and zeta potential values against MA time. **.....71**
Table 5.1 : Comparison of crystallite size and strain rates of VC and WC reinforced metal matrixes according to different approaches**.....78**

LIST OF FIGURES

Page

Figure 2.1 : Crystal structures in Group 4-8 transition metal carbides a) Rock salt: ScC, VC, NbC; b) hcp: β-Mo_2C, β –W_2C; c) Cr_3C and d) Fe_3C **7**
Figure 2.2 : Melting points of elements and compounds **8**
Figure 2.3 : Indexable inserts.. .....**12**
Figure 2.4 : Carbides in machinery: a) Two·pronged carbide bit used in rotary drilling, and b) rotating drum of a road planing machine **13**
Figure 2.5 : Various shapes of monoliths made from SiC for gas turbine engine **14**
Figure 2.6 : Classification of materials according to their particle/grain size **16**
Figure 2.7 : Nanocrystalline material types: 0D (zero-dimensional) clusters; 1D (one-dimensional) nanotubes, filaments and rods; 2D (two-dimensional) films and layers; 3D (three-dimensional) polycrystals **17**
Figure 2.8 : Mechanical properties of a SiC/zirconia-toughened mullite nano-composite as a function of nanosized SiC content **18**
Figure 2.9 : Schematic respresentations of three shapes of metal matrix composite materials **19**
Figure 2.10 : Increase in strength of TiC-reinforced Al nanocomposites with increasing volume fractions or decreasing diameters of dispersed-phase (TiC) particles **21**
Figure 2.11 : Nanoparticle synthesis methods **26**
Figure 2.12 : Ball-powder-ball collision of powder mixture during mechanical alloying **28**
Figure 2.13 : First stage including layered structure consist of initial materials **29**
Figure 2.14 : Intermediate stage of processing **30**
Figure 2.15 : The final stage of processing and consolidation **30**
Figure 2.16 : The Schematic illustration of microstructural changes during milling of a brittle - ductile combination of powders **31**
Figure 2.17 : The schematic definition of particle size, grain size, crystallite size and domain size **32**
Figure 2.18 : Minimum grain size obtained by mechanical milling of different pure metals with different crystal structures versus their melting temperature **32**
Figure 3.1 : Flowchart of experimental procedures.....**33**
Figure 3.2 : Partial liquidus surface projections in stable equilibria **34**
Figure 3.3 : a) WAB™ T2C Turbula blender, b) 8000D™ Spex mill, c) Pluslabs™ glove box.....**35**
Figure 3.4 : Linn™ 1800 M Vac Graphite furnace. **35**
Figure 3.5 : a) Micromeritics™ AccuPyc II 1340 Gas Pycnometer b) Mictotrac™ Nano-flex particle size analyser c) Malvern™ Mastersizer Laser particle size analyser.....**36**
Figure 3.6 : Bruker™ X-Ray Diffractometer (XRD). **36**

Figure 3.7 : a) FEI – Quanta FEG 250 and b) JEOL™ JCM-6000 Benchtop scanning electron microscope (SEM). **39**
Figure 3.8 : JEOL JEM-ARM200CFEG UHR transmission electron microscope (TEM). **39**
Figure 3.9 : Heraeus™ drying oven. **41**
Figure 4.1 : PSD of initial powders. **43**
Figure 4.2 : XRD graphs of initial powders. **44**
Figure 4.3 : XRD graphs of Cu25TaC, Cu25VC and Cu25WC against MA time. **45**
Figure 4.4 : Williamson – Hall plot analysis of Cu based composite powders Grafik scale aynı değil. **47**
Figure 4.5 : Peak shiftings of Cu (111) due to carbide type against MA time. **48**
Figure 4.6 : PSD of MA'ed Cu25TaC, Cu25VC and Cu25WC powders. **49**
Figure 4.7 : SEM photos of a) Cu25TaC, b) Cu25VC and c) Cu25WC for 2, 4 and 8h MA time from left to right, respectively. **51**
Figure 4.8 : SEM photos of Cu25WC after 8h MA time (BEI x1000). **52**
Figure 4.9 : SEM photos of Cu25WC after 8h MA time at high magnifications x10000 and x30000. ..... **52**
Figure 4.10 : SEM photos of a) Cu25TaC and b) Cu25VC after 8h MA time at high magnification x10000. ..... **53**
Figure 4.11 : EDS maps of 8h MA'ed a) Cu25TaC, b) Cu25VC and c) Cu25WC powders. **54**
Figure 4.12 : Diffraction patterns of Fe25TaC, Fe25VC and Fe25WC powders against MA time. **56**
Figure 4.13 : Williamson – Hall plot analysis of Fe based composite powders. **57**
Figure 4.14 : Peak shiftings of Fe (110) due to carbide type against MA time. **59**
Figure 4.15 : PSD of Fe25TaC, Fe25VC and Fe25WC powders against MA time. **60**
Figure 4.16 : SEM photos of a) Fe25TaC, b) Fe25VC and c) Fe25WC for 2, 4 and 8h MA time from left to right, respectively. **61**
Figure 4.17 : BEI of Fe25WC after 8h MA time (x3000). **63**
Figure 4.18 : SEM photos of a) Fe25TaC, b) Fe25VC and c) Fe25WC after 8h MA time at magnification x10 000. ..... **63**
Figure 4.19 : EDS maps of 8h MA'ed a) Fe25TaC, b) Fe25VC and c) Fe25WC powders. **65**
Figure 4.20 : Diffraction patterns of Ni25TaC, Ni25VC and Ni25WC powders against MA time. **67**
Figure 4.21 : Williamson – Hall plot analysis of Ni based composite powders. **68**
Figure 4.22 : Peak shiftings of Ni (111) due to carbide type against MA time. **69**
Figure 4.23 : PSD of Ni25TaC, Ni25VC and Ni25WC powders against MA time. **70**
Figure 4.24 : SEM photos of a) Ni25TaC, b) Ni25VC and c) Ni25WC for 2, 4 and 8h MA time from left to right, respectively. **72**
Figure 4.25 : BEI of Ni25WC after 8h MA time (x3000). **72**
Figure 4.26 : SEM photos of a) Ni25TaC, b) Ni25VC and c) Ni25WC after 8h MA time at magnification x10 000. ..... **73**
Figure 4.27 : EDS maps of 8h MA'ed a) Ni25TaC, b) Ni25VC and c) Ni25WC powders. **75**
Figure 5.1 : Schematic illustration of particle, grain and crystallite size. **78**
Figure 5.2 : Nano WC particles among 8h MA'ed a) Cu25WC, b) Fe25WC and c) Ni25WC composite powders. **79**

Figure 5.3 : a) Cu25WC particle and Cu ring pattern, b) Fe25WC particle and Fe ring pattern, c) Ni25WC particle and Ni ring pattern of composite powders after 8h MA. **80**
Figure 5.4 : SEM images of 8 h MA'ed a) Fe25WC and Ni25WC composite powders (x 240000). **80**
Figure 5.5 : EDS mapping of 8 h MA'ed a) Fe25WC and Ni25WC composite powders (x 120000). **82**
Figure 5.6 : EDS mapping of 8 h MA'ed a) Cu25VC and Ni25VC composite powders (x 120000). **82**
Figure 5.7 : Peak shiftings of brittle phase strongest peaks against MA time. **83**
Figure 5.8 : Cracks and fracture and rupture surfaces. **83**
Figure 5.9 : SEM images of composite powders from right to left Cu, Fe and Ni matrixes; up to down TaC, VC and WC after 8h MA, respectively (x 240 000). **84**
Figure 5.10 : SEM image of 8h MA'ed Cu25WC composite powder after leaching in H_2SO_4 at different magnifications a) x60 000 and b) x240 000. ..... **85**
Figure 5.11 : a) Calculated WC crystallite sizes after mechanical alloying in different metal matrixes and b) TEM micrograph of single WC particle detected in 8 h MA'ed Cu25WC composite powder. **86**
Figure 5.12 : XRD graph of WC particles after leaching of Cu from 8 h MA'ed Cu25WC composite powders **86**

OPTIMIZATION OF FRAGMENTATION BEHAVIOUR OF BRITTLE PHASE IN A DUCTILE MATRIX DURING MECHANICAL ALLOYING FOR THE PRODUCTION OF NANO COMPOSITE POWDERS AND FINAL PRODUCTS

SUMMARY

Transition metals and their carbides display outstanding properties such as high melting and elastic modulus with high mechanical properties such as extreme hardness. They are used in the applications required very high temperature and pressure owing to their high toughness and strength. In addition, they are also used in applications such as coatings against radiation, electrical conductors and diffusion barriers as a result of having optical, magnetic and electrical properties. These transition carbides can mostly find an application area directly such as refractory materials, corrosion and chemical resistive materials, nuclear materials, aircraft and aerospace materials, super hard and high wear resistant materials, thin films or as a reinforcement element to ductile matrix.

Based on the lack of solubility between the transition carbides and metals matrixes such as Al, Cu, Fe, Ni etc. and powder metallurgy (PM) is generally viable method for the production of these types of materials. However, these composites or composite powders cannot be fabricated easily by using conventional methods such as casting due to the high cost of processing, though. It is possible to produce metal matrix composites or composite powders in the whole range of matrix reinforcement compositions via powder metallurgy (PM) techniques by eliminating the segregation phenomena, which is typical in the casting processes, and to minimize the brittle reaction products and high residual stresses caused by solidification shrinkage. The most important point of production of these fiber/particle reinforced composite materials/powders is the homogeneity of reinforcement distribution. Therefore, the critical step for homogeneous distribution is the mixture process. Within this scope, high energy milling (HEM) and mechanical alloying (MA) as a forging, fracturing and welding process in micro/nano scale were developed in the last century. It is now well known that mechanical alloying can be an alternative solution to production of non-equilibrium systems. The increase in solubility of systems which normally do not have solubility between each other and obtaining fine and relatively homogeneous distributed hard reinforcement element by mechanical alloying can be set an example for this.

Nanocomposites lead to promising way for unique and new material designs with the development and improvement of nanomaterials. Despite assembling dissimilar materials and creating new and optimum properties from these materials are a hard and challenging process, processing dissimilar materials in nanoscales provides new material and properties far beyond the prediction of “mixture of rules”. The nanostructured composite materials/powders or metal-ceramic nanocomposites that are the nano fiber/particle reinforced metal matrix composite materials/powder can

be fabricated by mechanical alloying. During mechanical alloying, each powder particle is treated by numerous deformation, fracturing and cold welding processes in order to obtain homogeneous nanostructure.

In this study, the effect of properties such as lattice type, elastic modulus, thermal conductivity, density of ductile metal matrixes on the fragmentation behaviour of carbides and carbide reinforced composite powders during mechanical alloying was investigated. The high energy milling of sole carbide was previously examined and it was observed that the particle size and the amorphization tendency were increased by on-going milling after a certain time. Considering the theory of at least 15 wt.% ductile phase existence for a better mechanical alloying, the reverse situation was applied and reinforcing hard elements were added more than their amount and submicron/fine/nano particles were tried to be synthesized in different ductile matrixes.

One of the most significant aims of this study is to synthesize of nano particles in ductile matrix and to produce nanostructured composite powders, finally. In this scope, the constitution of solution between the systems having negligible solubility or immiscibility at the crystal level is also aimed.

Within the scope of this work, the correlation between crystallite size and particle size and the effects of strain rates on the final density properties of powders are also studied. In this sense, the deduction for crystallite size – particle/grain size relation was made by applying different X-ray diffraction (XRD) profile models/approaches.

Cu, Ni and Fe powders were mixed with 25 wt. % VC, TaC and WC powders in order to obtain the composition of Cu–25 wt. % VC, Cu–25 wt. % TaC, Cu–25 wt. % WC; Ni–25 wt. % VC, Ni–25 wt. % TaC, Ni–25 wt. % WC and Fe–25 wt. % VC, Fe–25 wt. % TaC Fe–25 wt. % WC (hereafter called as Cu25VC, Cu25TaC, Cu25WC; Ni25VC, Ni25TaC, Ni25WC and Fe25VC, Fe25TaC, Fe25WC). Mixed powders were then mechanically alloyed (MA'ed) for 2, 4 and 8h using a Spex high-energy ball mill. X-ray diffraction characterisation was performed for every step so as to see phase changes and identifications. Apparent, true and green densities were measured. The microstructural changes in morphology of particles during mechanical alloying were performed via scanning electron microscopy (SEM) and transmission electron microscopy (TEM) techniques. Different approaches were applied to calculate crystallite size and strain rates. The results of different crystallographic approaches were compared and the deformation mechanisms of particles during mechanical alloying were discussed after Williamson-Hall plot analysis.

Particle size and distribution (PSD) of powders were measured against increasing milling time. Particle size and distribution and zeta potential value of nano fractions was also measured and the result were compared to high resolution scanning electron microscopy (SEM) and transmission electron microscopy (TEM) findings. Besides, some of the metal matrixes were leached in order to obtain fine carbide particles and particle sizes of these particles were measured for the verification.

For the production of final composite powders, annealing process was applied. Annealing temperature for Cu, Ni and Fe based composite powders were chosen 400^{o}C, 550^{o}C and 600^{o}C, respectively. Strain rates, compressibility and green density of powders after annealing were calculated and compared to values before annealing.

X-ray diffraction results and the changes in two-theta positions, lattice parameters, and peak broadenings were investigated in depth, comparatively. In this scope, the crystallite size and strain rates were calculated by fundamental parameters approach (FPA) and pseudo-Voigt Approach (pVA) and compared to Williamson-Hall plot analysis. With the convergence of all approaches, particle size measurements and transmission electron microscopy (TEM) findings, mechanical alloying mechanisms and particle-crystallite size relation were discussed.

As a result, production of Fe, Ni and Cu based composite powders having different types of carbides have been realized via MA for the direct or indirect utilization in different engineering applications as final product.

MEKANİK ALAŞIMLAMA SIRASINDA GEVREK FAZIN SÜNEK MATRİS İÇERİSİNDEKİ UFALANMA DAVRANIŞLARININ OPTİMİZE EDİLMESİ VE NANO KOMPOZİT TOZU NİHAİ ÜRÜN ÜRETİMİ

ÖZET

Geçiş metalleri ve meydana getirdikleri karbürler yüksek ergime ve elastisite modülü ile birlikte ve yüksek sertlik gibi mekanik özellikler özellikler sergilemektedirler. Özellikle yüksek dayanım ve dayanıklılıkları nedeniyle çok yüksek sıcaklık ve basınç içeren koşullarda kullanılmaktadırlar. Bununla birlikte sahip oldukları ışınsal, elektriksel ve manyetik kimi özelliklerinden ötürü ışınsal kaplamalarda, elektrik kontaklarında, difüzyon bariyerlerinde gibi birçok uygulamada kendilerine yer bulmaktadırlar. Geçiş metallerin meydana getirdikleri bu karbür bileşikleri, refrakter malzemeler, korozyona ve kimyasallara dirençli malzemeler, nükleer malzemeler, uçak ve uzay malzemeleri, süper sert ve yüksek aşınma dirençli malzemeler, kaplama malzemeleri gibi birçok kategoride kendisine doğrudan veya sünek matris içerisine takviye eleman olarak ağırlıkça katılarak uygulama alanı bulmaktadır.

Bu tip malzemelerin üretimi, Al, Cu, Fe, Ni gibi metallerle alaşım yapamadıklarından dolayı kompozit toz haline gelebilmeleri ancak toz metalurjisi (T/M) yöntemi ile gerçekleştirilmektedir. Toz metalurjik yöntemler ile döküm esnasında oluşan segregasyon problemi elemine edilerek geniş çapta takviye edilmiş matrisli kompozit tozu/malzemesi üretilebilmektedir. Parçacık veya fiber takviye edilmiş kompozit malzemedeki en önemli nokta, takviye elemanın homojen bir şekilde dağıtılmasıdır. Takviye elemanın homojen dağıtılması için ise kritik basamak karıştırma işlemidir. Bu bağlamda son yüzyıl içerisinde yüksek enerjili öğütme ve mikro/nano ölçekte bir dövme, kırma ve kaynaklama işlemi olan mekanik alaşımla prosesleri geliştirilmiştir. Mekanik alaşımlamanın, birçok sorundan dolayı üretimlerinde sıkıntı olan sistemlere alternatif denge dışı çözümler sağladığı bilinmektedir. Buna örnek olarak, normal koşullarda birbiri içerisinde çözünürlük göstermeyen sistemlerin çözünürlüğünün mekanik alaşımlama yoluyla artırılması ve takviye edilen sert takviye fazının sünek matris içinde ince ve homojen dağılımının sağlanması verilebilir.

Nano malzemeler geliştikçe, nanokompozitler de özgün ve yeni malzeme tasarımları için umut verici pratik bir yol açmaktadırlar. Farklı malzeme tiplerini bir araya getirebilmek ve bu birliktelikten en uygun özellikleri yaratabilmek her ne kadar zor bir işlem olsa da, nanometre ölçeğinde birçok malzemenin bir araya getirilebilmesi, "karışımlar kuralının" öngördüğünün çok ötesinde işlevselliklere sahip yeni malzemelerin oluşmasını olanaklı kılmıştır. Nano yapılı kompozit malzemeler veya metal-seramik nanokompozitleri, nano metrik ölçülü seramik parçacıklarla takviye edilmiş metal esaslı malzemeler olup mekanik alaşımlama ile üretilebilmektedirler. Mekanik alaşımlama esnasında, her bir toz parçacığı sayısız deformasyon, kırılma ve soğuk kaynaklanma işleminden geçerken homojen bir karışımla birlikte nanoyapı da elde edilebilmektedir.

Bu çalışmada sünek matrislerin latis yapıları, elastisite modülleri, ısıl iletkenlikleri, yoğunlukları gibi özelliklerinin karbürlerin ve karbür takviyeli kompozit tozların mekanik alaşımlama sırasındaki ufalanma davranışlarına etkisi incelenmiştir. Daha önce yapılan ön çalışmalar sonucu karbürlerin tek başlarına yüksek enerjili öğütme davranışları incelenmiş ve devam eden öğütme sürelerinde parçacık boyutunun aglomera olarak tekrar arttığı ve/veya amorf bir yapıya doğru ilerlediği gözlemlenmiştir. İyi bir mekanik alaşımlama için en az % 15 sünek faz varlığı bulunması göz önüne alınarak takviye eleman malzemelerinin, genellikle ağırlıkça katıldığı oranların üzerine çıkılmış ve farklı sünek matrisler içerisinde mikron altı ve nano karbür parçacıkları sentezlenmeye çalışılmıştır.

Bu tez çalışmasının en önemli amaçlarından biri, sünek matris içeirisinden nano parçacık sentezlenebildiği ve nihai olarak nano yapılı kompozit toz üretilebileceğini göstermektir. Birbiriyle çözünürlüğü olmayan veya çözünürlüğü ihmal edilebilir olan malzeme çiftleri arasında kristalin seviyede bileşik oluşturabilmek veya denge dışı kabul edilen bu sistemlerden hareketle kompozit toz çiftleri elde edebilmek çalışma kapsamında amaçlanmaktadır.

Çalışma kapsamında irdelenen bir diğer konu ise parçacık boyutu ve kristal boyutu arasındaki ilişki ve ortaya çıkan gerinim değerlerinin tozların yoğunluklarına etkisidir. Bu bağlamda farklı X ışını kırınımı (XRD) profil modelleri uygulanarak parçacık/tane boyutuna yönelik çıkarımlar yapılmak istenmiştir.

Çalışma kapsamında Cu, Fe ve Ni tozlarına ağırlıkça % 25 oranında TaC, VC ve WC tozları ilave edilmiştir. Hazıranan toz karşımları Cu25WC, Fe25TaC, Ni25VC şeklinde isimlendirilmişlerdir. Karıştırılan tozlar 2, 4 ve 8 saat mekanik alaşımlanmıştır (MA). X ışınları karakterizasyonu her kademede yapılarak farklı faz oluşumları kontrol edilmiştir. Görünür, gerçek ve ham yoğunluklar ölçülmüştür. Mekanik alaşımlama süresine bağlı olarak tozların/parçacıkların morfolojisindeki değişim taramalı elektron mikroskobu (SEM) ve geçirimli elektron mikroskobu (TEM) kullanılarak incelenmiştir. Farklı yaklaşımlar tanımlanarak yazılım yardımıyla kristal boyutları ve gerinimleri hesaplanmış, Williamson – Hall analizi yardımıyla hem mekanik alaşımlama sırasındaki mekanizma irdelenmiş hem de farklı yaklaşımlar ile ile elde edilen sonuçlar karşılaştırılmıştır.

Mekanik alaşımlama süresine bağlı olarak tozların parçacık boyut ve dağılımları (PSD) ölçülmüştür. Kompozit tozlarının nano fraksiyonlarının boyut ve dağılımları da ölçülmüş ve yüksek çözünürlüklü taramalı elektron mikroskobu (SEM) ve geçirimli elektron mikroskobu (TEM) bulguları ile karşılaştırılmıştır. Doğrulama amacıyla sünek matrisler liç işlemine tabi tutulmuş ve süzülerek alınan kabür parçacıklarının boyutları ölçülmüştür.

Nihai toz üretimi için kompozit tozlarına gerilim giderme tavı uygulanmıştır. Tavlama işlemi Cu esaslı tozlar için 400^{o}C, Fe esaslı tozlar için 600^{o}C ve Ni esaslı tozlar için 550^{o}C seçilmiştir. Tavlama sonrası gerinim değerleri ölçülmüş, preslenebilirlikleri ve ham yoğunlukları hesaplanarak tavlama öncesi değerlerle karşılaştırılmıştır.

X ışınları sonuçları derinlemesine çalışılarak kaymalar, latis yerleşimleri, latis parametresindeki değişiklikler karşılaştırmalı olarak incelenmiştir. Bu kapsamda TOPAS 4.2 yazılımı içerisinde Fundemental Parameters Approach ve pseudo-Voigt Approach yaklaşımları ile hesaplama yapılmış ve ilgili değerler Williamson – Hall Plot Analysis sonucu elde edilen değerlerle karşılaştırılmıştır. Yakınsaklık

sağlanması sonrası elde edilen değerler ile MA mekanizmaları ve parçacık boyutu arasında ilişki irdelenmiştir.

Çalışma kapsamında, Fe, Ni ve Cu esaslı farklı türde karbür içeriğine sahip doğrudan veya dolaylı mühendislik uygulamalarında kullanım potansiyeli bulunan kompozit tozların üretimi MA yöntemiyle gerçekleştirilmiştir.

1. INTRODUCTION

In this PhD Dissertation, the fabrication of brittle phase reinforced ductile (Fe, Cu, Ni, Al etc.) nanocomposites, which the compounds are non-soluble within each other, is being aimed via different metallurgical routes. In this manner, the mechanical alloying behaviour of brittle particles into ductile matrixes were investigated. Ductile materials to be chosen due to their industrial usage and they are to be compared among their crystal structures, Young's modulus and thermal conductivities. Besides mechanical alloying, hydrometallurgical techniques were performed for the confirmation of different nano powder structures. In this scope, a comparison between different production methods and final properties of the resulting powders is tried to be made. In addition to this, X-ray crystallographic simulations and validations are performed by using different models. The studies focused on the effect of lattice parameters, Young's modulus, thermal conductivities on the mechanical alloying properties and the detailed characterization of final composite powders produced via room-temperature synthesis method and achievement of manufacturing different kind of composite powders.

It is possible to manufacture metal matrix composites within whole range of matrix reinforcement compositions via powder metallurgy techniques by eliminating the segregation phenomena, which is characteristic to the casting processes (Fogagnolo, 2003). Nevertheless, one of the obstacle points to this technique is to achieve a homogeneous distribution of the hard phase in the metal matrix. It is essential to distribute the reinforcing phase homogeneously throughout the metal matrix to maintain compromising performance for a composite material (Boselli, 2001). So the critical step for powder metallurgy is to mix the matrix and reinforcement in order to overcome numerous problems during handling, processing, and manufacturing caused by segregation when mixed powders are needed. (Ozkal, 2010; Boselli, 2001; Jain, 1993). Therefore, high-energy ball milling (HEM) has first developed by Benjamin (Benjamin 1974) and since then it has been used to develop particle distribution in the matrix. It has already been mentioned by Suryanarayana that

minimum 15 wt. % of ductile has to take part for a better mechanical alloying (Suryanarayana, 2001).

In Pagounis, Lou and Gassman's studies, it was shown in past three decades that composite materials with improved properties can be produced with the assistance of ceramic reinforcements into metal matrixes. These matrix materials were chosen from light metals such as Ti, Al, Mg etc. and reinforced by Al_2O_3, SiC, mostly (Pagounis, 1998; Lou, 2003; Gassmann, 1992). Although various carbides such as SiC, TiC has been used as reinforcement material with different kind of metals, especially, WC reinforced Fe, Ni, Cu and Sn metals has not been investigated by MA in detail. Within this scope, carbides which are essential for steel microstructure, particularly, Mo_2C, VC, NbC, WC, Cr_7C_3 have not been studied in detail by MA with other important most frequently used metals such as Ni, Cu, Sn (Mill, 1996; Razavi, 2011; Surender, 2004; Sauer, 1998). In Dalfrad's study, it was seen that this kind of carbides could make good impact on the last properties of Ni and Fe (Dalfard, 2012).

It is also possible to calculate crystallite size and strain rates by applying different models such as Fundamental Parameters and pseudo-Voigt approaches by using TOPAS software and Williamson – Hall plot analysis (Behrens, 2012; Prabhu, 2013; Prabhu, 2014; Beyerlein, 2010; Mittemeijer, 2012; Kandemir, 2014; Kamrani, 2011).

2. THEORETICAL BACKGROUND

Literature review of this dissertation comprises the general properties and application areas and production techniques of carbides and nanostructured composite powders, general information about mechanical alloying and detailed description of ductile - brittle systems which were used as ball-milling assisted solid state methods and their elaborative crystallographic studies were performed in the scope of this dissertation.

2.1 Transition Carbides

Term carbide refers to those compounds formed by carbon and other elements of lower or about equal electronegativity (Cotton, 1972). Particularly, transition carbides means the compounds of carbon and the transition metals in Groups 4 – 6 of periodic table. Transition metal carbides are composed of varied group of materials with numerous industrial applications. In addition to being great interest of technology and industry, they have a growing and promising future. Despite having new properties, use of direct or as a reinforcing element, refractory carbides have been used for the last decade (Pierson, 1996). Titanium and tungsten carbides were properly recognised after their extraction from steel around nineteenth century (Pierson, 1996). Since Henri Moissan discovered the production of tungsten carbide and titanium carbide in his electric arc furnace and Hüttig synthesized WC by the reduction of WO_3 and silicon carbide was first produced commercially by E.G. Acheson at the end of nineteenth century, the very first respectable study which was later in 1933 published as a book reference in German by K. Becker, carbides, specifically interstitial carbides, have been subjected to several research interests and industrial applications (Pierson, 1996; Kieffer, 1993; Hüttig, 1950).

It has been known for a long time that transition metal carbides from the Group 4 to Group 6 of the Periodic Table display unique physical, chemical and mechanical properties (Santhanam, 1996). However, their characteristics, structures and application areas will be shown in the oncoming titles, Group 5 and 6 of transition metal carbides have been mentioned in this dissertation.

2.1.1 Production techniques of carbides

Because of their strong bonding, being chemically inert and a common tendency to decompose upon melting points, production of carbides cannot be easily performed by conventional metallurgical techniques such as casting or forging or sintering without any sintering agents (Pierson, 1996; Ettmayer 1985). Various methods developed and introduced consisting of detailed production or preparation of carbides, covering the period prior to 1971 have been provided by many references (Kieffer, 1953; Toth, 1971; Kosolapova, 1971; Santhanam, 1992; Storms, 1967; Ettmayer, 1994; Benesovsky, 1981). Well-known and common techniques for production of polycrystalline carbides are techniques from powder metallurgy in which two main concepts were indetified as directly from elements, or from compounds containing these elements (Gusev, 2001).

These carbides can be fabricated in powder and bulk shapes, as coating material, fibers and whiskers, which is summarized in Table 2.1.

Table 2.1 : Fabrication process of carbides (Pierson, 1996).

Form	Process
Powder	Chemical preparation Vapor-based chemical reaction RF-plasma torch Sol-gel Self-propagating high temperature synthesis
Bulk/monolithic	Powder forming Reaction bonding Sintered reaction bonding Hot pressing Hot-isostatic pressing
Fiber/whisker	Chemical vapor deposition Sol-gel
Coatings	Chemical vapor deposition (CVD) Physical vapor deposition (PVD) Thermal spray

In addition to Pierson's table, mechanical, thermomechanical and/or mechanochemical methods have been developed over the last hundred years (Lipatnikov, 1990). Despite being cheapest and most commonly used commercial method for producing carbides are carbothermal reduction of transition metal oxides (Tulhoff, 1985), the great necessity of final compound/product high extent to homogeneity, high-energy ball milling techniques have been improved.

However, among the great variety of production methods of carbides, preparation process ways can be categorized into three groups:

A most used method for preparation of transition metal carbide powders is to constitute the reaction between metal oxide and carbon between the temperatures 1500°C and 2400°C, subject to the metal type (Tulhoff, 1985) with the exception of beta-SiC production by simple solid-state reaction in a microwave oven around 1000°C (Ramessh, 1994). Even though the carbide formation of elements were shown thermodynamically more suitable at lower temperatures, high temperatures were also engaged because of the solid-state diffusion confines (Oyama, 2008; Kosolapova, 1971). In this method, metal oxides and gaseous carbon reactions directly and the reaction of metal oxides in the presence of solid carbon can be applied, which the last one has been very useful to synthesis stable nitride forms of transition metals (Kosolapova, 1971). One of the other main mechanism in this group is the preparation of carbides by solid combustion synthesis that is also called self-propagating high-temperature synthesis, SHS (Merzhanov, 1973 and 1975; Munir, 1988 and 1990; Agrafiotis, 1991). This technique provides excellent thermodynamically stability at high temperatures for carbides by exothermicity of carbon dissolution in the metals.

In order to prepare carbide powders, particles, whiskers/fibers and supported foams, there are several methods in the second group such as the reactions of metals or compounds with gas-phase substances, reactions between metal oxide vapor and solid carbon, decomposition of metal halide vapors or compounds, liquid-phase methods and temperature-programed methods. Solid metals or oxides were directly got into reaction with flowing gas-containing carbon. Metal chlorides or oxychlorides can also be used to produce carbides. Gaseous hydrocarbons are added to the system in order to react them with metal chlorides or oxychlorides, which provides the purification of metals during process; therefore, it is one of the versatile and convenient technology for synthesizing limited extent of pure carbides (Oyama, 2008). It is possible to obtain carbides by decomposing metal chlorides with hydrogen, i.e. Mo_2C and W_2C can be obtained in the gas phase in case the compounds are unstable (Hojo, 1978; Haggerty, 1981). Another method for this group is to control the treating of precursor by giving it into reactive gas during the increasing of temperature. In this method, oxide, sulphide, nitride, or carbide can be

the precursor and the reactive gas can be composed of hydrocarbon and hydrogen mixture (Oyama, 2008). Optimal balance can be arranged by this technique and new compounds can be described (Marchand, 1991).

The third group of carbide preparation is for films and coatings. In this group, plasma techniques have been developed for having better case uniformity of carburizing on metal parts such as gears, shafts, bearings etc. which can be generated by two major types of plasmas: glow discharge plasmas (nonequilibrium, low-temperature, or plasmatron) and thermal plasmas (equilibrium, high-temperature, or plasma torch) (Ho, 1989; Dressler, 1991; Pye, 1992). The most known and commercially applied techniques are chemical vapor deposition (CVD) and physical vapor deposition (PVD). Among them, CVD is applied at low pressures using inorganic metal species like halides in general, while PVD distinguishes from CVD by the lack of surface chemical reactions that leads to dispense ions to the composition of films (Reniers, 1996). It is possible to produce single crystal transition metal carbide by CVD method as well (Reina, 2009). Several techniques have been developed under the CVD or PVD methods (PalDey, 2003).

For a quick summary of fabrication process of carbides subjected to this dissertation, TaC powder is produced via the by the chemical reaction between Ta_2O_3 with carbon at 1700^oC, while the reaction of vanadium oxide or ammonium vanadate with carbon is used to fabricate VC powders approximately at same temperatures to TaC. Both VC and TaC carbide coatings are deposited by two different CVD techniques: sputtering and reactive evaporation. Direct carburization of tungsten metal with carbon or graphite is used to produce WC powders between the temperatures 1400^oC and 2000^oC, unlike TaC and VC powder production. Even the powders at submicron particle sizes are now available to be fabricated by CVD and sol-gel methods. Other initial materials such as tungsten oxide, tungstic acid etc. can also be used for WC powder production. Nevertheless, WC coatings are deposited by thermal and plasma CVD (Rohde, 1994; Dunbar, 1994; McKenna, 1968; Kieffer; 1965).

2.1.2 Interstitial carbides, structure, composition and physicochemical properties

Transition metal carbides (with the exception of chromium) are often defined as interstitial compounds and are refractory meanwhile exhibiting metallic properties

(Greenwood, 1984). Even some of them display a range of stoichiometry that affects the crystalline structure and therefore the final properties of the carbide as a consequence of revealing of short and longer range ordering, where disordered carbide structures by randomly filled interstices were believed to be intrinsic to non-stoichiometric phases (de Novion, 1985). It can be then said that the crystalline structure, composition and physicochemical properties are strongly related to stoichiometry and the ordering of atoms.

It is known that excluding the second and third row's elements of periodic table, compounds may be constituted with the reaction of carbon with all transition metals. The crystal structures of these compounds exhibit substantial variation. Toward the left of the periodic table, structures are in the tendency of being simple, and very commonly are similar to their transition metals themselves. On the other hand, toward the right in the periodic table, the electropositive elements contained compositions are inclined to be complicated regarding to radius ratio of metal and non-metal atoms (Hagg, 1931; Oyama, 1996). Figure 2.1 shows an illustration of carbide crystal structures that effects the designation of final properties.

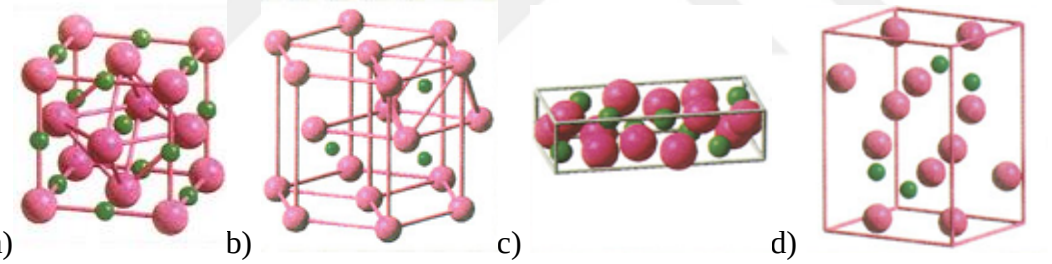

Figure 2.1 : Crystal structures in Group 4-8 transition metal carbides a) Rock salt: ScC, VC, NbC; b) hcp: β-Mo_2C, β –W_2C; c) Cr_3C and d) Fe_3C (Oyama, 1996).

Hagg first systemized the non-metal occupation of interstitial sites. He showed that electronic properties of metals, which are reflected in systematic crystal structure of carbides, are reason to this phenomenon (Oyama, 1996). This phenomena has been later theorized by Engel-Brewer which explains why the elements belong to left side of the periodic table constitutes body-centered cubic (bcc), while the center prefers hexagonal closed packed (hcp) structure and the right ones generate face-centered cubic (fcc) (Engel, 1939; Brewer 1967). Afterwards, the consequences of the shifts and occupations of valance electrons in mechanical properties have been studied deeply. For instance, the comparison of melting points were illustrated in Figure 2.2 (Adams, 1981; Cotton, 1980).

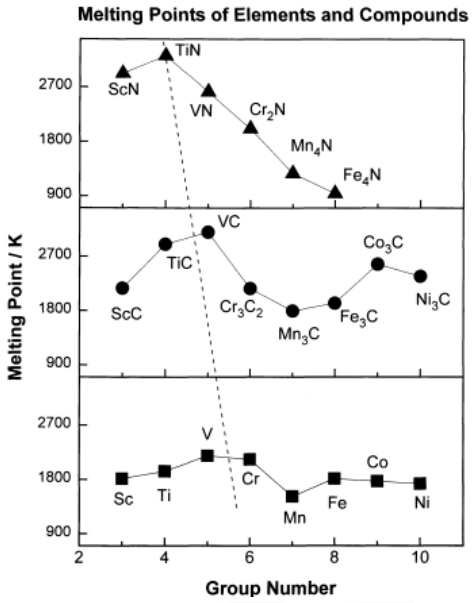

Figure 2.2 : Melting points of elements and compounds (Oyama, 1996).

By this graph, it was shown that M/X ratio is a factor in determining crystal type and strongly effective on the properties such as melting point. It can be seen from the graph that M/X ratio is maximum during the melting of metals for the Groups 5 and 6, while the maximum value shifts to Group 5 for carbides and to Group 4 for nitrides (Evans, 1979; Oyama, 1996).

In this group, the host metal generally consists of close-packed arranged atoms and the carbon atoms locate the interstitial sites that specified in the structure. The main transition metals, which meet the size and size availability criterions, are given in Table 2.2:

Table 2.2 : Transition elements fit the criteria (Hagg, 1931).

	Group IV	Group V	Group VI
4^{th} Period	Zirconium	Tantalum	Molybdenum
5^{th} Period	Titanium	Vanadium	Tungsten
6^{th} Period	Hafnium	Niobium	Chromium

Carbides formed from transition metals in the Groups IV – VI share some properties such as being refractory, having similar structure which allows to have a mixture of metallic, covalent and ionic bonding properties, similar carbon ordering, having high melting points, stability in terms of thermal and chemical, high hardness and strength even at high temperatures (Storms 1967; Toth, 1971). They have various compositions and structures, and major ones are given in Table 2.3.

Table 2.3 : Main compositions and structures of interstitial carbides (Pierson, 1996).

Group IV	Group V	Group VI
TiC_{1-x} (fcc)	V_2C (hcp) V_4C_3 * V_6C_5 * V_8C_7 * VC (fcc) *unidentified	$Cr_{23}C_6$ (fcc) Cr_7C_3 * Cr_3C_2 (hex)
ZrC_{1-x} (fcc)	Nb_2C (hcp) Nb_3C_2 * Nb_4C * NbC (fcc) *unidentified	Mo_2C (hcp) Mo_3C_2 * MoC (hex) *unidentified
HfC_{1-x} (fcc)	Ta_2C (hcp) Ta_3C_2 * Ta_4C_3 * TaC (fcc) *unidentified	W_2C (hcp) WC (hex)

During the constitution of carbide from metal, the M-M spacing increases for each transition metal carbide. This phenomenon influences strongly the hardness and melting point (Kisly, 1986; Weast, 1981; Van Uitert, 1981; Moffat, 1986). This switch of d-spacing in M-M atoms/planes from pure metal to carbide can also be seen at densities. Table 2.4 compares the density of transitions metals and their carbides:

Certain decrease in ratio of the melting points (carbide to metal) and the density (metal to carbide) from Group IV to Group VI is one of the remarkable finding wthat can be seen from the Table 2.4 (Kosolopova, 1971; Pierson, 1996).

Table 2.4 : Density of metals and their carbides (Pierson, 1996).

	Carbide	Carbide Density (g/cm^3)	Metal Density (g/cm^3)	Change (%)
Group IV	TiC	4.91	4.54	+ 8.1
	ZrC	6.59	6.51	+ 1.2
	HfC	12.67	13.36	- 5.1
Group V	VC	5.65	6.11	- 7.5
	NbC	7.79	8.56	- 9.0
	TaC	14.5	16.6	- 12.6
Group VI	Cr_3C_2	6.68	7.20	- 7.2
	Mo_2C	9.06	10.22	- 11.3
	WC	15.8	19.3	- 18.1

Table 2.5 shows the reviewed in more detail with relation between bond energy, Young Modulus, hardness and melting points of host metals and their carbides (Pierson, 1996; Zhurakovskii, 1974; Campbell, 1967; Kisly, 1986; Weast, 1981; Van Uitert, 1981; Moffat, 1986; Samsonov, 1964; Lide, 1967; Toth, 1971; Goldschmidt, 1967; McKenna, 1964; Oyama, 1992).

Table 2.5 : Reviewed physicochemical and mechanical properties of transition metals and their carbides.

		Bond Energy (eV)	Young Modulus (GPa)	Vickers Microhardness ($kg.mm^{-2}$)	Melting Point (°C)
Group IV	Ti	1.461 (Ti-Ti)	120	55	1660
	Zr	-	88	83 – 183	1850
	Hf	-	78	150 - 210	2230
	TiC	14.66 (Ti-C)	370	3200	3067
	ZrC	15.75 (Zr-C)	440	2550	3420
	HfC	17.01 (Hf-C)	352	2260 - 3050	3928
Group V	V	10.49 (V-V)	128	65	1890
	Nb	-	105	88 - 135	2468
	Ta	-	186	870 - 1200	2996
	VC	13.75 (V-C)	380	1500 - 1800	2830
	NbC	16.32 (Nb-C)	452	2400	3600
	TaC	16.98 (Ta-C)	285	1600 - 2000	3950
Group VI	Cr	6.72 (Cr-Cr)	279	108	1865
	Mo	-	329	140 - 270	2620
	W	-	411	370 - 470	3410
	Cr_3C_2	-	373 - 386	2280	1810
	Mo_2C	-	227 - 553	1950	2520
	WC	-	530 - 700	2600	2870

Interstitial carbides can be also defined as defect structure due to the misorientations, disorders and vacancies (Gusev, 2001; Moisy-Maurice, 1981). The interstitial carbides are known to be stable at high temperatures in the wide range of composition, however, structure of non-stoichiometric carbides in particular with these defects and vacancies should also be considered among them. The self-diffusion in carbides regulated by the amount of carbon vacancies is seldom defined as "structural vacancy", and these vacancies may reach highest percentages (Lorenzelli, 1969; Athanassiadis, 1987; Lipatnikov, 1997; Moisy-Maurice, 1982; Kaufinann, 1983; Metzger, 1983). Transitions carbides are therefore considered as defect structures that provide possibility to alter the properties and behaviour of these materials. It is now well known that the relationship between structure and properties

are intensely coupled with the atomic size, valances, bond energies and lengths, stoichiometry, ordering and vacancies. However, general properties of these carbides can be sorted as high hardness, high bond strength leading to high Young's modulus, very high melting points and refractories and high wear resistance.

2.2 Application of Transition Carbides

Application of metals in their pure state is very rare. They are generally applied in their alloy forms to overcome the expected conditions by strengthen or exploit desirable properties. In previous chapters, the physicochemical and mechanical properties of transition metal carbides superior to their pure metals were mentioned. The strength of interatomic bonding is very well known to be strongly effective on these properties (Kisly, 1986). Several studies have been reported formerly and the effects of bonding has been summarized previous chapters (Gubanov, 1994; Toth, 1971; Oyama, 1992; Lye, 1968). These carbides are therefore applied as direct to the materials (i.e. as a coating material), as reinforcement to different matrixes (i.e. composites) or as direct usage by addition of binder metal (i.e. WC – Co). Previously mentioned, the refractory carbides can be applied as powders, bulk/monolithic shapes, fibers, whiskers, and coatings (Pierson, 1996). They are subjected to various mechanical, thermal or tribological cycles. For the very reason, such properties were expected from them to exhibit such as hardness and chemical resistance (wear and corrosion applications), strength (structural applications), high thermal conductivity and electrical insulation (semiconductor applications) or high-temperature stability and resistance to radiation (nuclear applications). The properties that they exhibit make them so useful in industrial market. Several application areas of transition carbides have entered in the market in the last century. In addition to this, they have been gained significant importance in advanced applications over the last hundred years. By the synthesis of high specific surface area and ultrafine transition metal carbides, scientifically and technological interest in these areas stirred (Gleiter, 1992; Gusev, 1998; Dalfard, 2012; Fang, 2009; Kurlov, 2014).

The highest melting points are measured for the carbides of Group IV – VI transition metals as mentioned earlier. They can be operated at elevated temperatures and they can be applied in manufacturing industry where aggressive media under high loading cycles existd (Kurlov, 2013). Carbides such as WC, TaCy, VCy, NbCy etc. can also

be used a protective and hard coatings and can be added to the metal matrix in the shape of fibers, particulates or whiskers for various industrial areas (Veprek, 2002; Şelte, 2015; Abe, 2014; Hasegawa, 1993). Therefore, it is more appropriate to classify the transition carbides under industrial categories: tools and tool holding, machinery and equipment, automotive and aerospace, defense, nuclear, semiconductor and optical.

2.2.1 Tools and tool holding

This part covers some applications of carbides such as carbide blanks brazed to steel holders, milling cutters, grinding materials, or carbide coatings for steels. Indexable inserts, which are fully produced as carbide, are also in this group and have been used more than half decade in the industry. Particularly, cutting and grinding tools must have unique properties in terms of wear and corrosion resistivity. In case they are applied as abrasive-coated surface, great opposition to chipping is expected. Main failure mechanism in this area is wear that can be subgrouped as flank and abrasive wear (Lee, 1979). Therefore, in order to have effective functionality, a cutting tool must be harder than the substance or the material to machine. Like this, bulk WC tools (so-called WC – Co cemented carbides) as insert or mining or drilling materials have been developed. These inserts are now coated with other carbides (i.e. TiC), nitrides (i.e. TiN) or carbo-nitrides (i.e. TiCN) to prevent chipping and premature failures and to raise hardness of tool material against wear (Oyama. 1996; Clavel, 1991). This coated tools has a great impact on the extension of tool life and significant improve in productivity of metal cutting (Ekmar, 1974).

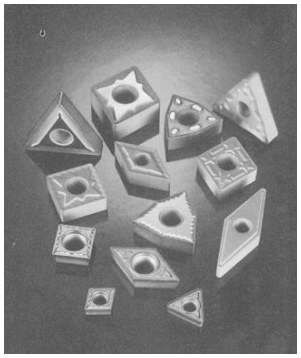

Figure 2.3 : Indexable inserts (Kennametal, Inc, Product Flyer A94-202, 1994).

2.2.2 Machinery and equipment

Transition metal carbides find wide range of applications in machinery and equipment such as metal and non-metallic forming, chemical processing, transportation and construction, structural components, coatings for metals and machine elements (Ashby, 1992). TiC for stamping and coining tools, deep drawing dies, extrusion dies for ceramic molding, sandblasting nozzles, components for abrasive processing and packing sleeves; WC for textile-processing, can-budy punches, rolls and shafts, swaging hammers and mandrels, extrusion punches and slitter knives; TaC for the protection of Ta metals, heat exchangers, or as reinforcement in particle-dispersed steels; Cr_7C_3 for especially sequential drawing dies and as corrosion resistant coating, NbC for the protection of Nb metals, or as grain growth stabilizer in micro-alloyed steels; SiC for valve liners, thermocouple wells, as heating elements, wear plates; VC laser cladded dies of new forming materials can be given as examples for machinery and equipment industry (Kurlov, 2013; Santhanam, 1996, Leunda, 2011).

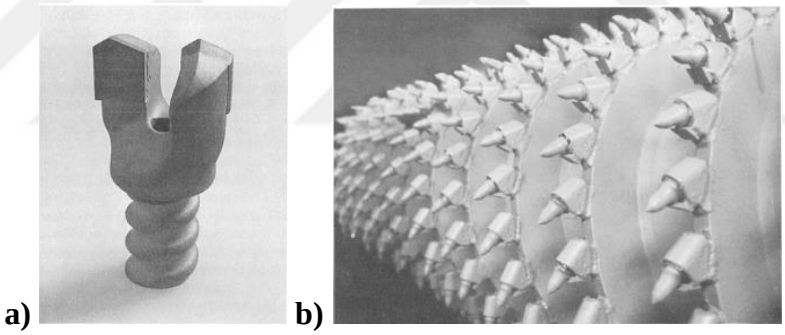

Figure 2.4 : Carbides in machinery: a) Two-pronged carbide bit used in rotary drilling, and b) rotating drum of a road planning machine (Santhanam, 1990).

2.2.3 Automotive and aerospace

In automotive and aircraft industry, cemented carbides are widely used materials for being a structural part. They are used in the applications where the high temperature and/or corrosion resistance are required. The bulk form of these carbides are usually applied in these areas. For instance, due to its high temperature resistivity even above 1700^{o}C makes SiC as one of the most used material for rocket nozzle application operating in a non-oxidizing atmosphere. In addition, TiC coated steel balls have been replaced in standard high-performance steel grades by providing enhanced properties such as higher hardness, a smoother surface with a lower

coefficient of friction. Typical example for TiC usage in automotive and aerospace industries is coated balls for bearings in space vehicles operating in vacuum and spin-axis gyroscope with oil lubrication (Savan, 1993, Pierson, 1996). Metal – ceramic composites such as carbide particle/fiber/whisker aluminum, copper, iron or titanium exhibit considerable increase in mechanical properties and find themselves application areas in aerospace as inner flaps, hypersonic fuselage skins, missile guidance tins and rocket nozzles and in automotive industry as ceramic substrate and coating material for honeycomb in gas turbine engine (Ho, 1992; Narula, 1996; Prater, 2014).

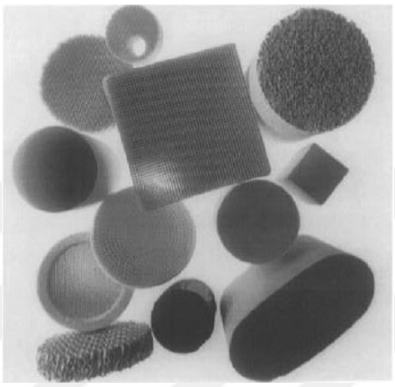

Figure 2.5 : Various shapes of monoliths made from SiC for gas turbine engine (Narula, 1996).

2.2.4 Transportation and construction

In this area, the usage of carbides are similar to machinery and equipment that involve soil stabilization, asphalt reclamation, trenching, tunnel boring etc.

2.2.5 Electronic and optical applications

SiC is a very promising material for both electronic and optical applications. Having high temperature potential, it has been used as semiconductor in the devices where high-voltage power, microwave and millimeter-wave required (Davis, 1993; Spearing. 2000). In addition, TaC can be an example for infrared to the near ultraviolet by its optical properties (Modine, 1984).

2.2.6 Nuclear applications

HfC, TaC, NbC, and ZrC coatings were introduced as an effective coating material for parts working at elevated temperatures between 2100 – 3200 K (Finseth, 1991).

Significant results have been reported for TiC and VC as well (Aguzzoli, 2010; Dahotre, 2001).

2.3 Composite Powders

Referring to ASM Metals Reference Book, composite material is described as a combination of two or more materials (reinforcement elements, fillers, binders etc.), diverging by shape of composition on a macro level (ASM Metals Reference Book, 1993). Phases or constituents do not dissolve or merge within each other and the miscibility is negligible. Since the immiscibility has been known between iron and copper, ball milling of iron and copper powders together constituted composite powders, which exhibited significant hardness, high strength due to the bcc/fcc interfaces between Cu and Fe after consolidating them to full density by sintering (Nakagawa, 1958; He, 1996). Having new and improved properties by producing composite powders has become well-known, and of course, optimizing the properties and ease of combining different kind of materials that are challenging to manufacture via conventional composite production, now is the main reason for production of composite powders (Llorca-Isern, 2013). Due to different structures, compositions and properties of constituents, they become multifunctional and correspond the several requirements such as a dense composite, a composite coating or in components where extremes of size are necessary, such as nanotechnology (Llorca-Isern, 2013; Ajayan 2003).

2.3.1 Nanocomposites and nanocrystalline materials

In this field of nano/microscale science and nanostructured or nanocrystalline materials, revolutional developments have been made for last decades which effected the every spot of humanity including community, politics, economics in particular with scientists and engineers from different disciplines such as chemistry, physics, materials science, computer technologies (Ohno, 2008). The more the size or the dimension decreases, the very new properties have become appear in bulk/powder materials which is first pointed out by Kubo in 1962 (Kubo, 1962). However, the idea of nanotechnology was first used by Richard Feynman in 1959 and the term “nanotechnology” first appeared by Norio Taniguchi in 1974. After then several

applications along with terminologies have been developed (Aliofkhazraei, 2011; Pitkethly, 2008).

Progressively, numerous nano based researches have been studied and it was seen that it is possible to obtain nanoparticle reinforced matrixes by forming impurities during heat treatment in steels, introducing second phases in submicron/nano scales, evaporating of metal particles onto substrates or dispersion of ceramic particles, constituting precipitates in metals, or by using precursors (Strudel, 1983; Eckert, 2002; Ajayan, 2003). Since the effect of crystallite and particle, size may result in great change in properties, production of nano-structured or -crystalline materials have paid attention in the last couple of decades (Gleiter, 1992; Gusev, 2004). These effects occurs when the grain size is at submicron scales or most evident below 100 nm. The common classification of these materials according to particle/grain size was illustrated in Figure 2.6.

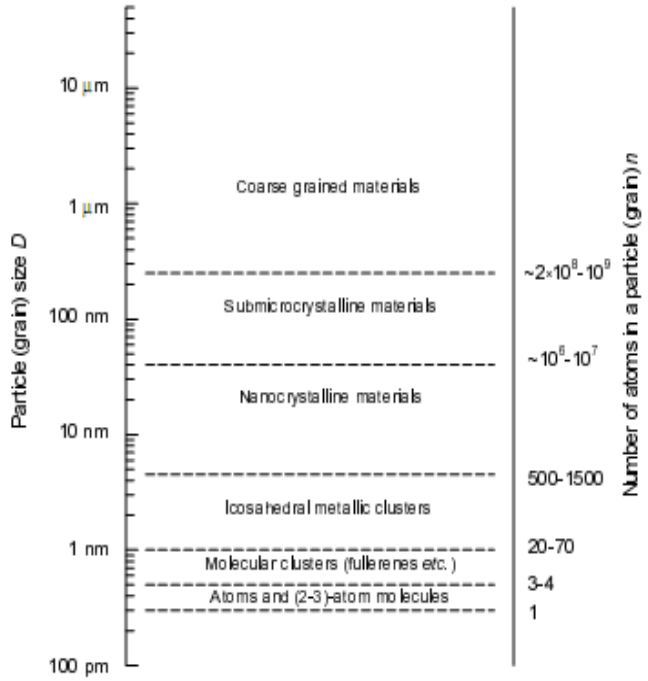

Figure 2.6 : Classification of materials according to their particle/grain size (Gusev, 2004).

Repeated distances between different phases in nanometer scale constitutes the so-called solid structure. These solid structures by combining of nano-dimensional phases with clear differences in the properties, chemistry and structure can be named as nanocomposite materials (Ajayan, 2003). Therefore, they can also classified as zero-dimensional (embedded clusters), one-dimensional (1D, nanotubes), two-

dimensional (2D, nanocoatings), and three-dimensional (3D, embedded networks) which can be seen in Figure 2.7.

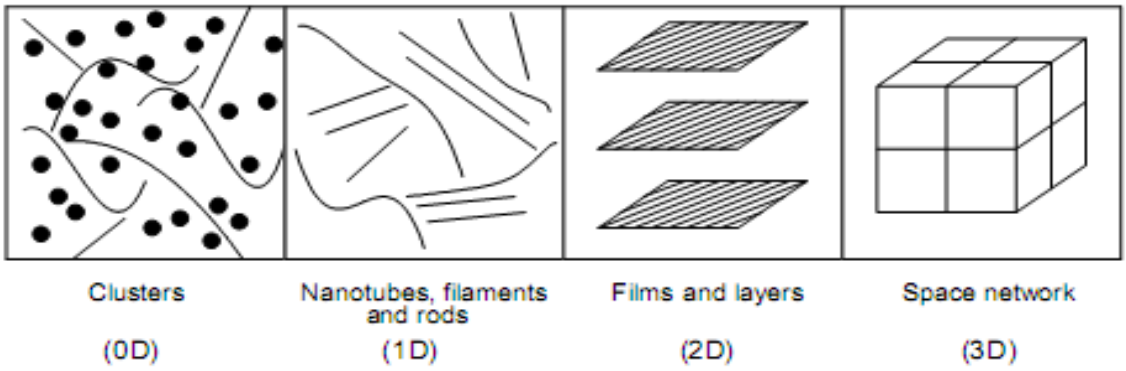

Figure 2.7 : Nanocrystalline material types: 0D (zero-dimensional) clusters; 1D (one-dimensional) nanotubes, filaments and rods; 2D (two-dimensional) films and layers; 3D (three-dimensional) polycrystals (Gusev, 2004).

They all consist of atoms of elements or clusters that constitute larger scales formed by nanoparticles or bulk nanostructures with nanosized crystallites (Shokuhfar, 2010). Despite the great influence of crystallite/particle/grain size on the final properties of composite, the high surface to volume ratio (A/V) is significantly effective to exhibit exceptional properties of nanostructured materials which is regulated by the precipitation of finer fractions/particles among grain boundaries and throughout the matrix in large quantities (Rezaie, 2013). One can say that the nanocrystalline materials is a representation of special state of condensed matter. It is now well known that these materials can be characterized by both specific factors of particles/crystallites and by their composite behaviours. Today, there are many wonders done by humans, just by relocating atoms and molecules, reducing their sizes to obtain advanced materials with excellent properties.

2.3.2 Properties of nanocomposite powders and materials

The physical properties of nano particles, isolated nanocrystals, or clusters have been investigated by several researchers and a large number of detailed reviews have been simplified (Buhren, 1998; Henglein, 1993; Perenboom, 1981; Halperin, 1986; Buffat, 1976). Among them, several techniques have been developed in order to determine the physical properties of fine particles, nanoparticles and particle beds (Hintz, 2009). Consequently, this chapter is limited to general properties of nanocomposite powders and nanostructured composite materials.

The field of nanocomposite have been an interest point of several researchers, scientists and engineers for a last couple of decades. Bulk or powder nanocomposites have been always under development and improvement in order to have promising properties for engineering applications. Besides ceramic based, metal based, polymer based, carbon nano tube (CNT) based composites, functional dimensional, particle dispersed magnetic, particle dispersed optical, inorganic, encapsulated, thin-film and various composite types were produced with the purpose of advanced technological applications (Ajayan, 2003; Ohno, 2008).

Critical mechanical properties of ceramics such as creep, thermal shock, fatigue resistivity and fracture toughness are improved by the dispersion and homogeneous distribution of submicron/nanometer-size second phase particles into ceramic matrixes (Ajayan, 2003). Considerable attention to these ceramic matrix composites (CMC) has also been devoted to "thin-films or multi-layer films" for coating technology. It has become possible to obtain better wear resistance, good stability at elevated temperatures and high friction properties with their enhanced hardness and Young modulus values (Veprek, 2005). Al_2O_3/W, Mo, Ni, Cu; ZrO_2/Ni, Mo; MgO/Fe, Co, Ni; SiC/Si_3N_4; TiC/TiCN nanocomposite powders can be cited for CMCs (Choa, 2000; Yoshimura, 1999; Nakahira; 1999; Choa 1999). The effect of nano SiC volume percentage on the strength and toughness of SiC/ ZrO_2-toughened mullite nanocomposite can be clearly seen from Figure 2.8.

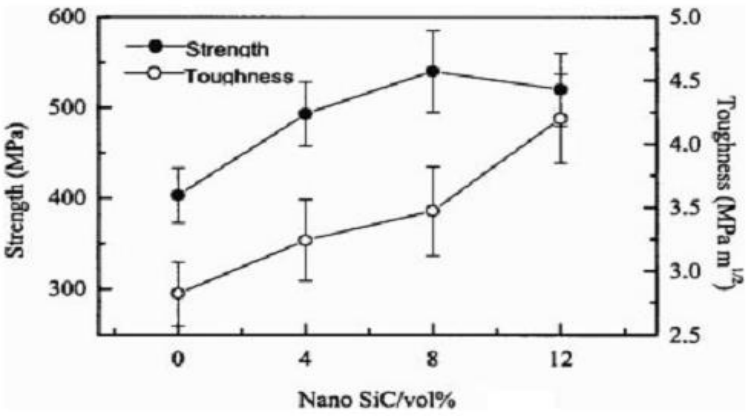

Figure 2.8 : Mechanical properties of a SiC/zirconia-toughened mullite nano-composite as a function of nanosized SiC content (Jin, 2002).

Besides, advanced bulk ceramics and powders are used owing to withstand high temperatures (>1500^{o}C), oxidation-resistivity and hardness (Tsuchida, 2005; Rezaie, 2013). They also exhibit excellent magnetic, electrical and optical properties and

superplasticity that are strongly related to particle/grain size of composite (Rezaie, 2013).

Metal matrix composites (MMCs), have been studied since the very beginning of 1960s and generally classified under two titles, e.g. a fibrous, whisker or particulate reinforced composites that is illustrated in Figure 2.9 (Chawla and Chawla, 2006). They are preferred as matrix materials owing to have:

- application allowance at elevated temperatures,
- generally high toughness,
- higher transverse stiffness and strength,
- advanced radiation resistances,
- excellent electric and thermal conductivities,
- higher strength-to-density, stiffness-to-density ratios, in addition to improved fatigue resistances, lower coefficients of thermal expansion (CTE) and superior wear resistances than with monolithic metals,
- possibility to be fabricated with conventional metal working equipment (Akovali and Uyanik, 2001).

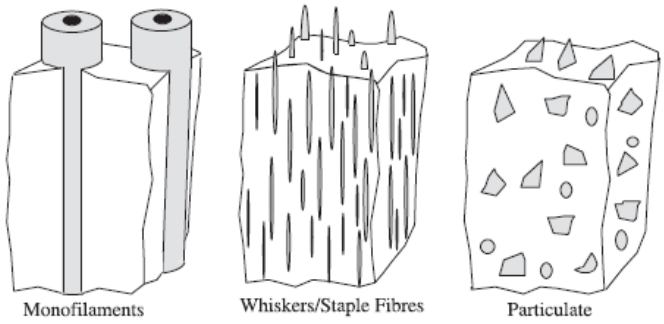

Figure 2.9 : Schematic respresentations of three shapes of metal matrix composite materials (Clyne and Withers, 1993).

Particle reinforced MMCs are paid attention mainly owing to their easier machinability, isotropic behaviour and often-lower cost. It is now well-known that particle size and distribution (PSD) is strongly correlated to the properties of particle reinforced MMCs. Wide range of MMCs are produced including large number of metals as matrix (Al, Cu, Fe, Ti, Ni etc) and reinforcing elements (carbides, borides, nitrides or their mixture). They display outstanding mechanical properties by the

formation of stable nanosized ceramic reinforcements (Ajayan, 2003). Goals of reinforcing metal matrixes with ceramic particles can be summarized as below:

- While preserving the high conductivity, increasing strength of conducting materials,
- Increase in creep resistance at low temperatures (reactionless materials),
- Development of burnout behaviour (electrical switch contacts),
- Development of wear resistance and behaviour (sliding contact),
- Longer operating times during spot welding by reduction of burnouts,
- Manufacture of layered composite materials for electronic parts,
- Manufacture of ductile composite superconductors,
- Manufacture of magnetic materials with special properties (Kainer, 2006).

MMCs family including particulate, fiber or whisker reinforced has drawn attention as a result of convenience to low-cost producibility, the process development in manufacture techniques in order to produce them with reproducible structure and properties and the availability of conventional metal working processes given at below:

- Combination of high strength and elasticity modulus (ceramic characteristics) with better toughness and ductility (metallic characteristics),
- Improved thermal stability,
- High specific modulus,
- Higher service temperature capabilities,
- Superior strength to shear and compression,
- Good chemical compatibility,
- High wear and friction resistivity (Ajayan, 2003; Kainer, 1994).

The reinforcement size and volume regulates the properties of MMCs significantly, as well as the type of interface between the matrix and reinforcement. Therefore, the effect of crystal/particle or grain is influential, dramatically. Change in tensile

strength of TiC reinforced – Al nanocomposites by volume fraction and diameter of TiC particles are illustrated in Figure 2.10:

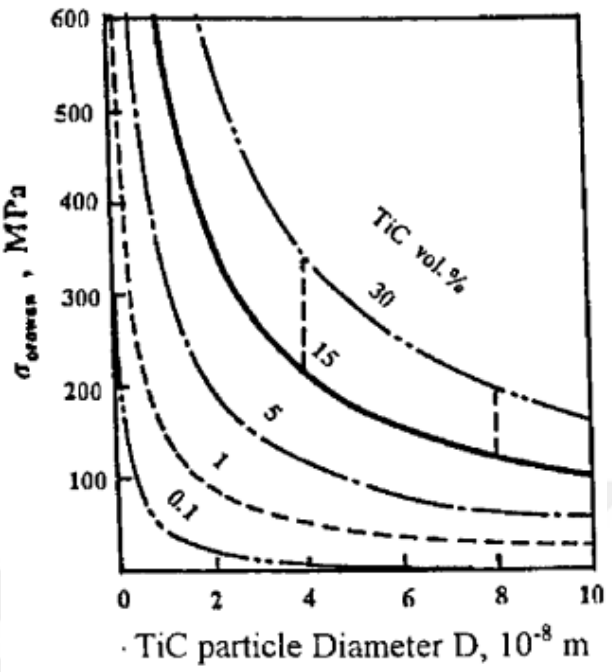

Figure 2.10 : Increase in strength of TiC-reinforced Al nanocomposites with increasing volume fractions or decreasing diameters of dispersed-phase (TiC) particles (Tong, 1998).

Moreover, Tjong and co-workers added silicon nitride nanoparticles (10 nm) to aluminium matrix and reported that the yield stress of 1 vol. % Si_3N_4/Al nanostructured composite is considerably superior to the 15 vol. % SiC-reinforced microstructured composite (Ma, 1996).

A large number of examples can be given for the nanocrystalline composite properties such as Fe-85 vol. % Fe_3C with the hardness value of 10.8 GPa, which is quite high, nanostructured M50 steel with the 8.5 GPa hardness in comparison with 7.8 GPa for conventionally produced M50 steel, Ni-TaC nanocomposite powders showing a high thermal stability, gaining ferromagnetism under 15 nm in radius etc. (He, 1996; Goodwin, 1997; Gonsalves, 1997; Wilde, 2001; Song, 1995). For detailed readings, Gusev's, Ohno's and Ajayan's books should be considered (Ajayan, 2003; Gusev, 2004; Ohno, 2008).

It is now well-known that we can engineer the prime of materials/devices/medicines with improved quality that corresponds the requirements of its application field and

responds the properties mentioned in this chapter by creating the “nanostructured materials”.

2.3.3 Application of nanocomposites and nanocrystalline materials

Nanomaterials and nanocomposites application in the systems were first in their powder form, without any consolidation or blending. Well-known example for this situation is the usage of nano zinc oxide and titanium dioxide powders in cosmetics for facial lotions and creams to protect from UV lights or nanoscale iron oxide powder for rouge and lipstick (Rezaie, 2013). Various examples can be multiplied for nano particle usage from defence industry to cutting tools through information technology to engineering components and coatings (Koch, 2007). Many uses of these particles have adapted to market and the usage of composite particles/powders have paid attention for scientific and technical equipment in the last decades. Nanocomposite particles/powders/materials are being developed including multiple shell structures, template-based approaches, coated particles, MMCs, CMCs, PMCs, coatings or self-assemble systems. Of several applications can be proposed for nanocomposites, only CMCs, MMCs and coatings are discussed here.

2.3.3.1 Nanocomposites for structural, electrical, magnetic applications

Metal based nanocomposites or composite powders have been used among the variety of applications. Particularly, light alloys find themselves a large number of application areas in automotive and aerospace engineering, which is mostly in the engine area. Construction units, pistons and piston pins, cylinder heads, crankshaft, valve train, engine block can be examples for the successful aluminium composite material applications within this range (Kainer, 2006). Al matrix composites, hard oxide, carbide or metal reinforced Cu, Mg, Ni, Ti matrix composites are utilized which is given in Table 2.6 as a compilation of potential and realized applications. Owing to their lightweight and tailorable properties, aluminum and magnesium alloys reinforced with carbon or boron fiber and aluminum reinforced with silicon carbide continuously have been used for a long time. In addition, the excellent incorporation between nanocomposites and nano particles makes them to exhibit superior improvements in their physical, mechanical and tribological properties, which was stated at previous chapter. For instance, reinforcing Cu with nano sized carbide particles provides sufficient increase in wear resistance and strength during

high temperature applications meanwhile Cu conducts electricity without any loses (Koch, 2007). Cu based MgO, TiB_2, MnO or Al_2O_3, WC, TiC composite powders are also produced for the electronic applications such as solid oxide fuel cells, microelectronics and semiconductors. Ti based composites are widely chose for the applications in medical industry such as implants owing to their high chemical stability and good biocompatibility. Pt-CeO_x powders are also good example of nanostructured composite powders with improved properties by optimizing the contact between the particle and diesel soot owing to the lower particle size, which needs relatively lower filter regeneration temperature (Llorca-Isern, 2013). Likewise, these reinforced metal matrix composite powders are a great candidate for reinforced plastics that is now used by Toyota and GM cars (Koch, 2007). Currently, metal matrix composites are widely applied in the defense, automotive and aerospace industries and it seems to be continued in mid-term future.

MMCs are not only composites for structural applications, but also CMCs are applied for load bearing applications. Al_2O_3/nanotube composites employed to positions that requires high toughness where high-contact damages occur. Similar results were obtained in Al_2O_3/graphite composites as well. BN/SiC membranes are another strong example to usage of CMCs. They are appropriate for gas separations, at least air separations by exhibiting of better permeability and selectivity comparing to than known polymers. Composite powders produced as encapsulated nanocomposite powders such as CNT/LaC_2, YC_2, TiC, V_4C_3, HfC, NbC, TaC, ZrC are a potential applications for magnetic recording media. Some of them (CNT/ TaC, NbC, MoC) are invaluable CMCs because of their excellent superconducting transitions at low temperatures regarding to their size (Bandow, 1993; Saito, 1994). For a further readings studies of Ohno (2008), Koch (2007), Eckert (2002), Chawla (2006) and Clyne (1993) and Ajayan (2003) should be noticed.

Table 2.6 : Potential and realistic technical applications of metal matrix composites (Kainer, 2006).

Application	Required properties	Material system
Automotive and heavy goods vehicle		
Bracing systems, piston rods, frames, piston, piston pins, valve spring cap, brake discs, disc brake calliper, brake pads, cardan shaft	High specific strength and stiffness, temperature resistance, low thermal expansion coefficient, wear resistance, thermal conductivity	Al-SiC, Al-Al_2O_3, Mg-SiC, Mg-Al_2O_3, discontinuous reinforcements
Accumulator plate	High stiffness, creep resistance	PbC, Pb-Al_2O_3
Military and civil air travel	High specific strength and stiffness, temperature resistance, impact strength, fatigue resistance	
Axle tubes, reinforcements, blade and gear box casing, fan and compressor blades		Al-B, Al-SiC, Al-C, Ti-SiC, Al-Al_2O_3, Mg-Al_2O_3, Mg-C continuous and discontinuous reinforcements
Turbine blades	High specific strength and stiffness, temperature resistance, impact strength, fatigue resistance	W super alloys, z. B. Ni_3Al, Ni-Ni_3Nb
Aerospace industry	High specific strength and stiffness, temperature resistance, low thermal expansion coefficient, thermal conductivity	Al-SiC, Al-B, Mg-C, Al-C, Al-Al_2O_3, continuous and discontinuous reinforcements
Frames, reinforcements, aerials, joining elements		
Energy techniques (electrical components and conducting materials)	High electrical and thermal conductivity, wear resistance	Cu-C
Carbon brushes	High electrical conductivity, temperature and corrosion resistance, burn-up resistance	Cu-C, Ag-Al_2O_3, Ag-C,Ag-SnO_2, Ag-Ni
Electrical contacts		
Super conductor	Superconducting, mechanical strength, ductility	Cu-Nb, Cu-Nb_3Sn, Cu-YBaCO
Other applications	Burn-up resistance	Cu-W
Spot welding electrodes		
Bearings	Load carrying capacity, wear resistance	Pb-C, Brass-Teflon

2.3.3.2 Nanocoatings

In recent years, surfaces of the components/parts exposed to severe damage failure mechanisms are coated with nanocoatings in order to improve the mechanical properties such as wear resistivity, corrosion, erosion etc. Layers, films under 100 nm thickness consist of nano particles/powders exhibit specific properties that they do not display for bigger dimensions. Applications can be classified as scratch and corrosion resistant coatings, medical, hygienic, optical applications, electric and electronic applications and the others (Aliofkhazraei, 2011). The usage of these nanocomposites varies from photovoltaic devices, biomedical equipment, nanoelectronics, etc. to protective applications in order to expand the lifetime of the parts, components or tools that are exposed to friction media for instance cutting tools, bearings, drills, gears etc. In addition to advantageous of nanocomposites improvements on mechanical properties, filling them with metallic nanoparticles (Ni, Co, Cu, etc.) showed superparamagnetic or ferromagnetic properties depending on

the cluster size (Martinez-Martinez, 2013). Application of nano Ag/TiO_2 composite powders in microbial and viral anti-pollution masks, coatings for prosthesis, coatings in food packaging, protective coating against bacteria are great cases for nanocomposite coatings in biomedical industry (Aliofkhazraei, 2011). Suzuki et al. have reported that polymer – iron oxide composite powders are excellent MRI contrast agent (Suzuki, 1996). Besides electronics, magnetics and biomedical devices, the most application field for nanocomposites is hard coatings. Most widely used coatings in this field are DLC, WC, TiAlN, TiC, TiN, TiB_2, Al_2O_3, MoS_2, CrN etc. However, composite powders have been applied for better thermal stability, lower friction, increased lifetime and toughness (Hauert, 2000). TiN/VN, TiN/Si_3N_4, TiAlN/CrN, WC/C nanocomposite coatings for tools, dies, bearings, rollers etc. were prospered within this context (Ajayan, 2003). With all that, laser cladding technology has been developed as a promising technique, recently. Substrate related metal matrix composites are enhanced for this technology. Al, Ni, Co, Cu, Fe / transition carbides or nitrides composite powders were used for tool, dies and moulds as laser-cladding coating material (Van Acker, 2005; Zhong, 2007; Vaz, 2000; Patscheider, 2001). The most important thing for all these applications is the well-known phenomena: size effect in nanostructured films owing to its unique and ultimate improvements.

2.3.4 Synthesis of nanocomposite powders

Composite powders/materials are produced via different production techniques. They cannot be fabricated easily by using conventional methods such as casting as a result of the high cost of processing. Wide range of matrix reinforcement compositions can be manufactured via powder metallurgy (PM) techniques by eliminating the segregation phenomena, which is typical in the casting processes, in order to minimize the brittle reaction products and high residual stresses caused by solidification shrinkage. However, notwithstanding this, it should be pointed out that favouring to use of the “bottom-up” approach in nanotechnology, while applying the “top-up” approach in conventional technologies is the key difference between nanotechnology and conventional technologies (Vollath, 2013). Powder production route presents an explanation for the difference between two approaches. Generally, chemical synthesis of powders exemplifies the “bottom-up” approach whilst the “top-down” approach means the crushing, milling, and comminution. The media,

which can be gas, liquid or solid, are always very effective on the formation of macroparticles, microparticles and nanoparticles. Therefore, the most preferred and important classification is focusing on media.

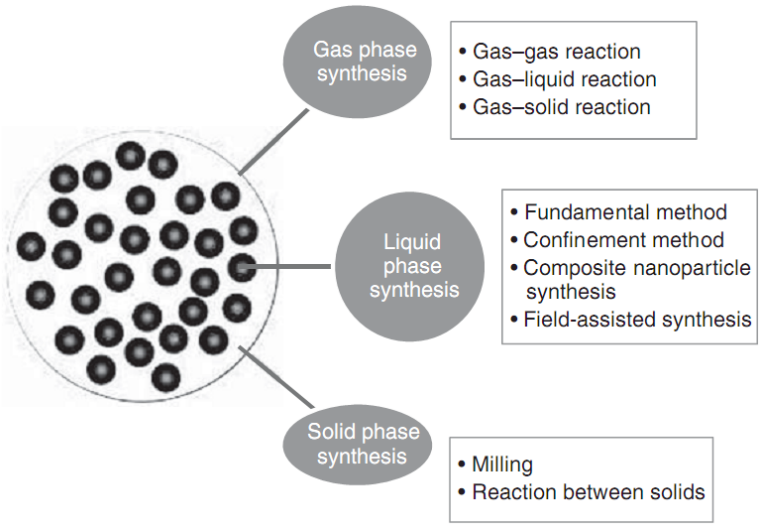

Figure 2.11 : Nanoparticle synthesis methods (Lu, 2012).

Although the dominant approach in nanoparticle synthesis is liquid-phase, other approaches are also widely used (Lu, 2012). Gas-phase approach covers the vapour condensations; vapour reactions and aerosol (vapour or spray pyrolysis). This method has the benefits of single-step production, involvement of solely inorganic and easy-to-obtain precursors, and fabrication of high-purity nanoparticles, however, because of random condensation, cluster collision by nature, particle size distributions is relatively broad, and agglomeration is evident (Wegner, 2002; Perez-Tijerina, 2008; Vollath, 2013). Liquid-phase consists of chemical precipitation and coprecipitation, hydrothermal, solvothermal, sol-gel, microwave heating, electrochemical processes (Llorca-Isern, 2013). The reason to liquid-phase approach become dominant is the requirement of nanoparticles to have control in nucleation and growth. This allows having more flexibility in controlling nanoparticle formation. However, it requires more control to obtain desired particle size, and it should be considered that different compounds may have different precipitation rates that may cause deviation from homogeneous precipitation (Lu, 2012). On the other hand, solid-phase synthesis consist of milling and reaction between solids. It contains cryochemical processing, mechanochemical processing, mechanical milling, solid-state synthesis and self-combustion methods. Sample material is grinded by given kinetic energy to reduce the particle size or to alloy or combine immiscible systems.

The high-energy process that causes for nanostructured materials introduces the severe plastic deformations.

Although there are various methods for synthesis of nano-structured powders, the main methods classified under three groups: mechanosynthesis, sol-gel methods and pyrolysis. Yet, only mechanosynthesis is the topic of interest concerning this dissertation.

2.3.5 Mechanosynthesis

It is known that manufacturing metal matrix composites in the whole range of matrix reinforcement compositions via powder metallurgy techniques is possible. It provides eliminating the segregation phenomena, which is typical in the casting processes (Fogagnolo, 2003). However, obtaining a homogeneous distribution of the reinforcement throughout the metal matrix appears as one of most important obstacle points. Hence, it is essential to provide the homogeneously distributed reinforcing phase in the metal matrix to maintain compromising performance for a composite material (Boselli, 2001). Therefore, the critical step for powder metallurgy is to mix the matrix and reinforcement (Fogagnolo, 2003; Boselli, 2001; Jain, 1993). Accordingly, high-energy ball milling was created by Benjamin in the 1960s (Benjamin, 1988), but it took some time to reach its full commercial position up to the 1980s (Fisher and Haeberle, 1988) and since then it has been used to obtain homogeneous particle distribution throughout the matrix. Mechanical milling (MM), mechanical alloying (MA) or mechanosynthesis (MS) and mechanochemical synthesis (MCS) or reactive milling (RM) are assigned to processes introducing mechanical energy generated in attritor mills, planetary ball mills, tumbling ball mills, vibratory mills or Spex mills, which they have different capacities, milling effects, cooling and heating units (Suryanarayana, 2001; Goff, 2003). The production of nancomposite powders has drawn interest of numerous researchers, because of the fact that the high-energy milling process substantially reduce the crystal or particle size. In the last decade, the synthesis of nanocomposite or nanostructured composite powders have been intensely subjected to many of the researches and studies. After the discovery of the capability of MA technique to synthesis these composite powders with the uniform distribution of nanoparticles, a great number of

nanocomposite systems has been studied in the wide range of material components (Llorca-Isern, 2013).

As a technique providing changes in mechanical, chemical and physical properties of materials through chemical, conventional thermal, mechanical and thermomechanical routes, mechanical alloying can be applied to improve the performance and properties of materials (Suryanarayana, 2001). Consequently, the processability of non-equilibrium systems and the ability to produce better and advanced materials, MA has become an interest of many scientists, researchers and engineers. Structure and property of advanced materials can be controlled much better under non-equilibrium conditions. MA is a PM technique to produce composite powders by repetitive cold welding, fracturing and re-welding of particles by obtaining controlled fine structure (Öveçoğlu, 1987; Benjamin, 1992; Suryanarayana, 2001). One of the most important advantages of MA is to allow alloying immiscible systems, which have normally not any miscibility or the miscibility is negligible. The reason for this phenomenon is that MA is a solid phase process and therefore there is not any limits related to phase diagrams (Benjamin, 1992).

2.3.5.1 Mechanism of mechanical alloying

During high-energy milling, the powder particles are repeatedly flattened, cold welded, fractured and rewelded. Trapped particles between the balls after a while starts to be plastically deformed by effect of the impact force that leads to work hardening and fracture (Figure 2.12).

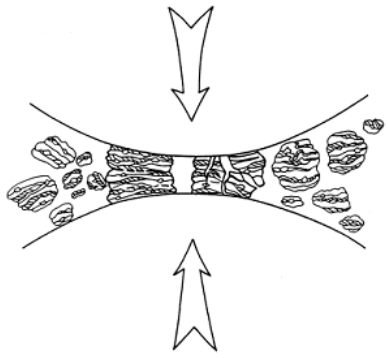

Figure 2.12 : Ball-powder-ball collision of powder mixture during mechanical alloying (Suryanarayana, 2001).

By fracturing, new surfaces are created which enables them to weld together and raises the particle size. At very beginning of the milling, the particles are soft, and so

have great tendency to agglomeration. A wide range of particle sizes shows up that bigger than the starting particles. While the deformation continues, the particles get work hardened and fracture by a fatigue failure mechanism and/or by the fragmentation of fragile fakes (Suryanarayana, 2001). Consequently, one can said that MA provides oxide dispersion, carbide dispersion, solid-phase and substructure/precipitation hardening (Öveçoğlu, 1987). MA must be divided into three stages for a better understanding. At the first stage, metallic particles are crushed and lapped over. Meanwhile, clean surfaces contact each other and cold-weld. Brittle constituents such as intermetallics and brittle additives clog between these interfaces (Goff, 2003). Figure 2.13 shows this stage that forms layers.

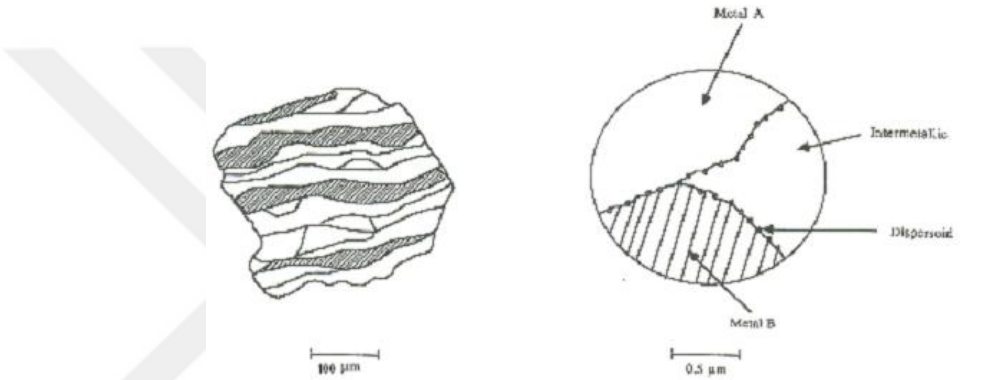

Figure 2.13 : First stage including layered structure consist of initial materials (Öveçoğlu, 1987).

The particles continue to get refined by repeated welding and fracturing of exceptionally work-hardened metallic phases and brittle intermetallics and/or dispersoids in the intermediate stage (Goff, 2003). At this stage, the fracture tendency becomes dominant over cold welding (Suryanarayana, 2001). The particles consist of convoluted lamellae. Areas of solute dissolution constitute throughout the metal matrix by the aid of increased microstructural mixing, high temperature of the powder constituents due to the adsorbed kinetic energy of milling balls and particle size reduction (Öveçoğlu, 1987). Thus, this potentially may lead to areas where new phases develop which is mainly due to an overall decrease in atomic diffusion distances between individual phases and decreased activation energies for diffusion due to the increase in temperature (Öveçoğlu, 1987; Goff, 2003). Consequently, the inter-layer spacing decreases and the number of layers in a particle increase (Suryanarayana, 2001). The reduction in particle size, dissolution of lamellae and

formation of new phases followed by the final stage of processing and consolidation are schematized in Figure 2.14 and Figure 2.15.

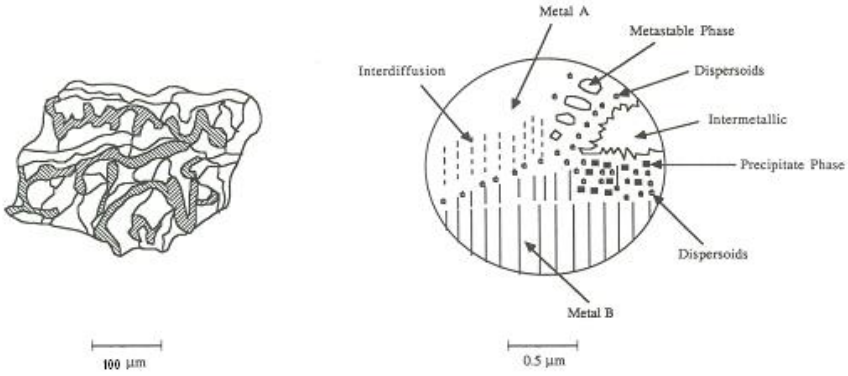

Figure 2.14 : Intermediate stage of processing (Öveçoğlu, 1987).

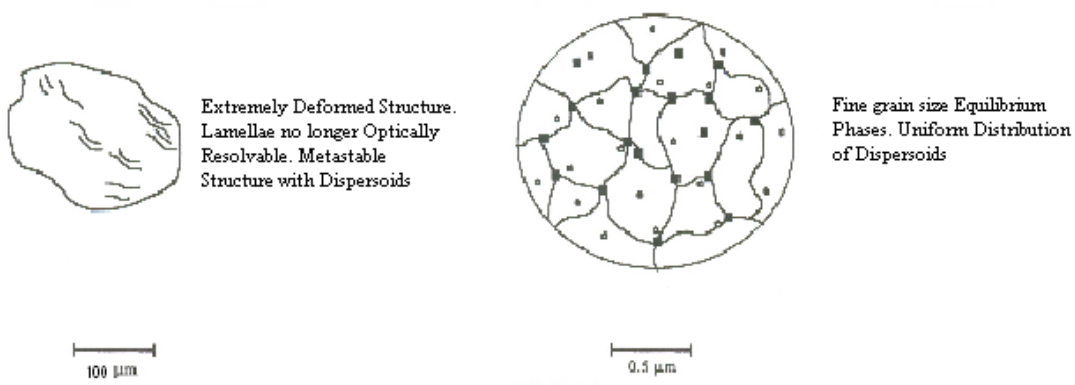

Figure 2.15 : The final stage of processing and consolidation (Öveçoğlu, 1987).

In the final stage, the balance between fracturing and cold-welding is reached. The smaller and finer particles become resistant to high deformation rates without fracturing. They gain high tendency for obtaining fine structures (Figure 2.15), (Suryanarayana, 2001). At this stage, particle size and distribution tighten and relatively homogeneous structure is produced.

2.3.5.2 Systems of mechanical alloying

Three different systems called ductile – ductile, brittle - brittle and ductile – brittle can be achieved by MA. They can be investigated in detail, individually (Fecht, 2002). It is considered that at least 15 % of ductile presence is ideal for better MA. This is a fact as a result of repeated cold-welding and particle fragmentation and it is known that cold-welding cannot occur without any ductile existence (Suryanarayana, 2001).

If this system contains two or more brittle constituents, it would be expected to alloying improbable. Absence of ductile constituent avoids any welding to occur, and without any welding, mechanical alloying is not expected to happen. However, some brittle – brittle systems were reported that the alloying has occurred such as Mn - Bi and Si - Ge (Davis, 1987; Davis, 1988). Yet at very small sizes, particles tend to behave like ductile, therefore further reduction in size is not possible (Harris, 1967). It was reported that harder component starts fragmentated and then becomes embedded to the softer one (Suryanarayana, 2001). This transfer can be considered as a result of possible mechanism happening during milling including (a) rise in temperature locally, (b) deformation on the surface, (c) micro-deformation in defect-free volumes, and/or (d) hydrostatic stress state in the powders (Davis, 1988).

At the beginning of ductile – brittle milling, brittle particles get fragmentated, while the ductile particles become flattened by the ball - powder - ball collisions. These comminuted particles are in tendency to become blocked by the ductile constituents and trapped into ductile particles. Meanwhile, the brittle particles are carefully settled between the gaps of lamellae and refined. With continued MA, ductile particles continue to be hardened, lamellae becomes convoluted and then finally, finer. Brittle particles disperse uniformly during lamellae gets closer by increasing milling (Figure 2.16). Particularly, insoluble brittle particles disperse in the ductile matrix in this way (Suryanarayana, 2001).

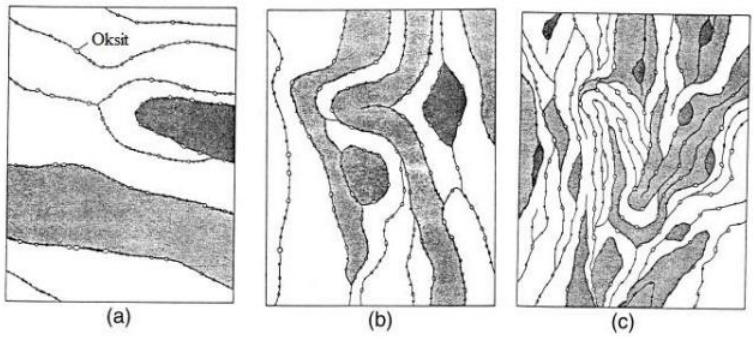

Figure 2.16 : The Schematic illustration of microstructural changes during milling of a brittle - ductile combination of powders (Suryanarayana, 2001).

2.3.5.3 The effect of grain size

As mentioned in previous chapters, the grain size can be reduced by milling until a saturation level by establishing balance between the fracturing and cold welding. One can said that the minimum grain size, d_{min} changes depending on material type,

milling condition, and is strongly in correlation with crystallite size and particle size. This is because smaller sizes constitute the larger structure that can be seen in Figure 2.17.

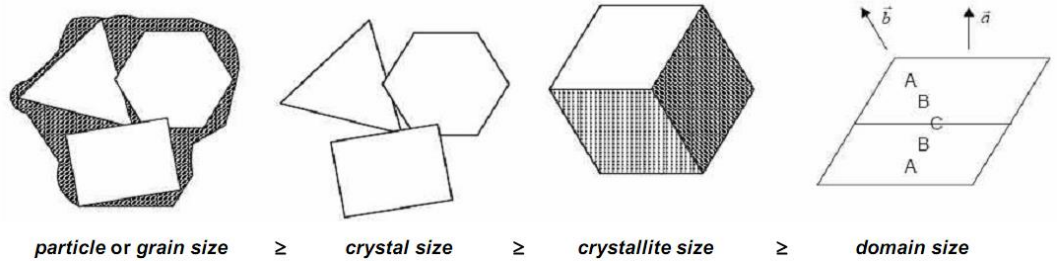

Figure 2.17 : The schematic definition of particle size, grain size, crystallite size and domain size (TOPAS Users Manual, Bruker AXS).

It was reported that 5 – 50 nm minimum grain size was achieved, and it appears that nanostructures by mechanosynthesis is possible for various kind of materials. However, the explanation of why and how nanometer-sized grains are obtained are lacking of comprehensive investigations. In addition to this, several studies have shown that the value of d_{min} is determined by plastic deformation via dislocation motion, which is regulated by lattice type (Suryanarayana, 2013). For instance, the minimum grain size can be obtained in nano scales for the most of the metals. Nevertheless, metals with a body centered cubic (bcc) crystal structure can reach much finer particle sizes comparing to metals with the other crystal structures. Eckert et al., noted that mechanical and physical properties of the material are strongly related to d_{min}, which can reduce by increasing melting temperature (Eckert, 1992). The correlation between grain size and the melting temperatures of some metals regarding to their lattice type is presented in Figure 2.18.

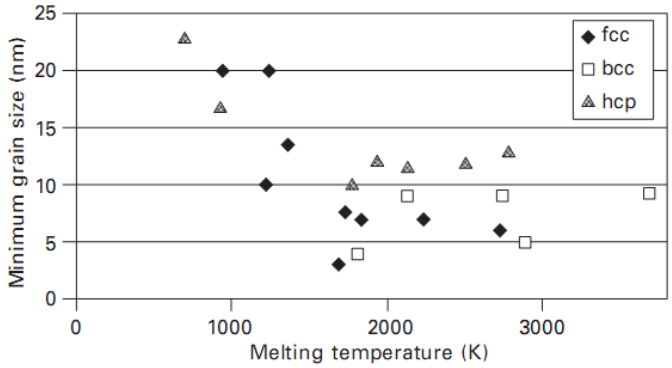

Figure 2.18 : Minimum grain size obtained by mechanical milling of different pure metals with different crystal structures versus their melting temperature (Suryanarayana, 2013).

3. EXPERIMENTAL PROCEDURE

The experimental procedure of this dissertation comprises the identification of raw materials, mechanical alloyed (MA'ed) powders, and their detailed crystallographic characterization. Furthermore, hydrometallurgical techniques were used to obtain nano fractions in order to confirm the manufacture of nano particles. Flow chart of the experiments are illustrated in Figure 3.1.

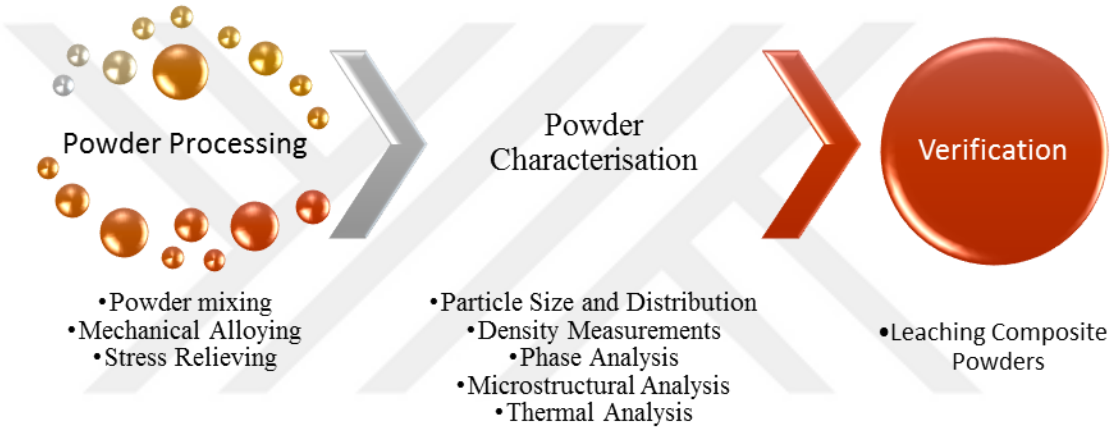

Figure 3.1 : Flow chart of experimental procedures.

3.1 Materials

Synthesis of finer brittle particles and optimization of fragmentation behaviour of brittle particles in order to obtain nanostructured composite powders via MA technique is one of the major purposes of this dissertation. Brittle compounds were selected according to their density and elastic modulus values and the purity of them was cared. Ductile matrixes were decided due to their elastic modulus and thermal conductivity values considering their crystal type. Table 3.1 shows the characteristics of the raw materials used in the experiments.

Insolubility or negligible solubility between these metal matrixes and carbides constituted also basis for the selection process of these materials. However, some ternary phase diagrams of these materials were reported as for Cu-V-C (Savitskii, 1961), Cu-W-C (Yasinskaya, 1966), Fe-V-C (Arnold, 1912; Vogel, 1931), Fe-W-C

(Hultgren, 1920; Jellinghaus, 1968), Ni-W-C (Edwards, 1952; Whitehead, 1956), Ni-V-C (Edwards, 1952; Holleck, 1984) and Ni-Ta-C (Edwards, 1952; Vasileva, 1975). Partial liquidus surface projections in stable equilibria only for Fe-V-C, F-W-C and Ni-W-C were illustrated by MSI Eureka in Figure 3.2. Rest of the material graphs are lacking in literature.

Table 3.1 : Raw materials used in the experiments.

	Cu	Fe	Ni	TaC	VC	WC
Provided from	Alfa Aesar	Alfa Aesar	Alfa Aesar	Alfa Aesar	ABCR	Alfa Aesar
Purity (%)	99.9	99.2	99.9	99.9	99.9	99.9
Mean Particle Size	-100 mesh	-20 mesh	-100 mesh	-325 mesh	3-5 µm	-325 mesh
Density (g/cm3)	8.96	7.874	8.908	14.3-14.65	5.77	15.6
Elastic Modulus (GPa)	110-130	≈ 211	≈ 200	≈ 285	≈ 380	≈ 550
Thermal Conductivity (W/m·K)	401	80.4	90.9	21		110
Melting Point (°C)	1084.62	1538	1455	3850	2810	2785
Hardness (Mohs)	3.0	4.0	4.0	8.5	9 – 9.5	≈ 9.0

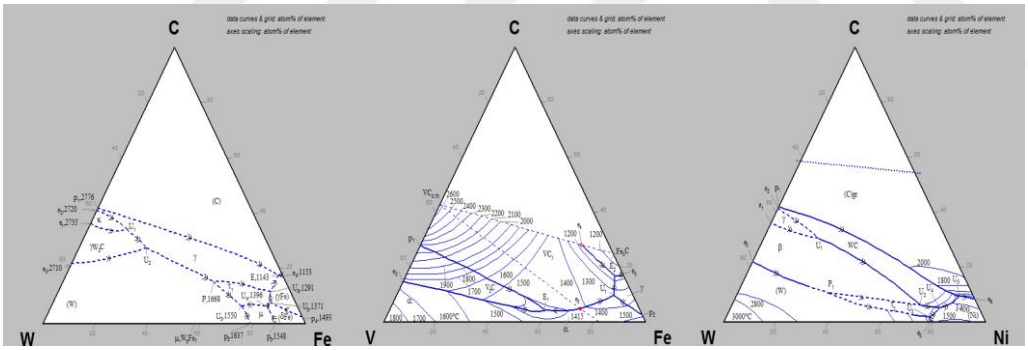

Figure 3.2 : Partial liquidus surface projections in stable equilibria.

3.2 Powder Processing

TaC, VC and WC powders were added to Cu, Fe and Ni powders to constitute 75Cu/Fe/Ni-25TaC/VC/WC (wt. %) powder mixtures, which are hereafter called as Cu25TaC, Cu25VC, Cu25WC; Fe25TaC, Fe25VC, Fe25WC and Ni25TaC, Ni25VC, Ni25WC. The mixtures were mixed in laboratory scale turbula blender for homogenization and then mixed powders were mechanically alloyed (MA'd) for 2, 4 and 8h using a Spex™ Duo Mixer/Mill 8000D with a speed of 1200 rpm in a tungsten carbide (WC)-cobalt (Co) vial with WC–Co balls having a diameter of 6.35

mm (1 = 4 inches). The ball-to-powder weight ratio (BPR) was 10:1. The vials were sealed inside a Plaslabs™ glove box under purified Ar gas (99.995% purity) to prevent oxidation during MA (Figure 3.3).

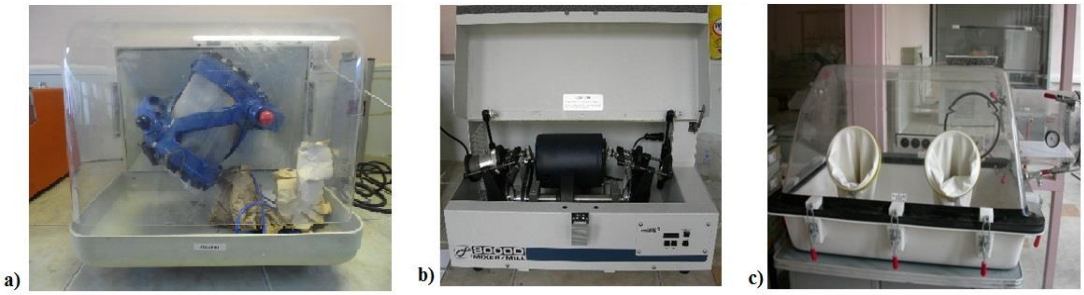

Figure 3.3 : a) WAB™ T2C Turbula blender, b) 8000D™ Spex mill, c) Pluslabs™ glove box.

Stress relieving treatment was applied for Cu based composite powders at 400°C, Fe based composite powders at 600°C and Ni based composite powders at 550°C by using Linn™ 1800 M Vac Graphite furnace. Holding time was 2 hours for all powders according to ASM Handbook (ASM International, 1991).

Figure 3.4 : Linn™ 1800 M Vac Graphite furnace.

3.3 Powder Characterisation

All powders were dried at 100°C to remove moisture for measuring true densities that were measured in Micromeritics™ AccuPyc II 1340 Gas Pycnometer under He atmosphere. Density result of each powder product includes the arithmetic mean of ten successive measurements and standard deviations. Green densities were calculated by pressing the powders at MSTEC™ BM-0805" hydraulic press machine at same pressure rate 200 MPa in the cylindrical dies with 12 mm radius. Powders were stirred by using Bandelin™ Sonorex ultrasonic bath for 10 minutes and then

powder particle size and distributions (PSD) were carried out in a Malvern™ Mastersizer Laser particle size analyser according to Mie's theory. Powders before and after leaching were stirred by using Bandelin™ electronic UW 2200 homogenizer for 30 seconds and finer particle fractions of MA'ed powders were measured at Microtrac™ Nano-flex particle size analyser.

a) 

b) 
c) 

Figure 3.5 : a) Micromeritics™ AccuPyc II 1340 Gas Pycnometer b) Mictotrac™ Nano-flex particle size analyser c) Malvern™ Mastersizer Laser particle size analyser.

The phases of all initial and MA'ed powders were identified using a Bruker™ D8 Advanced Series X-ray diffractometer (XRD) with CuKα (λ=0.154 nm) radiation in the 2θ range of 10-100° with 0.02° steps at a rate of 5°/min (Figure 3.6). International Centre for Diffraction Data (ICDD) powder diffraction files (PDF) were utilized for the crystalline phase identification of the raw materials.

Figure 3.6 : Bruker™ X-Ray Diffractometer (XRD).

The determination of crystallite sizes is derived the following equation relating the width of a diffraction line to the crystallite size (Scherrer, 1918):

$$\beta = \frac{\lambda}{D \cos\theta} \tag{3.1}$$

where β is the full width half-maximum, D is the volume weighted domain size (crystallite size) and θ is the diffraction angle. This equation has been used for years and is still used as modified in integral breadth methods to calculate the crystallite size of a material (Ida, 2002; Suryanarayana, 1998). Afterwards, the crystallite size D was first estimated by the Debye - Scherrer equation:

$$\boldsymbol{D = \frac{\kappa\lambda}{\beta cos\theta}} \tag{3.2}$$

where κ is a constant which depends on the crystallite shape and is usually unknown, but is often assumed to be 0.89, λ is the x-ray wavelength, β is the integral breadth (IB) or full width at half maximum (FWHM) of the diffraction angle. In this context, IB of the diffraction line or FWHM intensity is usually employed for many cases. Contributions regarding to the observed, broadened diffraction lines in terms of parameters, which used in materials science such as dislocation densities, faulting probabilities and crystallite size and strain rates are confrontation for scientists. In order to extract microstructural parameters from profile parameters of a single line or multiple/whole powder diffractions, development of advanced methods have been increase, dramatically (Mittemeijer, 2012). Practically, fundamental parameters approach (FPA) is applied for most cases as a result of being superior to other empirical or phenomenological methods, which the crystallite size and strain rates of the powders related to this dissertation were calculated by using TOPAS software according to FPA (Wang, 2008). This approach can be employed either with Gaussian or with Lorentzian or with convolution (Voigt) of both line profiles, which all are strongly related to diffraction line shape. For microstrain broadenings Gaussian distribution functions, for the emission profiles and intensity changes Lorentzian (Cauchy) distribution functions, or weighted linear addition of a Gaussian and Lorentzian functions for asymmetric shapes or considering shape parameters Pearson VII functions are commonly applied. The ratio of the integral breadth, β, and the full width at half maximum (FWHM), 2w, is used to define The Voigt parameter, φ (Mittemeijer, 2012):

$$\boldsymbol{\varphi = \frac{2\omega}{\beta}} \tag{3.3}$$

Original and extended Thompson-Cox-Hastings (TCH) pseudo-Voigt formulas were applied for approximating the Voigt profile and calculate the crystallite size (Thompson, 1987; Ida, 2002). For this purpose, in this dissertation, both profiles were applied to FP approach to estimate crystallite size and strain rates, which the strain broadening is calculated by following equation (3.4):

$$\boldsymbol{\varepsilon_0 = \frac{\beta}{4\cos\theta}} \tag{3.4}$$

On the other hand, based on the microstructural broadening assumptions, several analysis methods were developed without referring to a specific microstructural model that can be seen in Table 3.2.

Likewise, Williamson-Hall plot analysis was also applied to approximate information respecting size D and microstrain ε by the equation given below:

$$\beta cos\theta = \frac{0.89\lambda}{D} + 4\varepsilon sin\theta \tag{3.5}$$

Table 3.2 : Summary of basic assumptions made in line-profile decomposition methods and the type of size and strain data obtained (Lucks, 2004).

Method	Assumptions	Size	Strain
Williamson – Hall conventional plot 1949, 1953	Lorentz-shaped peak profiles for size - and strain -broadened profile	Volume-weighted column length	Maximum strain, ε related to local mean-squared strain ε_0^2 for Gaussian strain distributions
Warren–Averbach 1950, 1952	Gaussian strain distribution or small strains	Area-weighted column length	Mean-squared strain $(\varepsilon_L)^2$, related to A^D (L, S_i)
Alternative method 1994	Small strain gradients and broad size distribution	Area-weighted column length	No analytical relation between $(\varepsilon_L)^2$ and the strain Fourier coefficients

A^D (L, S_i) is the strain (''distortion'') Fourier coefficient of a line profile and L is the correlation distance perpendicular to the diffracting planes.

Afterwards, $\boldsymbol{\beta cos\theta}$ versus $\boldsymbol{4sin\theta}$ graph generated for selected diffraction patterns in order to approximate strain and crystallite size. The slope of line(s) was obtained for calculating strain by $\boldsymbol{y = \varepsilon.x + {}^{1}/_{D}}$ and to estimate crystallite size from the y-axis intercept; in other words the plot of $\frac{\beta cos\theta}{\lambda}$ vs $\frac{\sin\theta}{\lambda}$ result in explicit crystallite size and strain rates from the ordinate intersection and the slope of the linear fit of

the experimental points (Prabhu, 2014; Gonzalez 2012). In addition, the Thompson-Cox-Hastings pseudo-Voigt formula was applied for this end, IB, FWHM values were employed to Williamson-Hall plot analysis, and the relation between the crystallite, and particle sizes regarding the different assumptions and methods were tried to be established.

Microstructural characterisations of the powders were conducted using an FEI – Quanta FEG 250 Scanning Electron Microscope (SEM) coupled with an energy-dispersive X-ray spectrometer (EDX) - energy dispersive spectrometer (EDS) and JEOL™ JCM-6000 Benchtop scanning electron microscope (SEM) (Figure 3.7). For SEM analysis of the powders, the specimens of the powders were prepared by following the procedure of dissolving the powders in the ethanol (Merck^{TM}, in purity of 99.9 %), syringing them onto a base plate, drying them in air and coating their surfaces with a thin layer of gold using a Polaron^{TM} SC7620 Sputter Coater to enhance their conductivities. Microstructural and crystallographical investigations were also held at JEOL JEM-ARM200CFEG UHR transmission electron microscope (TEM) as shown in Figure 3.8.

a)  b) 

Figure 3.7 : a) FEI – Quanta FEG 250 and b) JEOL™ JCM-6000 Benchtop scanning electron microscope (SEM).

Figure 3.8 : JEOL JEM-ARM200CFEG UHR transmission electron microscope (TEM).

3.4 Verification

The mechanical properties of the composites can be simulated by a two- or three-dimensional periodic finite-element model considering the gradient in the matrix, while the composite and interfaces are under damage on the uniaxial tensile elastic-plastic behaviour of metal matrix composites (MMCs) consisting of either spherical or cubic particles in random or identical distribution (Weng, 2015). Besides, deriving the mechanical properties of MMCs is strongly correlated with fiber/particle shape and arrangement. With the aim of that, several micromechanical approaches were developed and employed to MMCs using cell models changing with cell model shape (rectangular, square, ellipsoid etc.), particle/fiber shape (sphere, cubic, random) and continuity or discontinuity (Schmauder, 2009). One can said that for all models, the strengthening of a composite depends on reinforcing particle size, particle shape, volume fractions, and interface relations between particle and matrix. Therefore, considering as microscopic structure of materials, representative volume element (RVE) model has become popular and the modeling technique of the microstructural geometry and the size effect of RVE, have been extensively investigated in many studies. Obtaining the distribution of reinforcement particles and volume fractions in order to approximate the grain size and modelling of finite size to reflect the overall material behaviour RVE should be exist in the strict sense (Chen, 2015; Böhm, 2002; Segurado, 2002).

Besides the particle size, which was previously mentioned, grain size is highly effective on the final property of material. However, studies show that the particle dispersion, shape and volume are much related to grain size (Nishizawa, 1997; Kamrani, 2011). This was first proposed by Zener-Smith with following equation (Zener, 1948):

$$\boldsymbol{d_m = \frac{4\alpha d_p}{3v_p}} \tag{3.6}$$

where d_m is the grain size, α is the proportional constant which can be assumed as 1, and Vp is the volume fraction of particle reinforcement. Because of this reason, it is essential to determine the smallest particle size and fine fraction ratio in order to make assumptions for the final material properties.

MA'ed powders were leached to solve ductile matrix in order to verify nano-sized carbide particles. To this respect, concentrated H_2SO_4 for Cu and Ni, concentrated HCl for Fe were applied for dissolution of mentioned metals. The solutions were put onto magnetic stirrer for 24 hours at the room temperature (24°C) under the oxygen atmosphere according to stabilize following equations (Pierson, 1992; Lascelles, 2005; Ebbing, 1990):

$$2Cu_{(s)} + 2H_2SO_{4(aq)} + O_2 + 8H_2O_{(aq)} \rightarrow 2CuSO_4.5H_2O_{(aq)} \quad (3.7)$$

$$2Fe_{(s)} + 6HCl_{(aq)} \rightarrow 2FeCl_{(aq)} + 3H_{2(aq)}$$

(3.8)

$$Ni_{(s)} + H_2SO_{4(aq)} \rightarrow NiSO_{4(aq)} + H_2 \quad (3.9)$$

Finally, the solutions were filtered through nano porous membrane and then, nanostructured powders were dried in the Heraeus™ drying-oven (Figure3.9). Apparent densities were measured by pycnometer machine. Zeta potentials and particle size distribution (PSD) were measured in Nano Flex and Stabino machine.

Figure 3.9 : Heraeus™ drying oven.

4. RESULTS AND DISCUSSION

4.1 Initial Powder Characterizations

Initial powder densities were measured as given in Table 4.1. The measured values corresponds the literature density values

Table 4.1 : Theoretical and true densities of initial powders.

Sample Name	Theoretical Density (g/cm^3)	True Density (g/cm^3)
Cu	8.96	8.89
Fe	7.87	7.80
Ni	8.90	8.90
TaC	14.30 – 14.65	14.38
VC	5.77	5.75
WC	15.60	15.63

Particle size and distribution of initial powders are illustrated in the Figure 4.1.

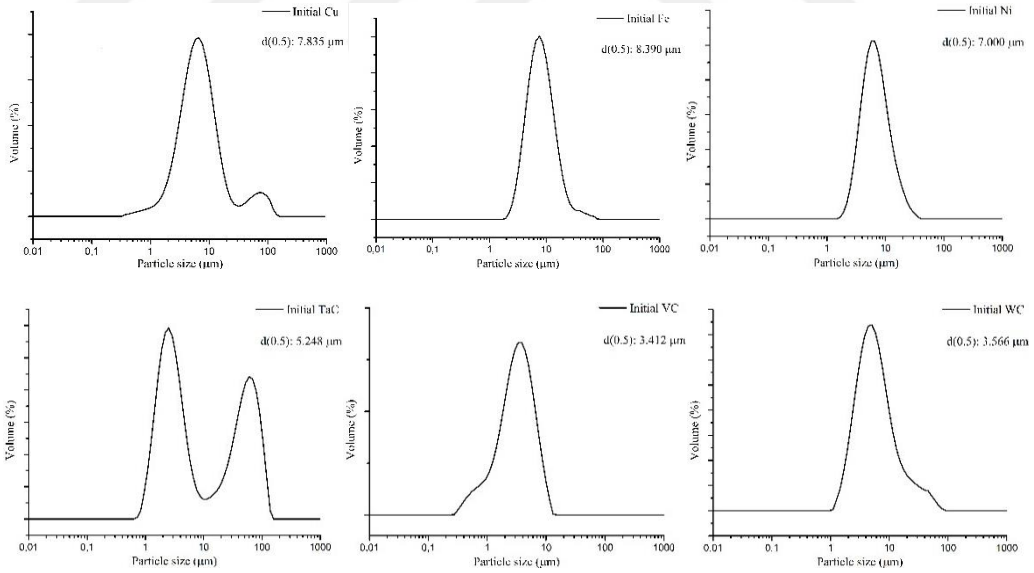

Figure 4.1 : PSD of initial powders.

According to particle size measurements, D50 mean sizes were found for Cu, Fe, Ni, TaC, VC and WC as 7.83 µm, 8.39 µm, 7.00 µm, 5.24 µm, 3.41 µm and 3.56 µm, respectively.

The X-ray diffraction patterns of initial powders were drawn as seen in Figure 4.2.

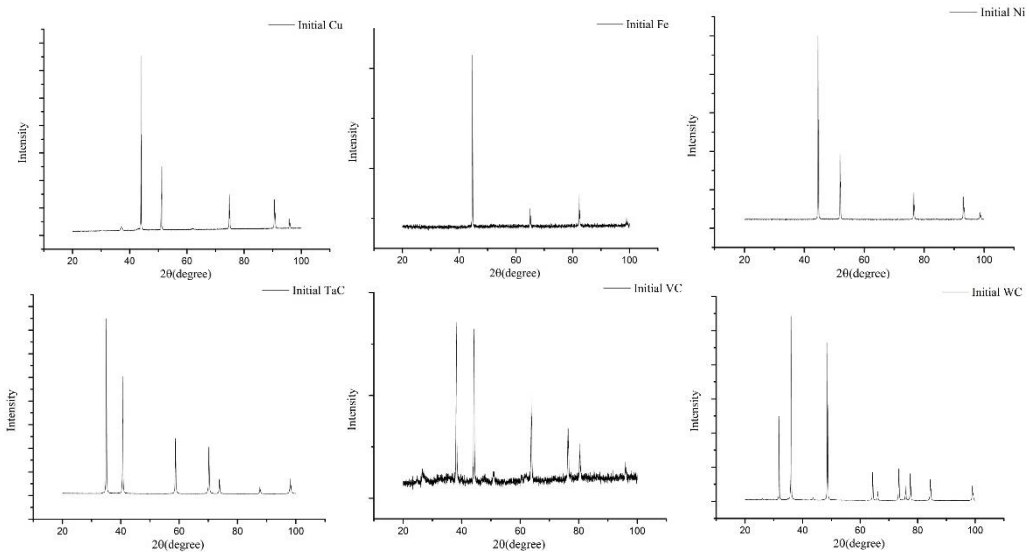

Figure 4.2 : XRD graphs of initial powders.

All peaks fit for the characteristic positions of materials. The strongest peak, its d-spacing, $2\theta^o$ position and lattice parameter of Cu (ICDD No: 065-9743), Fe (ICDD No: 065-4899), Ni (ICDD No: 065-2865), TaC (ICDD No: 065-7114), VC (ICDD No: 065-8074) and WC (ICDD No: 065-4539) powders are given in Table 4.2.

Table 4.2 : Crystallite size and strain rates of Cu25TaC, Cu25VC and Cu25WC powders against MA time.

	Cu	Fe	Ni	TaC	VC	WC
Lattice type	FCC	BCC	FCC	FCC	FCC	Hexagonal
Lattice parameters (nm)	a: 0.3607	a: 0.2867	a: 0.3523	a: 0.4449	a: 0.4164	a: 0.2900 c: 0.2831
Strongest pea	(111)	(110)	(111)	(111)	(200)	(100)
Strongest peak $2\theta^o$	43.459	44.663	44.619	35.028	43.417	35.750
d-spacing of strongest peak (nm)	0.2083	0.2027	0.2034	0.2568	0.2082	0.2511

4.2 Fragmentation Behaviour of Brittle Phase in Cu Matrix

The X-ray patterns of Cu25TaC, Cu25VC and Cu25WC powders after 2, 4 and 8 hours MA time were illustrated in Figure 4.3.

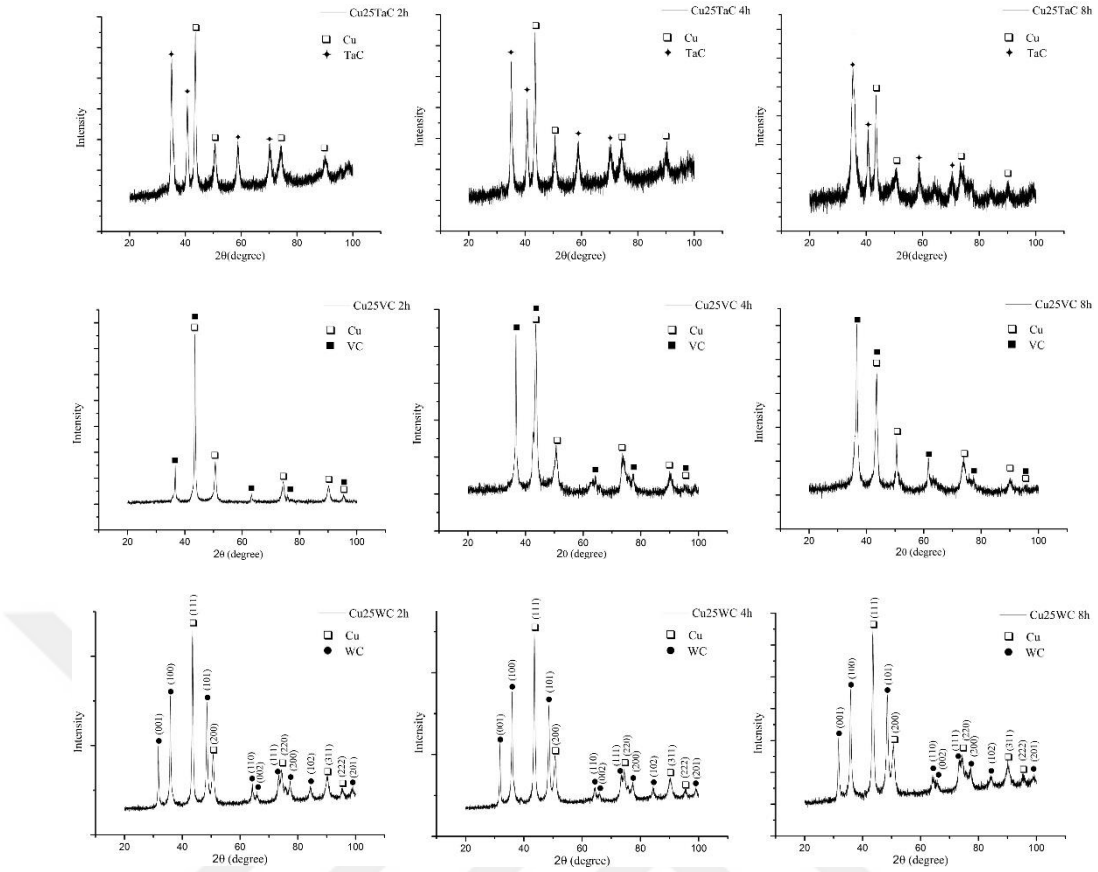

Figure 4.3 : XRD graphs of Cu25TaC, Cu25VC and Cu25WC against MA time.

There is not any contamination observed for three powder compositions. All peaks were obtained as belong to Cu, TaC, VC and WC phases, separately. Also there was not any compound constituted between two phases Cu - WC, Cu - VC and Cu – WC according to XRD analysis. Considering the intensities of carbides in Cu matrix, it was seen that VC peak intensities increased dramatically depending on MA time. On the contrary to VC peaks behaviour, very few increase in WC peak intensity was seen, where the peaks were broadened due to MA. Particularly, TaC peaks broadened and the noise level seemed to be high comparing to VC and WC. This was concluded as a consequence of crystal lattice distortion (micro-strain) due to dislocations, structural faults or concentration gradients in non-stoichiometric compound. It is also known that the smaller the particle the broad the diffraction peaks. In addition, the reduction of the intensity and the increase of full width at half maximum (FWHM) of the diffraction peaks with increasing milling time can be aspect to the increasing lattice strain and grain size reduction. This can be considered as a common behaviour to high-energy ball milled powders. Crystallite size and strain rates with the lattice

parameter and d-spacings of strongest peaks of composite powders belong to Cu phase are given in Table 4.3.

Table 4.3 : Crystallite size and strain rates of Cu25TaC, Cu25VC and Cu25WC powders against MA time.

Sample	MA time (h)	FPA		Williamson-Hall		Lattice parameter (nm)	d-spacings (nm)
		D, nm	ε, %	D, nm	ε, %		
Cu25TaC	0						
	2	15.87	0.61	12.89	0.56	0.3694	0.2076
	4	15.15	0.69	9.20	0.98	0.3684	0.2079
	8	21.50	0.90	12.82	0.78	0.3700	0.2080
	annealed	65.1	0.60				
Cu25VC	0						
	2	19.85	0.86	17.46	0.22	0.3700	0.2079
	4	22.90	1.53	10.11	0.36	0.3700	0.2077
	8	10.10	1.21	13.47	0.32	0.3623	0.2078
	annealed	100.9	0.58				
Cu25WC	0	141.3	0.14				
	2	29.63	0.50	22.44	0.49	0.3502	0.2076
	4	29.43	0.94	20.13	0.90	0.3606	0.2075
	8	16.99	1.39	14.63	1.31	0.3699	0.2077
	annealed	19.73	0.81				

Among all composite powders, minimum crystallite size was found in those 8 h MA'ed powders. FPA calculations and Williamson – Hall plot analysis show that the crystallite size decrease by increasing milling time as the same situation happens to particle size. However, strain rates inversely correlated to crystallite size as it was expected. After annealing the strain due to lattice distortion relieved. Marques (2007) reported that Cu crystallite size reaches a stable value below 30 nm with the presence of 20 wt. % WC only after 32 h of milling in planetary ball mill that was operated at a rotating speed of 400 rpm (Marques, 2007). The similar trend was observed for Yusoff's study (Yusoff, 2011), where Cu-W-C MA'ed in order to fabricate ex-situ composite powder with the final composition Cu-30 vol. % WC (approx. 42.7 wt. % WC), Cu crystallite size becomes under 30 nm barely after 60 h milling in a planetary ball mill with 400 rpm rotary speed. On the other hand, with the addition of 5 vol. % TaC crystallite size was found around 50 nm for 10, 20, 30 hours milling at 500 rpm using an Attritor mill via in situ generation of tantalum carbide (TaC) nanodispersoids in a Cu matrix (Manotas-Albor, 2014).

Lattice parameter of Cu changed significantly as seen in Table 4.3 for all powder mixes. In particular with WC presence, it was considered that Cu crystal was under tensile loadings extremely which can be seen as continuously increase in lattice

parameter. However, both values d-spacings and lattice parameter of Cu25TaC powders were also obtained as increasing and close to linear. Of these phenomena can be supported by Williamson – Hall plot analysis by illustrating in Figure 4.4.

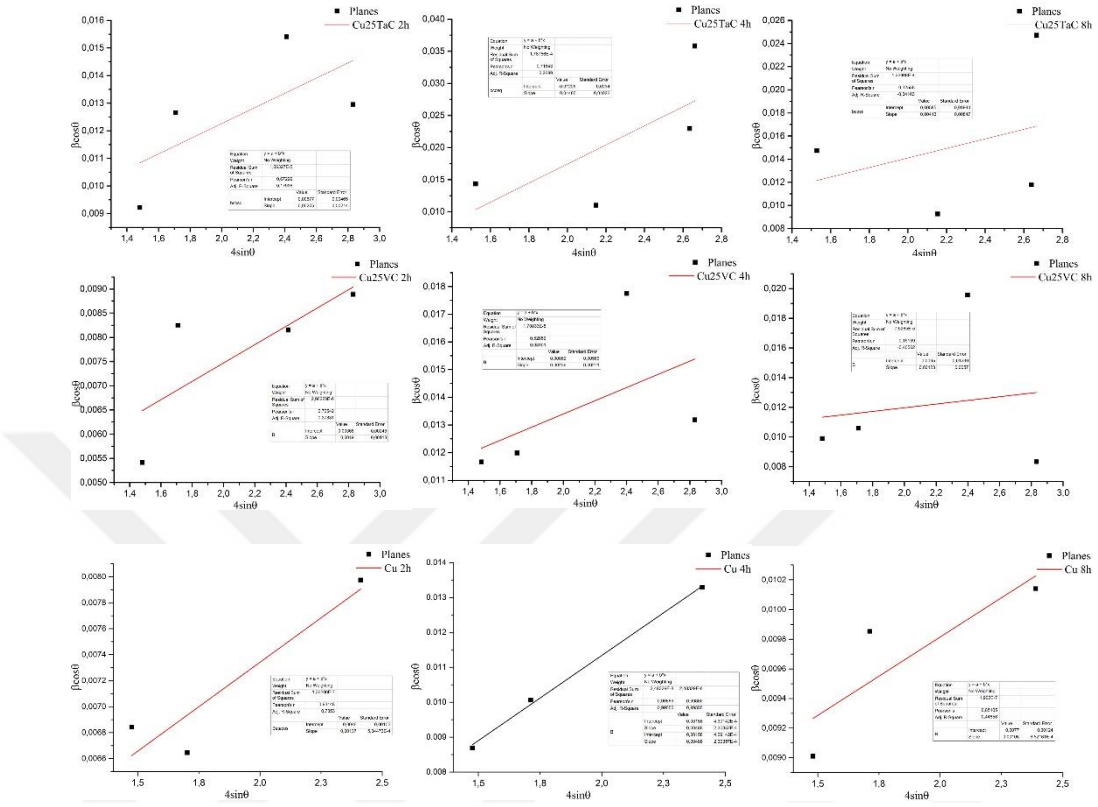

Figure 4.4 : Williamson – Hall plot analysis of Cu based composite powders.

The change and distortion of crystal lattice of Cu by changing carbide type and MA time can also be revealed by determining of Cu strongest peak position that is presented in Figure 4.3 and Table 4.4.

As seen from the table, 2-theta position of Cu (111) shifted lower angles by the TaC existence, where it shifted to higher angles in the presence of VC and WC. However, 2-theta position of VC and WC reinforced Cu (111) shifted alternately with continuous milling. As also seen from the Figure 4.5 and considering the determination of Cu (111) positions, it can be said that TaC affected Cu lattice to shift on the same direction which can be clearly seen as decreasing slope at Williamson – Hall plot analysis (Figure 4.4). On the contrary to TaC, WC and VC presence between two loading types: compressive and tensile in which one was thought to be more effective than the other one against MA time. On the other hand, one can say that the effect of MA time on the intensity of Cu (111) plane is stronger

than the other by the presence of VC. This can be related to the density of carbide that causes to be high in volume percentage.

Table 4.4 : Change in position of Cu (111) due to carbide type against MA time.

Plane	MA time (h)	Change in position, 2θ (degree)		
		Cu25TaC	Cu25VC	Cu25WC
Cu (111)	2	0.1956	0.0644	0.1864
	4	0.0345	0.1818	0.2807
	8	-0.0069	0.1312	0.1427

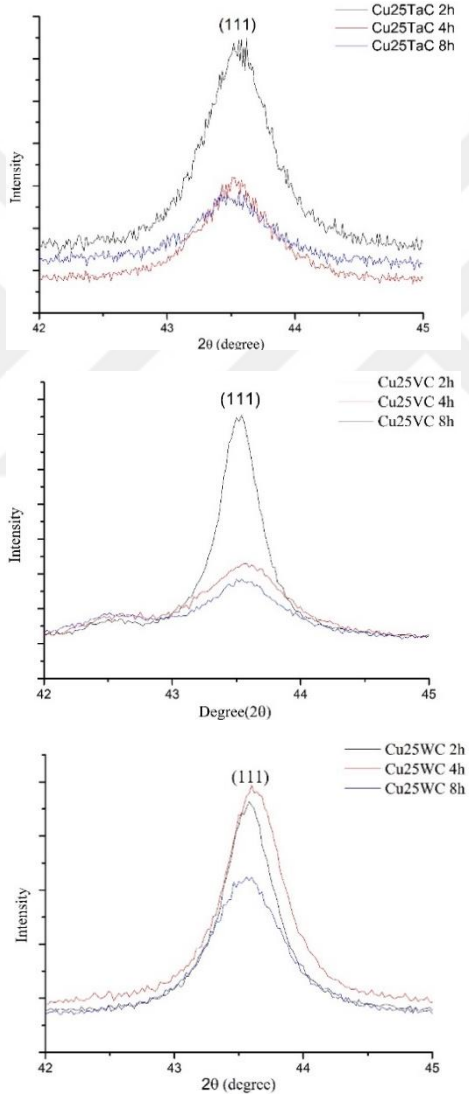

Figure 4.5 : Peak shiftings of Cu (111) due to carbide type against MA time.

Particle size and distribution of Cu25TaC, Cu25VC and Cu25WC powders against MA time is given in Figure 4.6.

a)

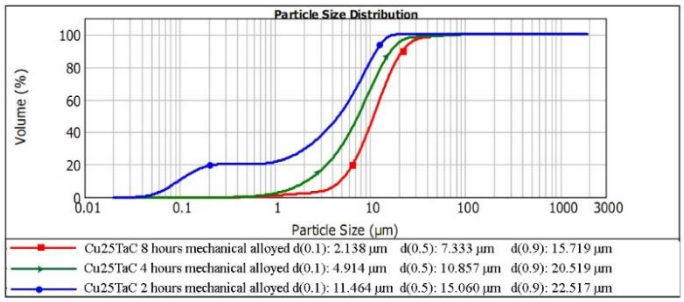

b)

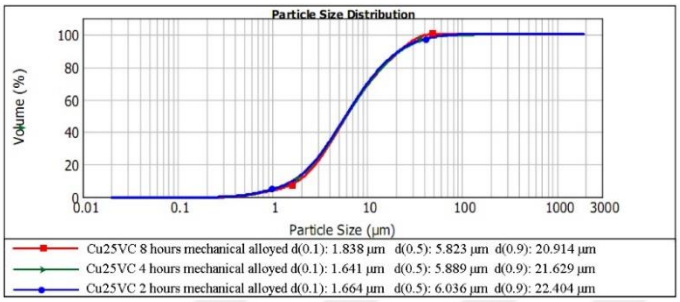

c)

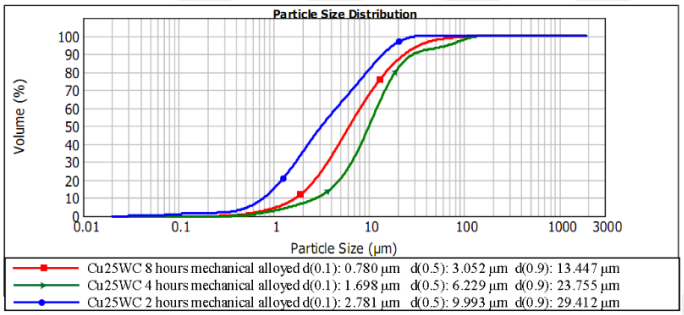

Figure 4.6 : PSD of MA'ed a) Cu25TaC, b) Cu25VC and c) Cu25WC powders.

As it is clearly seen from the cumulative particle size graphs of the powders, mean particle size has dramatically shifted to the right, which indicates the decrease to the submicron scales for Cu25TaC and Cu25WC. The size of the particles was decreased with increasing milling time of TaC and WC within ductile Cu matrix. However, Cu25VC particle size and distribution seem to be more homogeneous and less changed due to MA time. Nano fractions of powders were also measured against time. Minimum and average particle size of nano fractions were detected as given in Table 4.5 with the zeta potential values.

The apparent densities of powders seem to be changed very slightly, which provides information on the flowability of powders (Table 4.6). As it was expected decrease in the particle size results in the increase in the apparent density. Within this context, true densities decreased against MA time. It was thought that this occurred because of high deformation rates. Similar true density values were obtained after annealing.

These results prove that the suitable process was applied without oxidation or with negligible contamination rates.

Table 4.5 : PSD of nano fractions and zeta potential values against MA time.

Sample	MA time (h)	D50 (nm)	Minimum Particle Size (nm)	Zeta Potential (mV)
Cu25TaC	2	369	109	-43.0
	4	387	253	-40.6
	8	253.3	199.3	-43.2
Cu25VC	2	1190	297.9	-66.2
	4	660	302.3	-64.2
	8	425	223	-66.1
Cu25WC	2	934	515.2	-60.8
	4	876	199.1	-56.4
	8	236.4	93.49	-53.3
Leached Cu25WC	8	158.3	52.73	-62.9

Table 4.6 : Density values of composite powders against MA time.

Sample	MA time (h)	Theoretical density (g/cm^3)	Apparent density (g/cm^3)	True density (g/cm^3)	Green density (g/cm^3)
Cu25TaC	2	9.88	3.93	9.70	6.39
	4		3.71	9.58	6.22
	8		2.72	9.29	5.82
	annealed		-	9.32	6.28
Cu25VC	2	8.16	1.55	6.85	4.63
	4		1.52	6.81	4.25
	8		1.27	6.22	4.19
	annealed		-	6.20	4.80
Cu25WC	2	10.02	4.80	9.79	6.67
	4		4.79	9.75	6.47
	8		4.63	8.86	6.18
	annealed		-	8.86	6.22

The SEM micrographs of powders by increasing milling time were given in Figure 4.7.

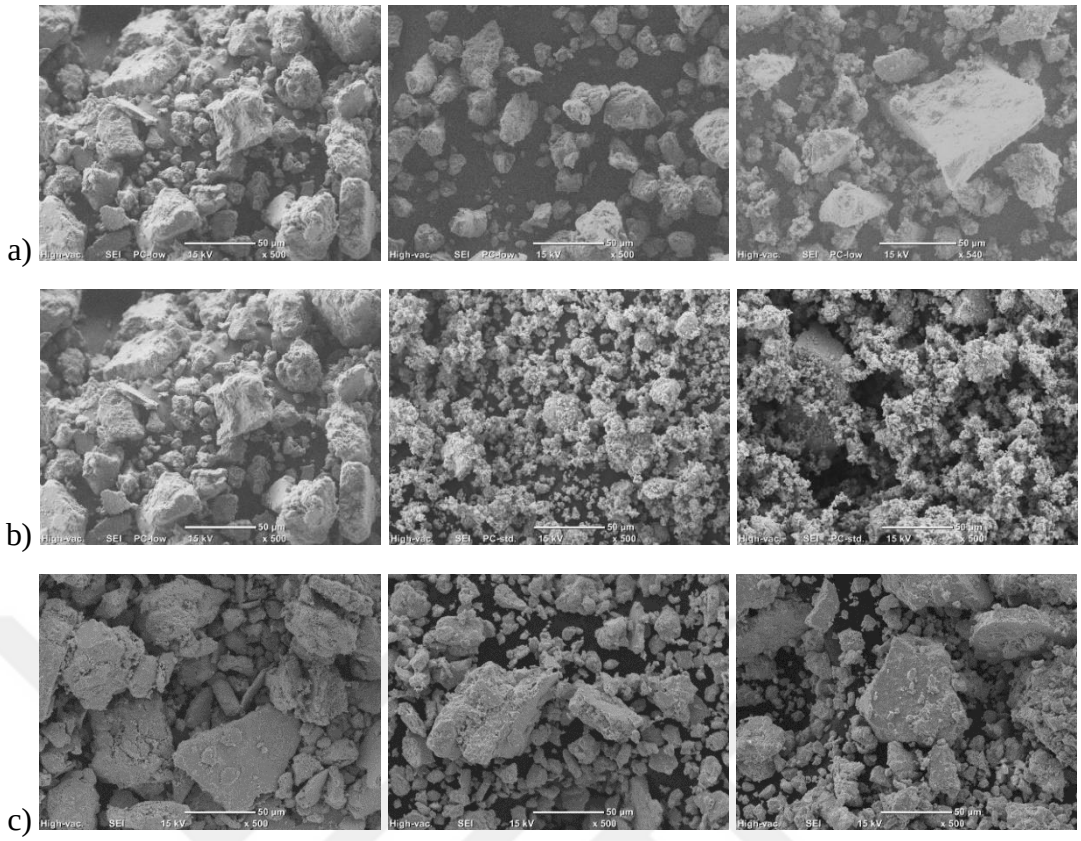

Figure 4.7 : SEM photos of a) Cu25TaC, b) Cu25VC and c) Cu25WC for 2, 4 and 8h MA time from left to right, respectively.

Particle behaviours during MA can be clearly observed from SEIs. Fractures and disintegrations occurred for three compositions. Brittle phase is quietly well distributed in the ductile matrix. However, VC particles seemed to be dispersed in everywhere as a consequence of low density that leads to high volume constitution compared to TaC and WC. Large single ductile particles did not fracture, but deformed and thus formed with little change. Those ductile particles seemed to be deformed and changed into a flake shape after 8h MA time for Cu25TaC and Cu25WC particularly (Figure 4.7a and c). Small, fine particles that instituted by fracturing and ruptured from brittle particles were easily distinguished by BEI of Cu25WC (Figure 4.8). Owing to density difference, BEI provided the contrast/brightness distinction that allows distinguishing carbide particles. As seen from the Figure 4.8, fine particles were obtained after 8h MA time and they observed as embedded onto larger particles.

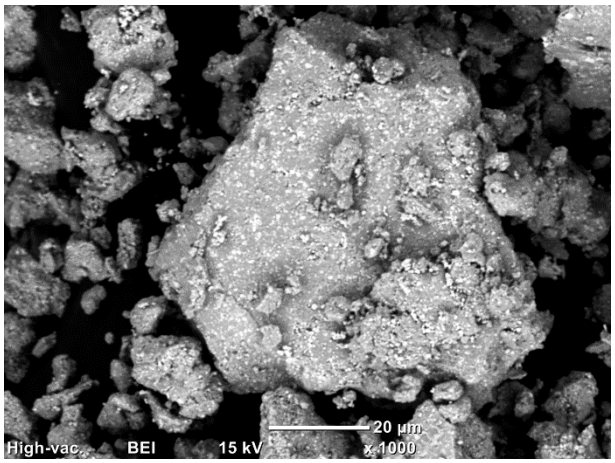

Figure 4.8 : SEM photos of Cu25WC after 8h MA time (BEI x1000).

At higher magnifications, the engagement of both phases were noticeably observed in Figure 4.9. It was considered that small particles belong to WC have cold-welded to Cu particles thereby composing hard-core solid solution.

a) 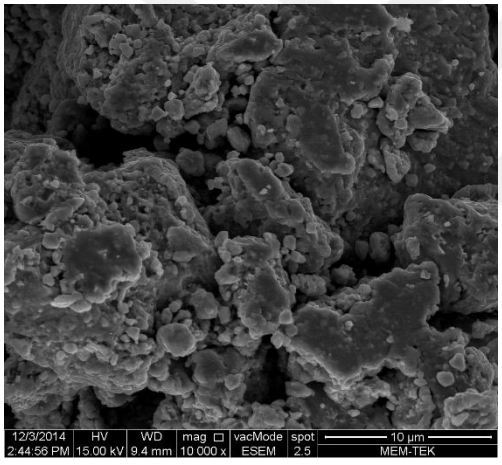

b) 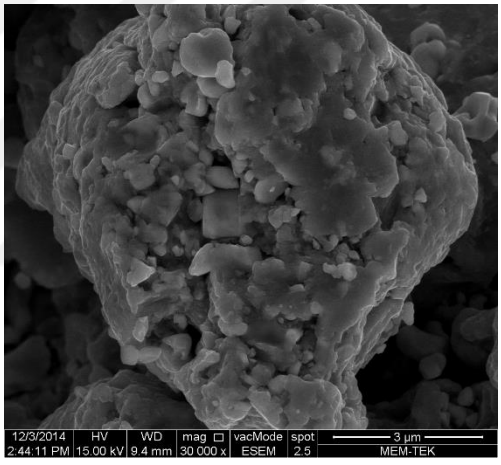

Figure 4.9 : SEM photos of Cu25WC after 8h MA time at high magnifications a) x10000 and b) x30000.

However, as seen from the Figure 4.9, the stage of on-going welding and fracturing mechanism has continued even after 8 hours milling time. It was noted that the same situation occurred in particular with Cu-TaC powder mixture in contradiction to Cu-VC fragmentation behaviour (Figure 4.10). As seen from the figure, the same phenomenon of WC is effectual to TaC. On the other hand, despite the on-going fracture of Cu particles of Cu25VC composite powders, VC particles were in agglomerated form, which was also accordance with particle size and distribution measurements.

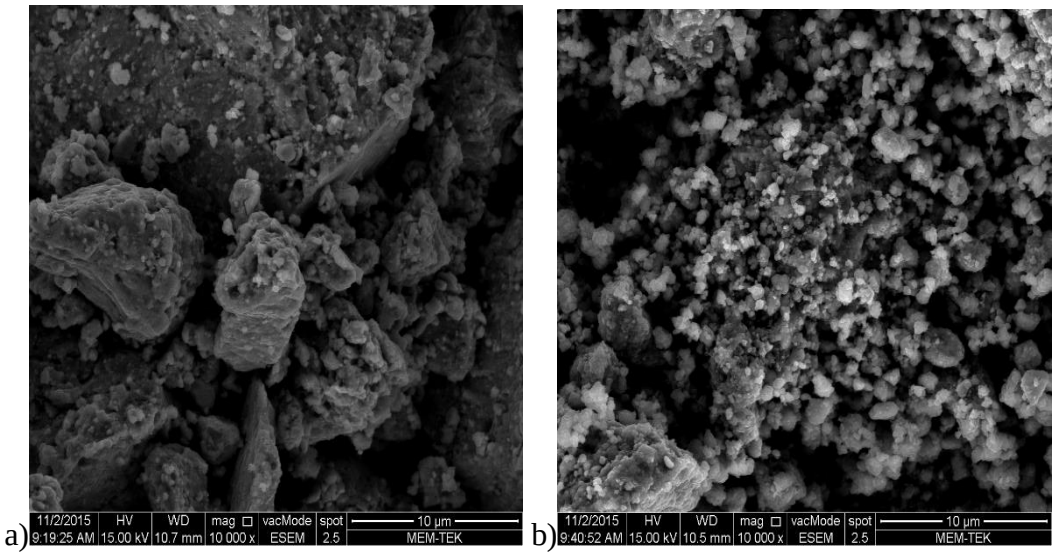

Figure 4.10 : SEM photos of a) Cu25TaC and b) Cu25VC after 8h MA time at high magnification x10000.

The EDS maps for three powder mixtures displayed homogeneous distribution of each phases (Figure 4.11). Particularly, being lighter than TaC and WC, VC particles were well-distributed than the others which is also promoted by PSD measurements.

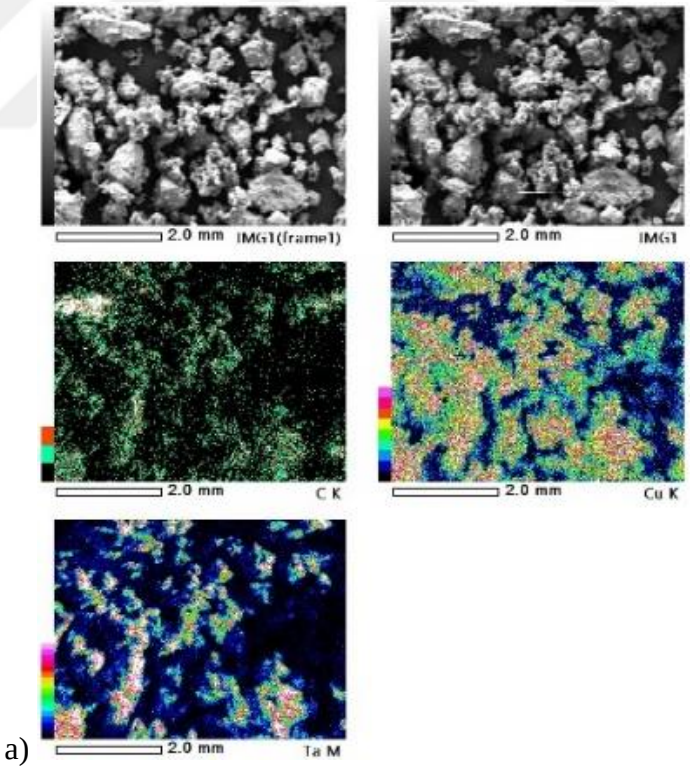

a)

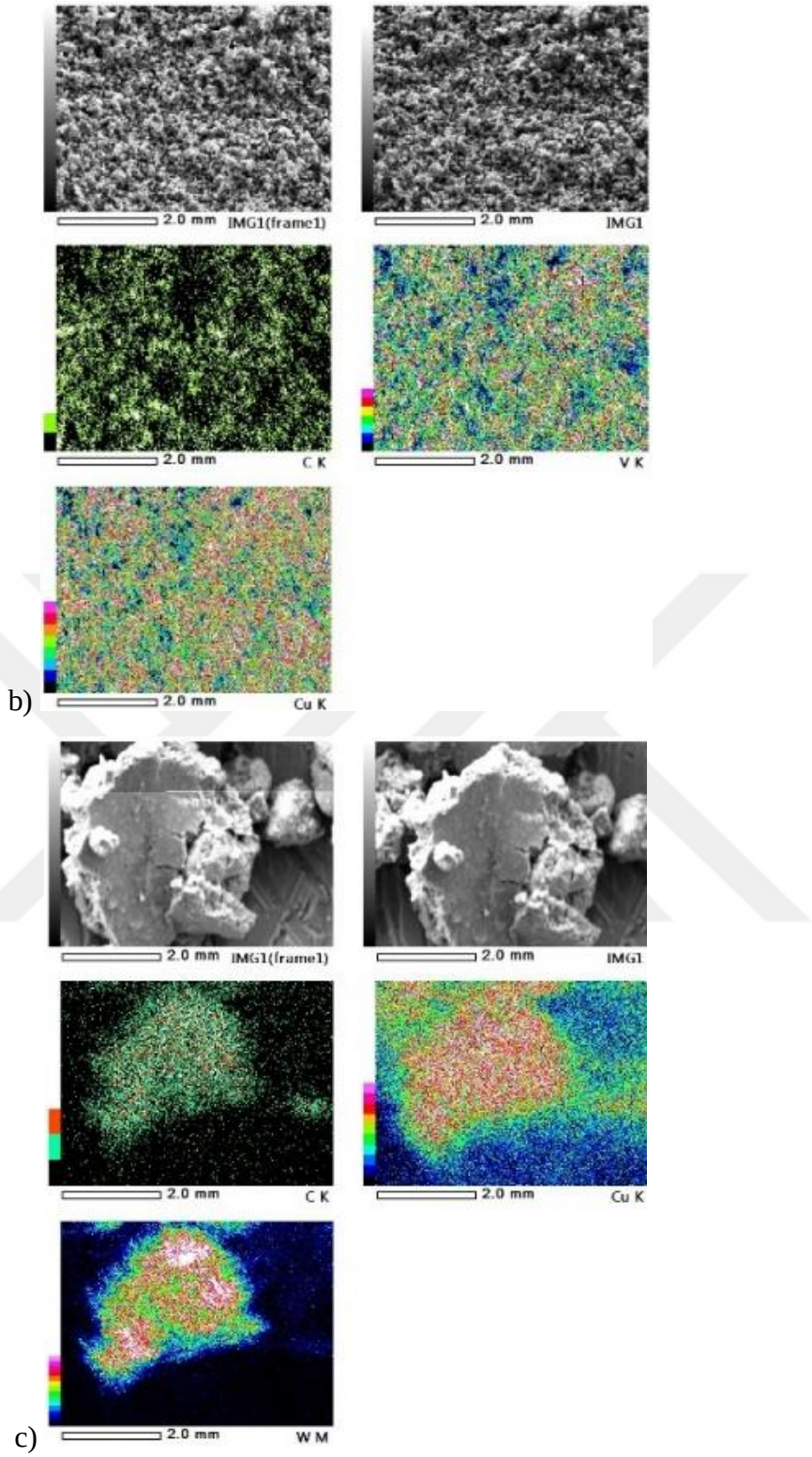

Figure 4.11 : EDS maps of 8h MA'ed a) Cu25TaC, b) Cu25VC and c) Cu25WC powders.

4.3 Fragmentation Behaviour of Brittle Phase in Fe Matrix

As stated in Table 4.7, true densities were measured lower than theoretical calculations for all compositions. The true density values decreased by increasing milling time, which was expected as the nature of imperfection regulated by MA. Almost for all cases, green density values increased after heat treatment. The internal stresses must be revealed by the heat treatment, which is compatible with strain calculations of domains/crystallites of particles. The change in apparent densities calculated for WC reinforced powders was obtained in higher rate than TaC and VC reinforced ones. This was concluded because of high hardness and elastic modulus that effects the fragmentation of particles.

Table 4.7 : Density values of composite powders against MA time.

Sample	Mechanical alloying time (h)	Theoretical density (g/cm^3)	Apparent density (g/cm^3)	True density (g/cm^3)	Green density (g/cm^3)
Fe25TaC	2	9.53	2.72	8.80	5.24
	4		2.56	8.51	4.94
	8		2.43	7.37	4.55
	annealed			8.37	5.14
Fe25VC	2	7.34	1.68	6.68	6.47
	4		1.40	6.46	6.18
	8		1.27	6.29	6.67
	annealed			6.36	6.72
Fe25WC	2	9.80	3.37	9.42	5.08
	4		3.36	8.65	5.24
	8		3.33	8.82	5.34
	annealed			8.84	5.38

Density values of the powders were shown in Table 4.7. True densities were expected to be obtained lower that theoretical density values after introducing the deformation. The misorientations, fractures and ruptures for all three compositions and MA durations, except Fe25WC 8h MA'ed powders, were in progress. However, the same phenomena happened to Cu based composite powders without any exception. It was also noted that Cu based composite powders' apparent densities inclined by increasing MA time, while Fe based ones' were alternating. This was thought to be a result of lattice type and Young's modulus effect that creates resistance to plastic deformation. Besides the thermal conductivity of Cu is higher than Fe which is also operative on MA behaviour of particles. The phase analysis was conducted by X-ray characterization technique and explained by graph as given in Figure 4.12.

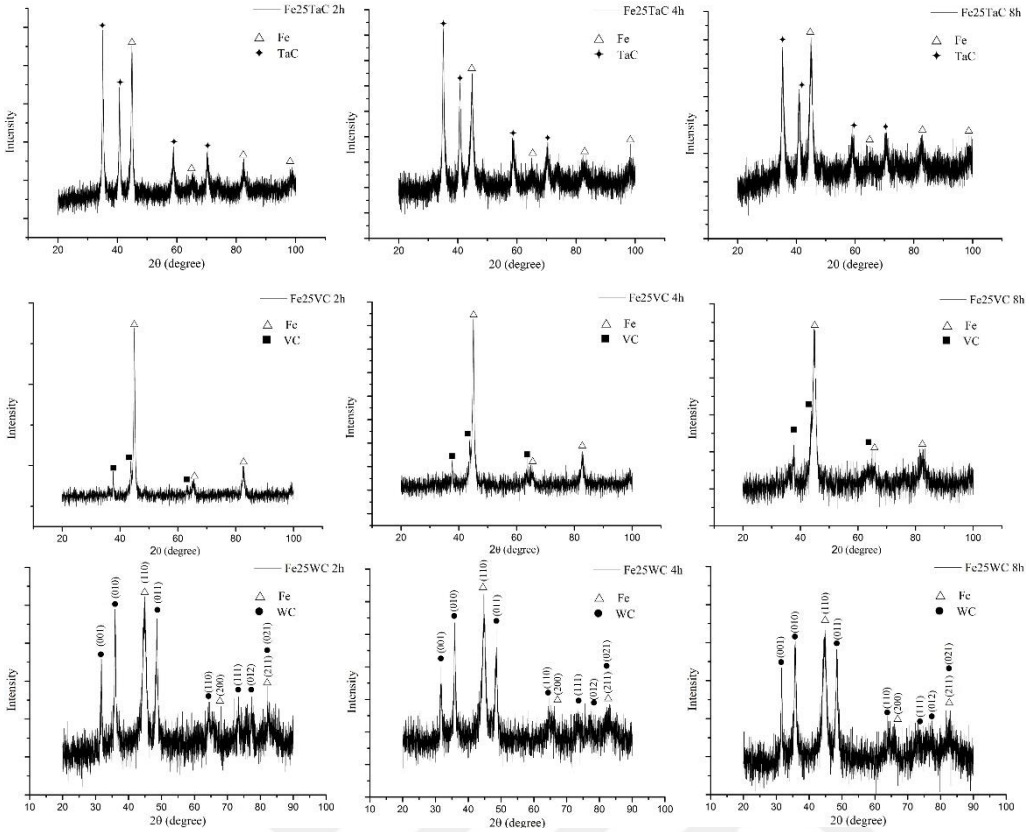

Figure 4.12 : Diffraction patterns of Fe25TaC, Fe25VC and Fe25WC powders against MA time.

All the peaks were found as belong to Fe, TaC, VC and WC phases. No any contamination was observed. Peak intensities of TaC in Fe matrix decreased after 4h MA which is compatible with true density measurements. Fe25TaC and Fe25WC powders peaks were also broadened comparing to Fe25VC peaks for the same milling duration as seen from the Figure 4.12. VC peak intensities increased by increasing milling time that can be considered as the homogeneous mixture on the contrary to TaC and WC peaks. They both broadened and their peak intensities increased owing to continuous milling time. The crystallite sizes of composite powders decreased by increasing milling time, and as it was expected all strain rates increased that can be a proof of the peak broadening, which was assumed to be result of microstresses, coherency strains and crystallite smallness that was also measured and calculated as given in Table 4.8. However, the lattice parameter of Fe did not alter by milling time but it has exhibited a fixed parameter even with increasing milling time. This can be due to highest level of crystal deformation for this milling time. D-spacings of Fe planes have also change a little.

Table 4.8 : Crystallite size and strain rates of Fe25TaC, Fe25VC and Fe25WC powders against MA time.

Sample	MA time (h)	FPA		Williamson-Hall		Lattice parameter (nm)	d-spacings (nm)
		D, nm	ε, %	D, nm	ε, %		
Fe25TaC	0						
	2	20.03	0.19	20.53	0.14	0.2860	0.2018
	4	13.30	1.72	8.75	1.40	0.2860	0.2021
	8	14.90	1.58	9.55	1.29	0.2860	0.2015
	annealed	63.6	0.33				
Fe25VC	0						
	2	20.03	0.81	14.66	0.17	0.2860	0.2016
	4	14.10	1.50	7.13	0.21	0.2860	0.2012
	8	15.90	1.27	9.23	0.38	0.2860	0.2016
	annealed	40.5	0.23				
Fe25WC	0	108.2	0.12				
	2	13.35	0.48	13.22	0.26	0.2860	0.2019
	4	10.00	0.81	10.23	0.44	0.2860	0.2019
	8	7.60	1.23	8.86	1.25	0.2860	0.2025
	annealed	92.9	0.27				

The Williamson – Hall analysis was also employed to calculate crystallite size and provide information and peak profile analysis to support particle behaviour during MA (Figure 4.13).

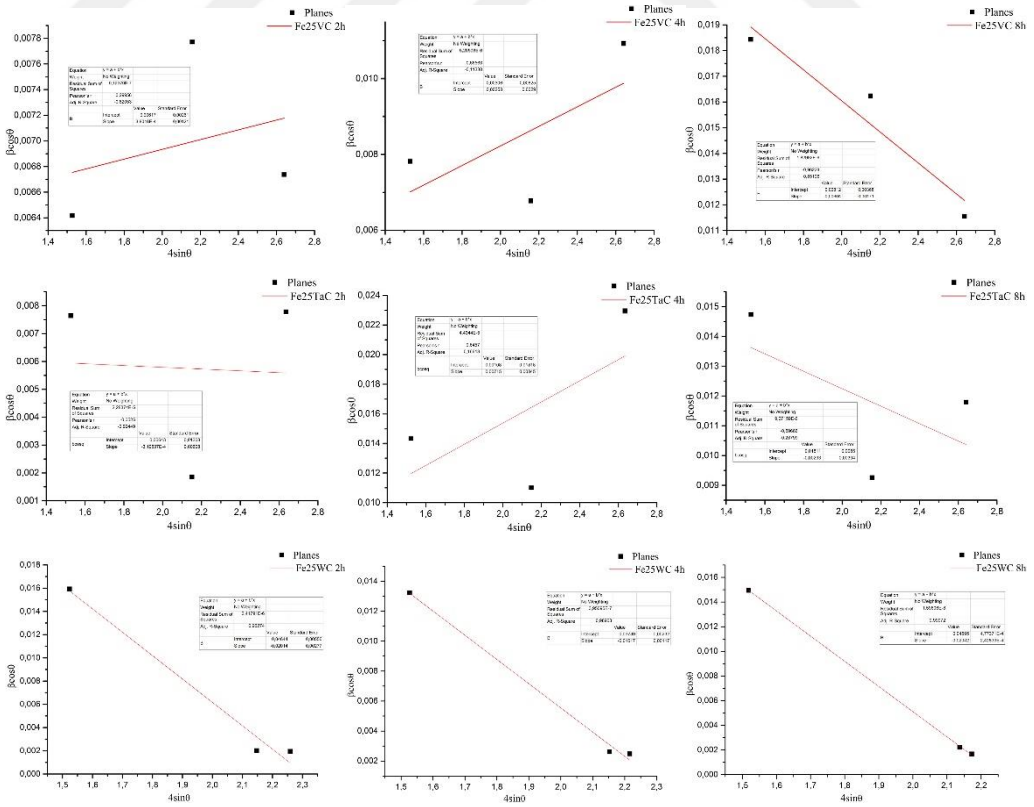

Figure 4.13 : Williamson – Hall plot analysis of Fe based composite powders.

Williamson – Hall crystallite sizes were determined in convolution with TOPAS software results. The change in sizes was obtained very much similar in the trend of the true density decreasing. Correlation between the crystallite size and the density can be understood from results: the smaller the crystallite size, the lower the density. The W – H graphs also revealed the mechanism of plastic deformation of crystals in where negative slope indicates compressive loading that its strain broadening must be very small and negative slope indicates tensile loadings that it has not reached minimum contribution of strains. Slopes and changes in crystallite size were found agreeable within each other. Kumar et al. reported that Fe crystallite size reaches around 12 nm after 20 h of MA by the addition of Cr and Al with 250 rpm rotary speed (Kumar, 2016). The interesting study of Tung and his colleagues was revealed that Fe nanoparticles can be fabricated by high-energy ball milling with the speed of 450 rpm and crystallite size can be obtained 10 nm after 16 h (Tung, 2016). In the presence of MnO, Fe crystallite size was obtained under 30 nm after 20h milling (Pati, 2014). Kirino and his colleagues has showed that in-situ generated TaC crystals can be obtained about 5 nm size prepared by sputtering (Kirino, 1996). On the other hand, VC crystallite size was found in the range of 10-30 nm in the Lomeava's study which was focused the production of Fe–VC–Fe_3C nanocomposites via mechanical synthesis at planetary mill (Lomeava, 2012).

Fe peak intensities seemed to be changed slightly and broadened by increasing milling time. However, all peaks belong to Fe (110) plane shifted to the same direction. The change in 2θ positions were illustrated in Figure 4.14. Peak belonging to (110) of Fe were shifted to the same direction comparing to initial places (Table 4.9). It was concluded that these attitudes appeared as a result of distortion and misorientation in lattice of Fe and Ni owing to tensile and compressive loadings occurred by mechanical alloying.

Table 4.9 : Change in position of Fe (110) due to carbide type against MA time.

Plane	MA time (h)	Change in position, 2θ (degree)		
		Fe25TaC	Fe25VC	Fe25WC
Fe (110)	2	0.4791	0.5866	0.4344
	4	0.2821	0.7568	0.4030
	8	0.6000	0.5642	0.0896

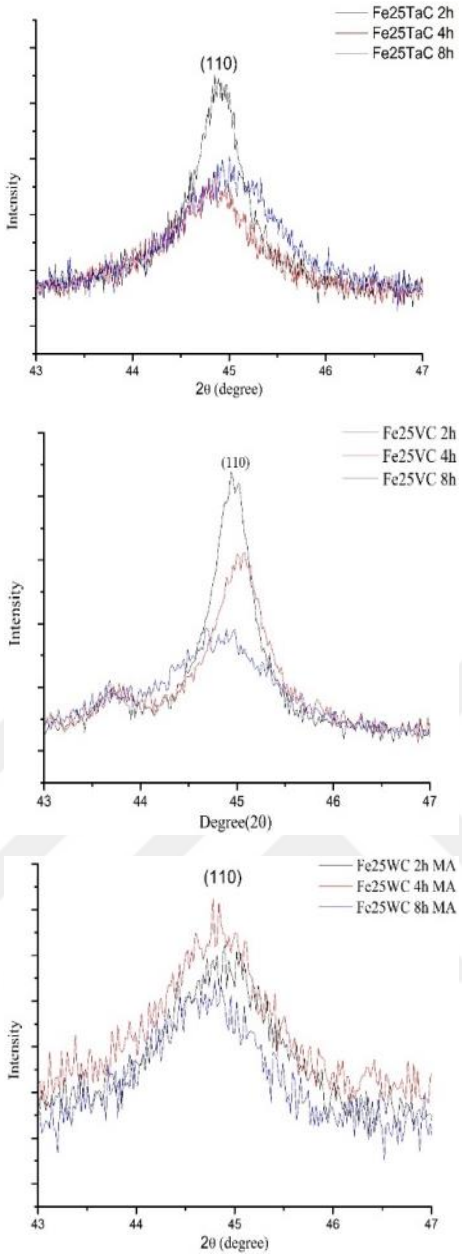

Figure 4.14 : Peak shiftings of Fe (110) due to carbide type against MA time.

On the contrary to Cu matrix, 2-theta position of Fe (110) changed alternately towards to higher angles by the presence of TaC and VC. With the existence of WC, 2-theta position of Fe (110) plane first increased, but with continuous milling, peak belongs to Fe (110) decreased and approximately returned to initial position. The Williamson-Hall plot analysis is in good agreement with the change of Cu (111) plane with various carbide type. The situation of peak shifting was completely reversed comparing to Cu. One cause for the difference of these peak shiftings was thought to be nature of lattice type, which was related to slip systems, for Cu as FCC and for Fe as BCC. Besides surface relaxation/compression can be one of the reason.

This alternation of TaC reinforced powders can also be related to difference between elastic modulus of carbides that provides resistivity to plastic deformation.

Particle size and distribution of Fe25TaC, Fe25VC and Fe25WC powders against MA time are given in Figure 4.15. Nano particle size and zeta potential measurements can be followed in Table 4.10.

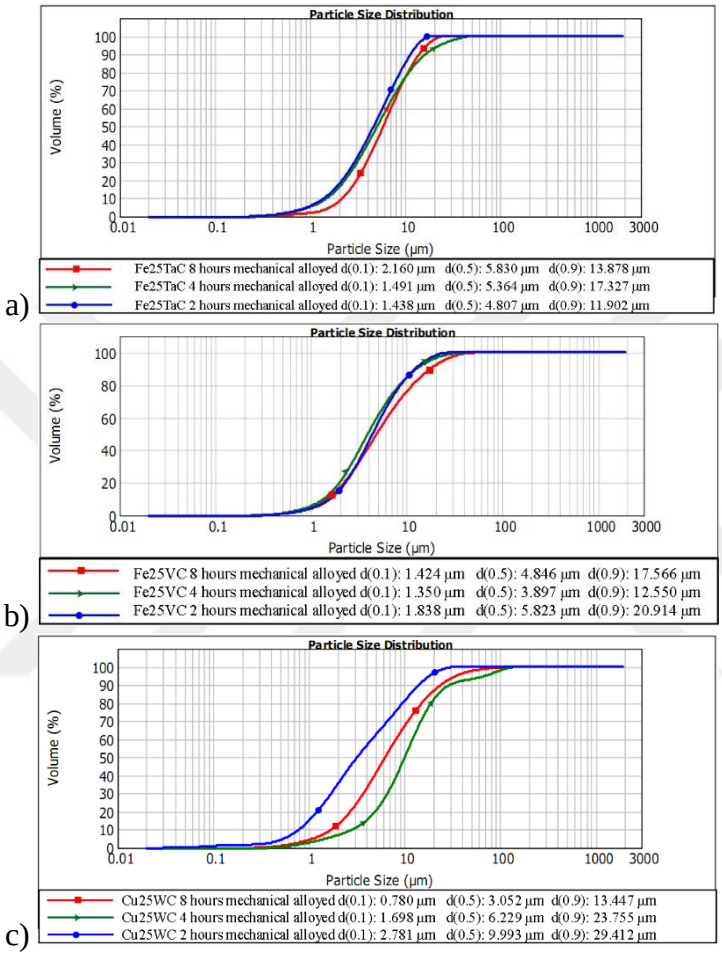

Figure 4.15 : PSD of Fe25TaC, Fe25VC and Fe25WC powders against MA time.

Change in D50 value of Fe based composite powders exhibit similar trend. However, the particle size of Fe25TaC powders decreased by MA duration, while Fe25VC powders demonstrate fluctuant behaviour. Particle sizes did not change by a wide margin. In addition, the cumulative graphs indicated that the fine fractions came into existence by on-going MA.

Table 4.10 : PSD of nano fractions and zeta potential values against MA time.

Sample	MA time (h)	D50 (nm)	Minimum Particle Size (nm)	Zeta Potential (mV)
Fe25TaC	2	394	116.5	-41.6
	4	324	190.8	-42.0
	8	212.8	145	-41.2
Fe25VC	2	934	376.2	-60.1
	4	876	153	-65.5
	8	236.4	109.7	-62.0
Fe25WC	2	489	182.5	-56.8
	4	391	183	-57.9
	8	270.2	117	-50.5
Leached Fe25WC	8	173.7	80.52	-59.6

Figure 4.16 shows SEM images of Fe25TaC, Fe25VC and Fe25WC composite powders after mechanical alloying for 2, 4 and 8 hours.

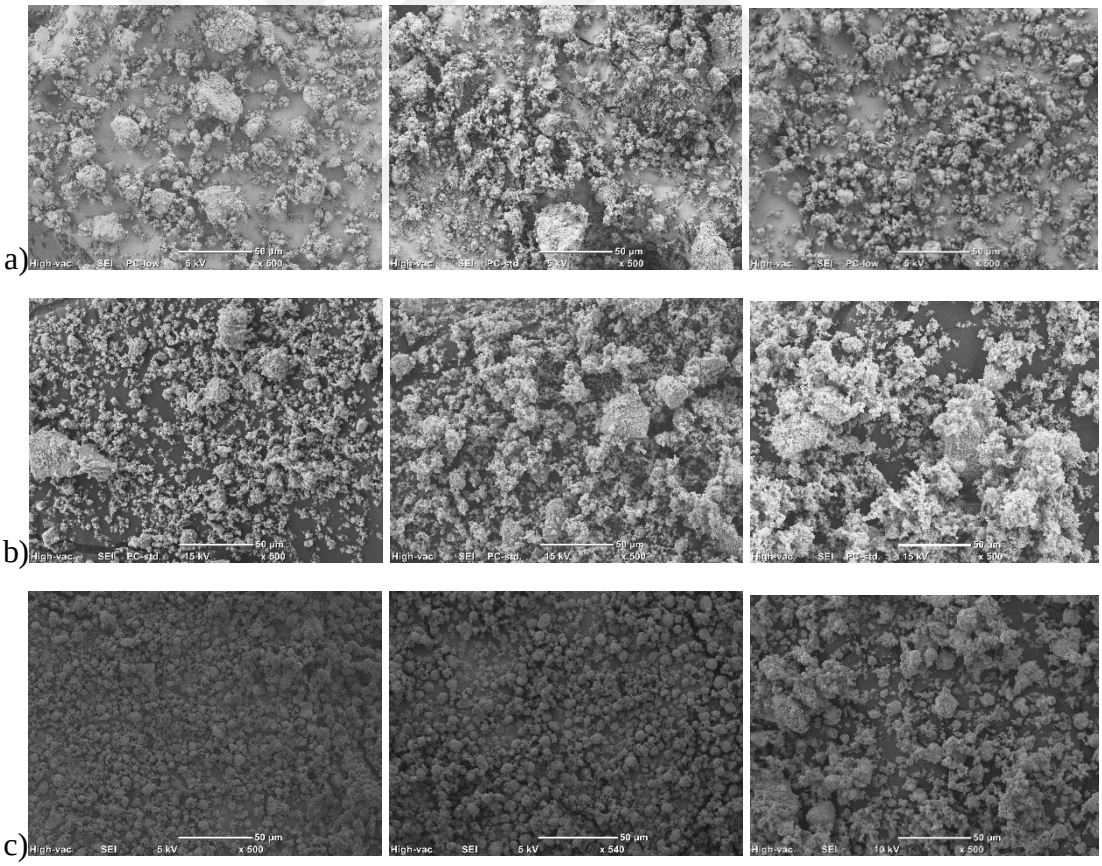

Figure 4.16 : SEM photos of a) Fe25TaC, b) Fe25VC and c) Fe25WC for 2, 4 and 8h MA time from left to right, respectively.

Minimum particle size for Fe25TaC was determined powders as 90.21 nm (Table 4.10). D(50) values revealed that average particle size of fine fractions were obtained lower for Fe25VC than the others. Fine particles were synthesised from Fe25TaC powder composition that was also promoted by zeta potential rates. After leaching Fe25WC and extracting Fe, submicron and nano sized WC particles were obtained and measured. Similar tendency were observed for WC in Cu matrix concluded as a result of WC lattice type.

After 8 h milling time, small particles with the size of 1 – 2 μm were observed among larger ones with the size of 10 – 20 μm. This means that some amount of initial powder particles was not refined at all. From Figure 4.16a, Fe25TaC particles were observed as formed in irregular shape consist of pancake, flake particles that having the least flowability, and tend to be retained between balls – powder surfaces that cause increasing cohesion that leads into agglomeration with decreasing particle size. The PSD results and detailed XRD characterizations including crystallite size and peak shiftings were found compatible with SEM images, reasonably. For the Fe25VC powders' MA behaviour, it can be said that the agglomeration tendency increased by continuing MA due to its lower density than TaC and WC. This condition has also revealed itself in the more homogeneous distribution of VC particles and higher visibility of VC presence shown in Figure 4.17. On the contrary to them, Fe particles in Fe25WC powder were plastically deformed only after 4 hours MA which the initial Fe particles were observed even after 4h MA. This situation was considered to be led the decrease and fluctuation in density and crystallite measurements which were given in Table 4.7 to 4.8. In early stages of milling, Fe particles kept their spherical shape and agglomerated which can be seen from the Figure 4.16c. It can be clearly seen that the particles formed from irregular particles that ease fatigue failures, fragmentation, fracture and then to agglomeration by mechanical interlocking of coarse, rough surfaces occurred only after 8 MA. However, the mean particle size of Fe25WC powders remained almost constant, even though the nano fractions were obtained. The noticeable agglomeration was observed for all powders that may be due to high rotation speed of Spex and as a consequence, owing to the heating of the powder. In Figure 4.17, BEI of Fe25WC composite powders can be seen. The smaller and finer particles mainly covering the bigger Fe particles can be easily distinguished.

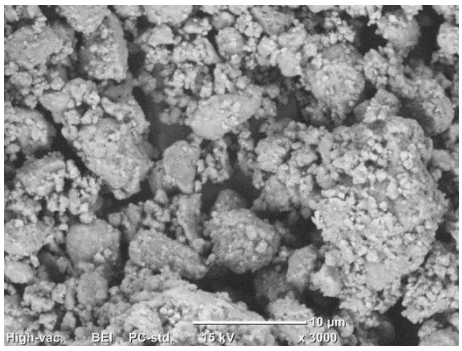

Figure 4.17 : BEI of Fe25WC after 8h MA time (x3000).

The powders MA behaviours can be better understood at higher magnifications. The morphology of the particles shows irregularity in shape especially for the powders with TaC and WC reinforcements. It is seen that the process reaches a steady state when fracturing and welding are almost in balance. The fine particles were observed after 8 hours milling time among the larger ones. Each particle becomes a composite/incorporating one synthesized by mechanical alloying, presenting a fine and homogeneous distribution of the nanometric reinforcement throughout the whole particle, as shown in Figure 4.18.

a) 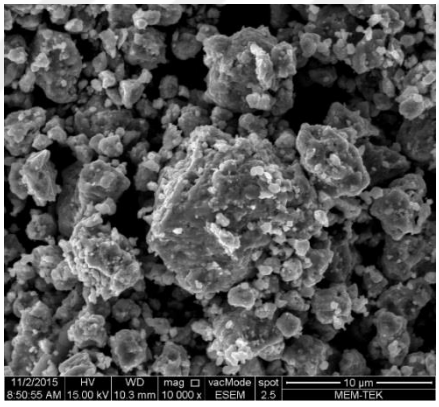

b) 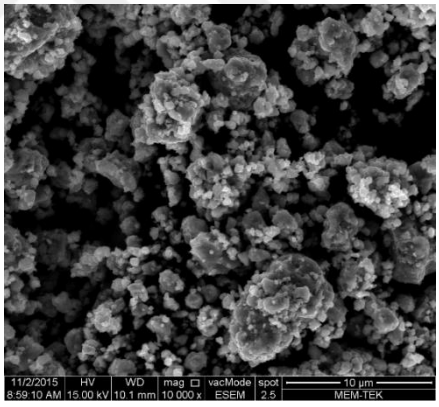

c) 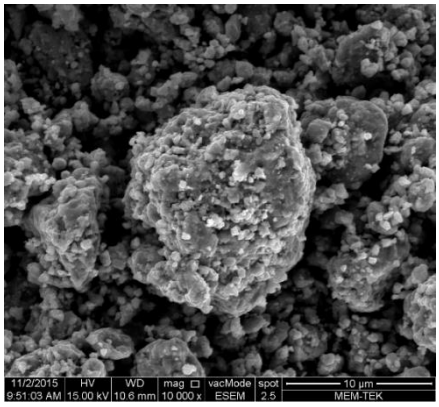

Figure 4.18 : SEM photos of a) Fe25TaC, b) Fe25VC and c) Fe25WC after 8h MA time at magnification x10 000.

A supportive EDS analysis was obtained that shows the relative homogeneous composite powders (Figure 4.19). This was concluded as due to density of reinforcing element that plays critical role to obtain more homogeneous distribution. At same magnification, it is to be said that the balance was reached between agglomeration tendency and on-going fragmentation, even though the production of finer and nano sized particles within composite powder batch.

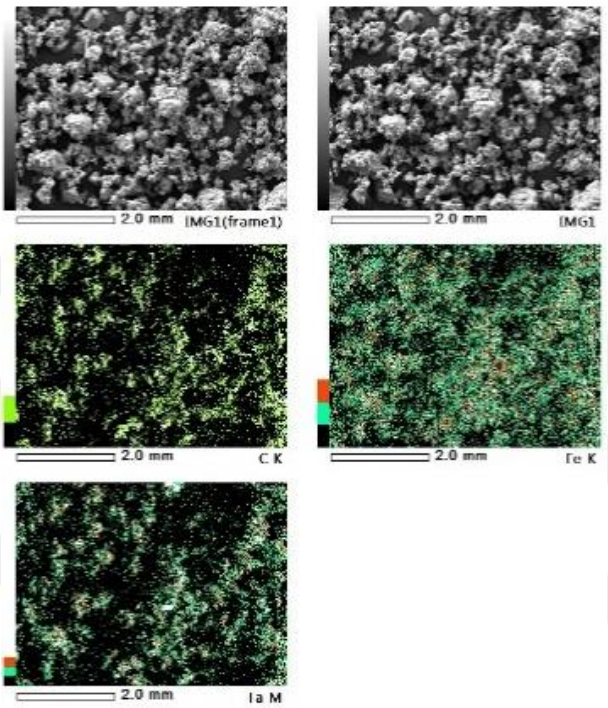

a)

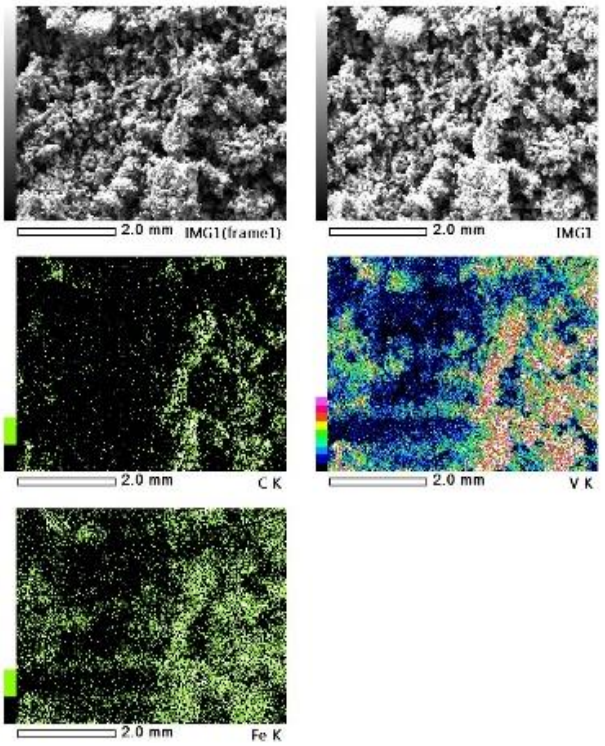

b)

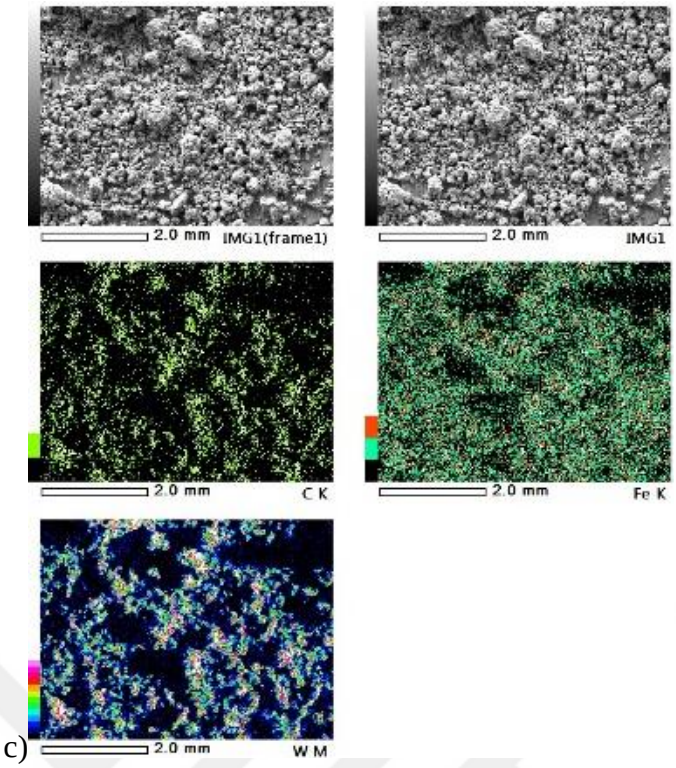

c)

Figure 4.19 : EDS maps of 8h MA'ed a) Fe25TaC, b) Fe25VC and c) Fe25WC powders.

4.4 Fragmentation Behaviour of Brittle Phase in Ni Matrix

With increasing MA time, the true density of the powder mixture decreased as given in the Table 4.11. The true densities of Ni25VC were noticeably lower than theoretical density for all MA time. However, this occurred for Ni25TaC and Ni25WC composite powders only after 8 hours. Both Ni25TaC and Ni25WC powders true densities were changed dramatically after 8 hours milling time on contrary to alteration and slight decline in density value of Ni25VC. Apparent densities that can be evaluated and related to flowability of powders were also calculated. From the Table 4.11, it can be clearly seen that the change of flowability was strongly connected with by particle size change.

Figure 4.20 shows the XRD patterns of the 2-4-8 hours MA'ed Ni25TaC, Ni25VC and Ni25WC powders. All the detected peaks are characteristic of Ni, TaC, VC and WC, individually. As shown from the Figure 4.20, no secondary phase or contamination has been observed. XRD patterns of MA'ed powders exhibited a broadening of diffraction peaks and some decline in intensity.

Table 4.11 : Density values of composite powders against MA time.

Sample	MA time (h)	Theoretical density (g/cm^3)	Apparent density (g/cm^3)	True density (g/cm^3)	Green density (g/cm^3)
Ni25TaC	2	10.30	4.03	10.27	5.94
	4		3.42	10.00	5.77
	8		3.02	9.80	6.10
	annealed			9.78	6.22
Ni25VC	2	8.12	1.63	7.78	4.50
	4		1.66	7.13	4.72
	8		1.57	6.80	4.53
	annealed			6.80	5.02
Ni25WC	2	10.58	4.36	10.45	6.08
	4		4.12	10.11	5.87
	8		3.63	10.01	5.94
	annealed			10.21	6.09

The crystallite sizes of Ni based composite powders decreased by increasing milling time, and as it was expected all strain rates increased that can be a proof of the peak broadening which was assumed result of microstresses, coherency strains and crystallite smallness that was also measured and calculated as given in Table 4.12. However, the lattice parameter of Ni did not alter dramatically by milling time but it gave close values even with increasing milling time. However, the lattice parameter of Ni was increased by milling time. It can be said that the raise (average 4.9 %) in the lattice parameter of Ni can be considered as hard-core solid solution. Increase in lattice parameter also leads an increase in cell volume that gives rise to tensile strain and reflects the effect of plastic deformation and initiation of distinct defects during mechanical alloying process. This phenomenon can be seen from same table as the strain rate changed in direct proportion to reduction in cell volume. Minor changes in d-spacing of Ni (111) planes were observed.

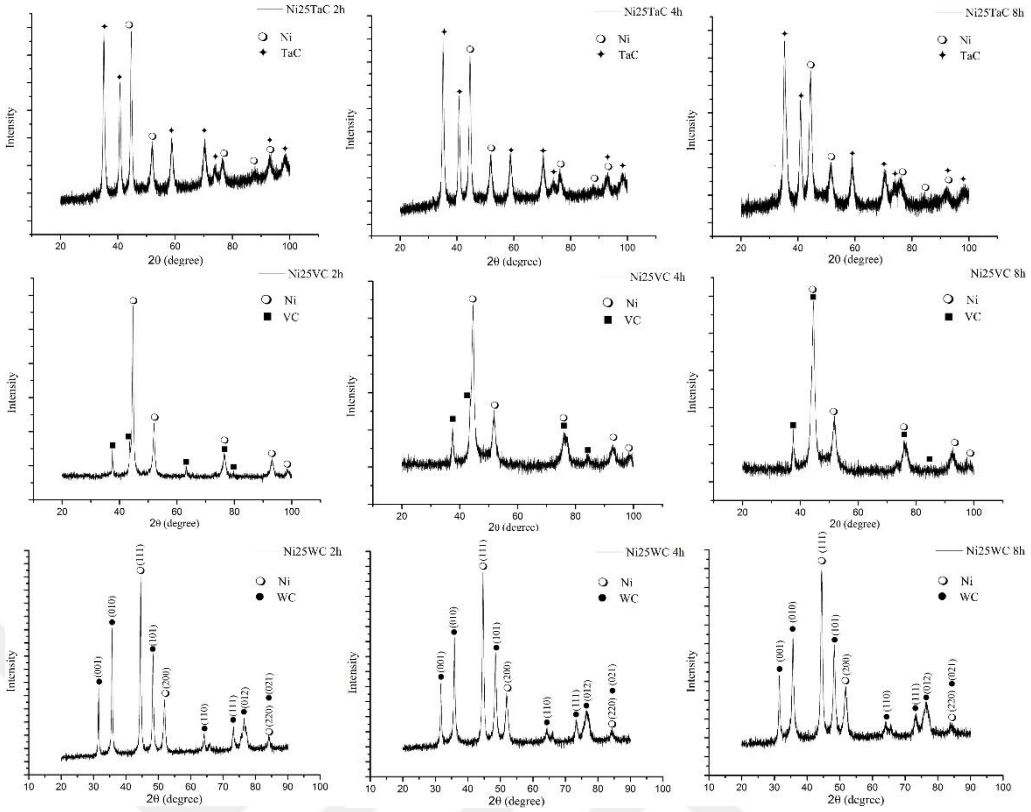

Figure 4.20 : Diffraction patterns of Ni25TaC, Ni25VC and Ni25WC powders against MA time.

Decrease in crystallite size and increase in lattice strain can be contributed by the reduction of the intensity and the increase of full width half at maximum (FWHM) as can be seen in Table 4.12. This is a common behaviour to high-energy ball milled/mechanical alloyed powders. Rane et al. achieved Ni crystallite size between 15-29 nm after 80 hours milling in planetary ball and below 10 nm after 30 hours milling in shaker mill by the presence of 15 % W (Rane, 2013). Average crystallite size of Ni was obtained 58 nm by milling in planetary ball by mechanical coating method (Yazdani, 2015). Ni was also mechanical alloyed with Ti and its crystallite size reached below 40 nm only after 50 hours of MA where the rotating speed is 300 rpm (Sharma, 2016). In addition WC, Chao and his colleagues has studied in-situ synthesis of Ni-TaC by laser cladding in order to obtain 0.5 – 2 μm grain sizes (Chao, 2008) and also Greer showed that nanocrystalline structures with crystallite size even below 5 nm are possible by devitrification of sputter deposition (Greer, 2001). However, Ni-VC are lacking.

Table 4.12 : Crystallite size and strain rates of Ni25TaC, Ni25VC and Ni25WC powders against MA time.

Sample	MA time (h)	FPA		Wiliamson-Hall		Lattice parameter (nm)	d-spacings (nm)
		D, nm	ε, %	D, nm	ε, %		
Ni25TaC	0						
	2	15.40	0.53	15.83	0.25	0.3700	0.2026
	4	12.43	1.23	10.48	0.40	0.3699	0.2026
	8	15.87	0.86	12.89	0.29	0.3534	0.2040
	annealed	22.6	0.68				
Ni25VC	0						
	2	22.90	0.84	23.61	0.23	0.3544	0.2029
	4	12.56	1.22	6.26	0.47	0.3565	0.2033
	8	11.50	1.77	12.96	0.36	0.3517	0.2035
	annealed	63.25	0.23				
Ni25WC	0	145.6	0.07				
	2	40.35	0.14	46.47	0.10	0.3699	0.2032
	4	23.80	0.55	13.92	0.53	0.3698	0.2027
	8	17.65	1.13	12.86	0.66	0.3699	0.2035
	annealed	43.15	0.27				

The Williamson – Hall analysis was also employed to calculate crystallite size and provide information and peak profile analysis to support particle behaviour during MA (Figure 4.21). Shiftings of strongest peaks belong to Ni (111) due to carbide type against MA time was shown in Figure 4.22.

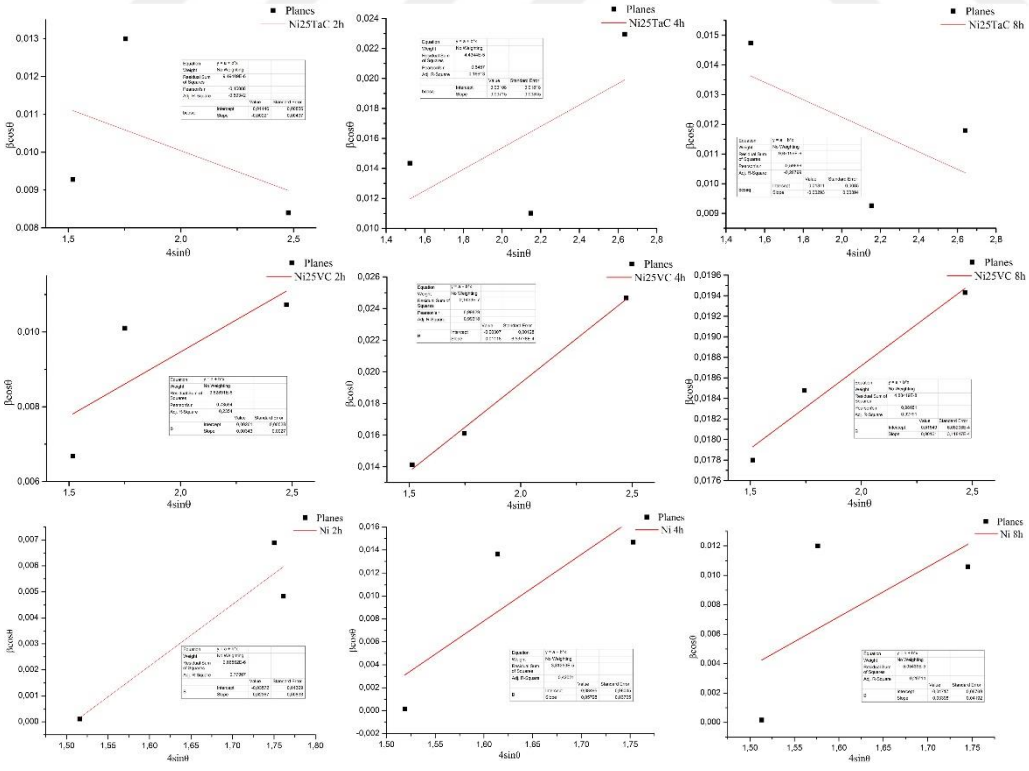

Figure 4.21 : Williamson – Hall plot analysis of Ni based composite powders.

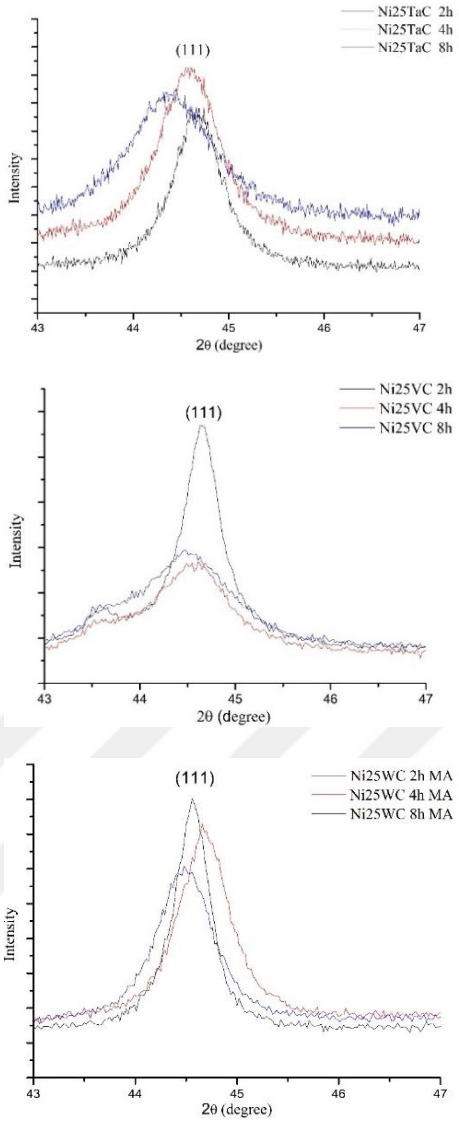

Figure 4.22 : Peak shiftings of Ni (111) due to carbide type against MA time.

Changes in position of Ni (111) due to carbide type against MA time was given in Table 4.13.

Table 4.13 : Change in position of Ni (111) due to carbide type against MA time.

Plane	MA time (h)	Change in position, 2θ (degree)		
		Ni25TaC	Ni25VC	Ni25WC
Ni (111)	2	0.1546	0.0067	- 0.1883
	4	- 0.2084	- 0.1995	0.1031
	8	- 0.4057	- 0.3496	- 0.3339

Figure 4.23 shows the cumulative distribution of Ni25TaC, Ni25VC and Ni25WC powders against MA time.

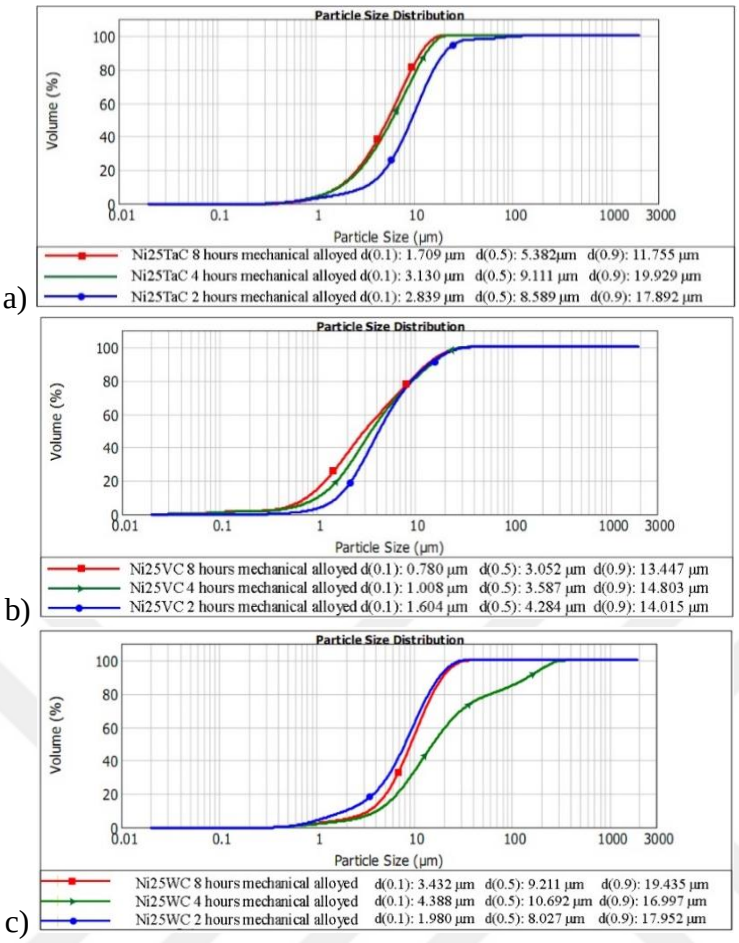

Figure 4.23 : PSD of a) Ni25TaC, b) Ni25VC and c) Ni25WC powders against MA time.

On the contrary, Cu and Fe, Ni based composite powder particle size and distribution exhibited fluctuated aspect except VC reinforced ones. Comparing to Cu based powders; the size and distribution were obtained in wide range that was considered as a result of higher Young modulus despite having same lattice type. Although the agglomeration tendency increased after 4 hours MA for Ni25TaC and Ni25WC composite powders, mean particle size of them decreased below initial particle size, finally. Only with VC reinforcing particles, the mean particle size decreased by increasing milling time, disagreeably. This situation was thought to be a consequence of effect of VC density, which resulted in high volume percentage. The ZPs and minimum particle size of nano fractions can be easily followed in the Table 4.14.

Table 4.14 : PSD of nano fractions and zeta potential values against MA time.

Sample	MA time (h)	D50 (nm)	Minimum Particle Size (nm)	Zeta Potential (mV)
Ni25TaC	2	697	218.7	-58.0
	4	450	83.8	-47.3
	8	204.4	32.8	-59.2
Ni25VC	2	493	191.5	-59.1
	4	440	186.2	-58.9
	8	389	166.7	-51.2
Ni25WC	2	443	227.8	-46.2
	4	330	154.2	-49.3
	8	298.9	107.3	-40.5
Leached Ni25WC	8	260.2	28.1	-59.3

Zeta potentials were measured far below zero that indicates instability of particles owing to its presence of nano fractions. The relation between ZPs and minimum particle size of nano fractions can be easily noticed from the Table 4.14. Minimum average particle size of nano fractions were measured for Ni25TaC powders, also the minimum particle size was detected. Although, the particle size of nano fractions was determined as increasing agglomeration tendency, 28.1 nm size was measured after leaching 8 hours MA'ed Ni25WC powders.

Figure 4.24 shows the morphologies of the Ni reinforced composite particles with wt. 25% TaC, VC and WC after 2, 4 and 8 h of milling. After 2 h of milling, very large particles appeared. Although, there is a certain drop in the particle sizes with increasing milling time. These agglomerates also contain very fine particles that are cold-welded together due to the very hard plastic deformation. However, agglomeration tendency was observed as increased after 4h MA for all powder compositions. Fragmentation of particles continued and fine and nano scaled particles were observed and detected after 8h. Fracture and fragmentation were clearly seen for TaC and WC reinforced Ni powders comparing to VC ones. Although nano fractions were measured, agglomerated particles occurred. Fine and coarse particles can be observed for all powder batches and MA durations. The MA'ed Ni25WC powders of low apparent densities show a laminar morphology after 8 h, while the ones with the high apparent density show equiaxial morphology. In a later stage of the process, the morphology of the particles of Ni25WC changes again

to an equiaxed one, with better powder packing and an increase in the apparent density. Figure 4.25 is a back scattered SEM micrograph showing the presence of the spherical like fine particles that clung onto the larger/agglomerated particles after 8 h. White nanoparticles homogeneously embedded into bigger particles can be seen in this micrograph. These white nanoparticles are thought to be WC phase, which could not be dissolved in Ni lattices during MA.

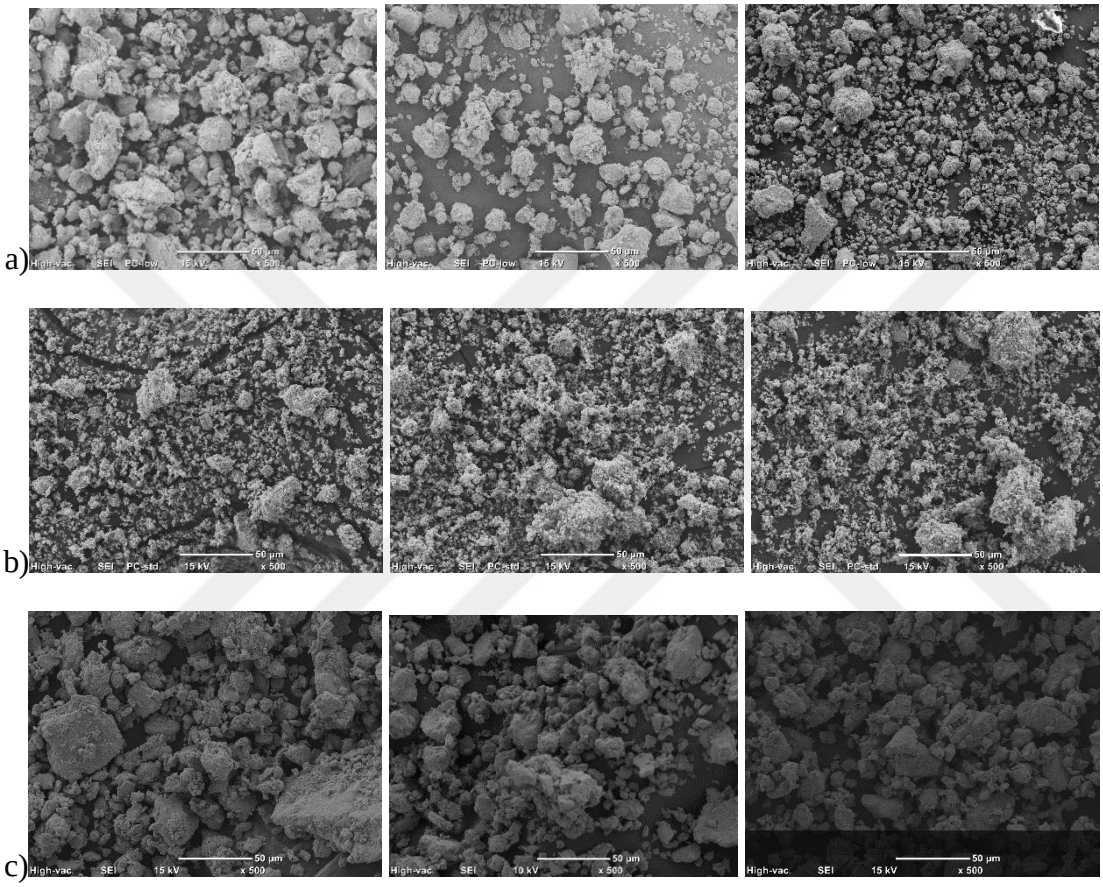

Figure 4.24 : SEM photos of a) Ni25TaC, b) Ni25VC and c) Ni25WC for 2, 4 and 8h MA time from left to right, respectively.

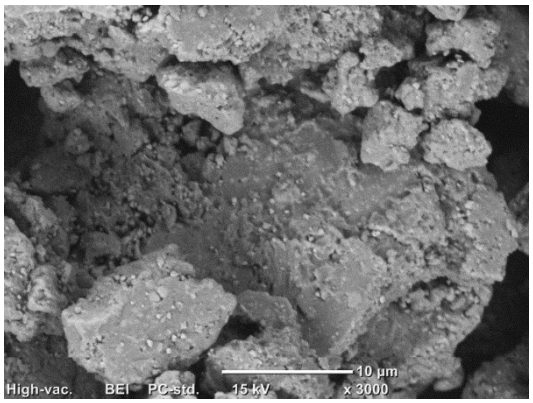

Figure 4.25 : BEI of Ni25WC after 8h MA time (x3000).

Higher magnifications disclose the on-going fractures and presence of fine fractions after 8 h MA for all powder compositions as shown in the Figure 4.26.

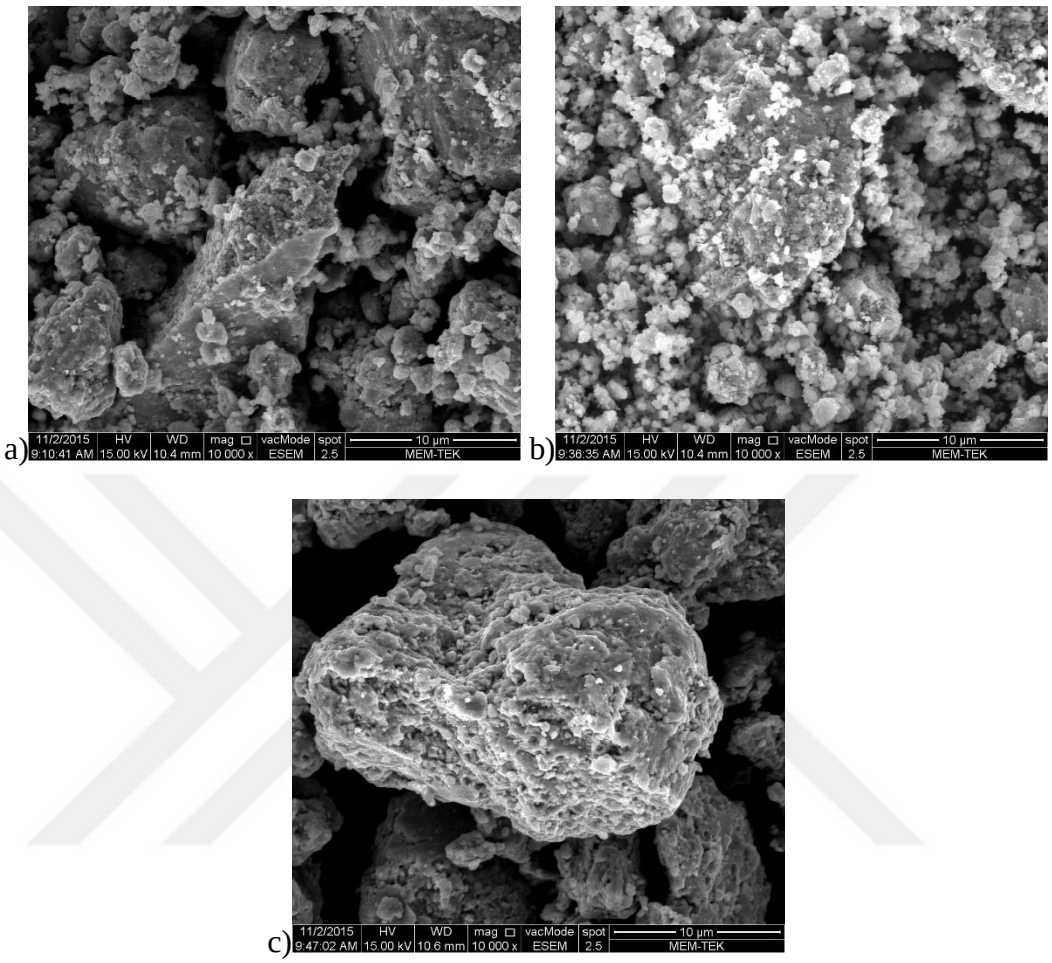

Figure 4.26 : SEM photos of a) Ni25TaC, b) Ni25VC and c) Ni25WC after 8h MA time at magnification x10 000.

Fracture surface of Ni particle can be observed from Figure 4.26a. It should be noticed that submicron particles are in existence among with coarse particles. Finer fractions were thought to be produced by both fragmentation of Ni and TaC. VC particles seemed to have more homogeneous distribution. The finer particles detected as WC phase can be seen easier from Figure 4.26c as embedded onto bigger particles. The distribution of these brittle phases was confirmed by EDS mapping as given in Figure 4.27. VC was observed as to be well distributed than TaC and WC which was also remarked in Cu and Fe matrixes. Some particles were in lack of C (white regions) that indicates the lack of the compound of brittle phase TaC and VC. The same observation was obtained for Cu and Fe matrixes; therefore this was concluded as result of higher Young modulus and thermal conductivity of WC than TaC and VC which effects the MA.

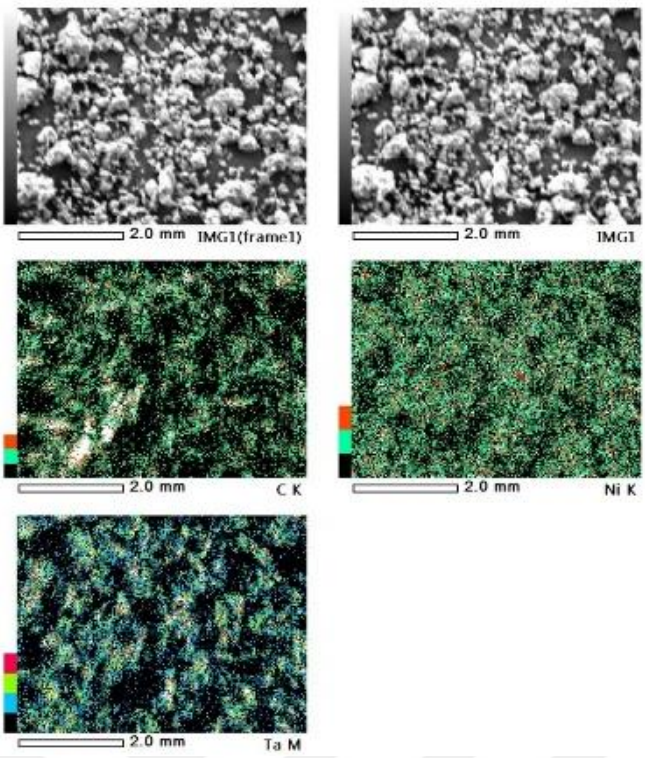
2.0 mm
IMG1(frame1)
2.0 mm
IMG1
2.0 mm
C K
2.0 mm
Ni K
2.0 mm
Ta M

a)

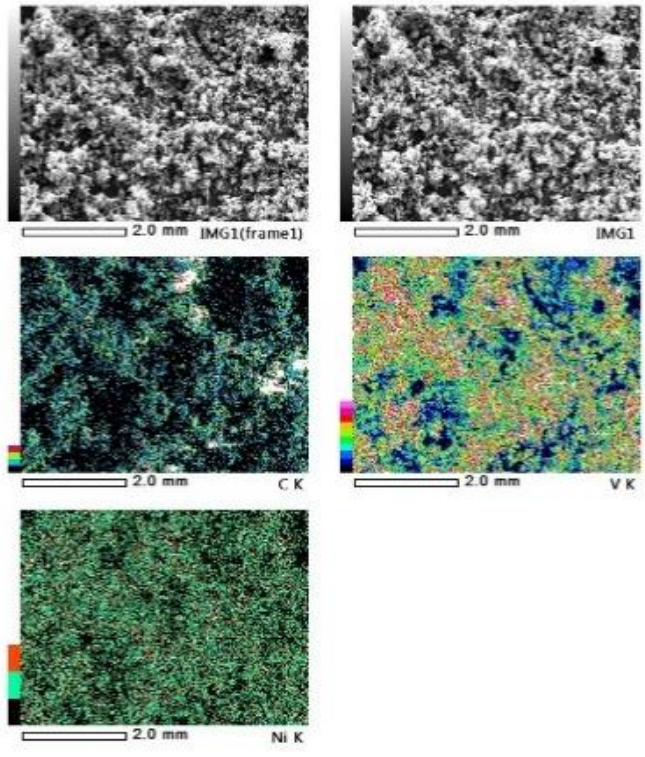
2.0 mm
IMG1(frame1)
2.0 mm
IMG1
2.0 mm
C K
2.0 mm
V K
2.0 mm
Ni K

b)

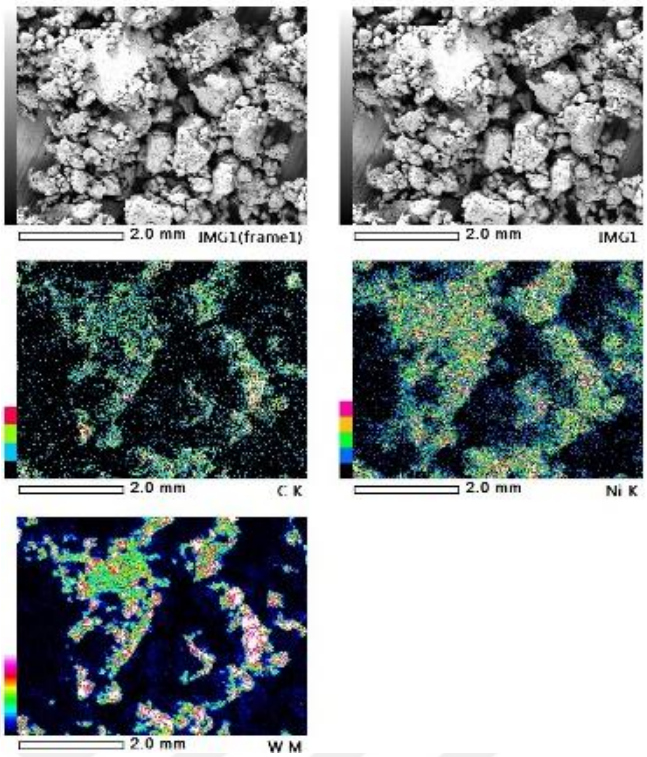

c)

Figure 4.27 : EDS maps of 8h MA'ed a) Ni25TaC, b) Ni25VC and c) Ni25WC powders.

5. BROAD DISCUSSION

Crystallite, particle and grain sizes are frequently confusing (Figure 5.1). It is commonly stated that the average size of crystallites is determined from XRD, the distribution of crystallites is determined from TEM, while the average size of particles is measured by SEM and particle sizers. It is also known that a crystallite is a long-range order of atoms. However, a particle, though not necessarily, often has more than one crystallite. Even though XRD gives the crystallite size but not the particle size, we can sometimes find good agreement between particle sizes obtained from TEM and XRD analysis, especially in nanoparticles. This may be the case when the nanoparticles are single crystalline. However, a particle is composed of several crystallites and can contain multiple domains. The grain and the domain sizes are seldom the same in a polycrystalline aggregate but it is accepted that they can be the same in a proper nano sized powder. Different crystallite size models and approaches together with particle size, SEM, TEM techniques and leaching were applied for correlation of crystallite and particle sizes. In view of what actually XRD tells us is the coherent crystalline or domain size including grains, sub grains, twins and other extended defects like stacking fault and anti-phase boundaries. Therefore, a good agreement can be established between grain size and crystallite size from XRD and TEM only when sample does not contain sub grains, twins and extended defects. In our study, crystallite size and grain size can be used interchangeably. However, the density values, the strain rates and the results of TEM studies revealed that our system is full of deformation and consisting of poly-crystals which makes it difficult to correlate of two (or even three) sizes.

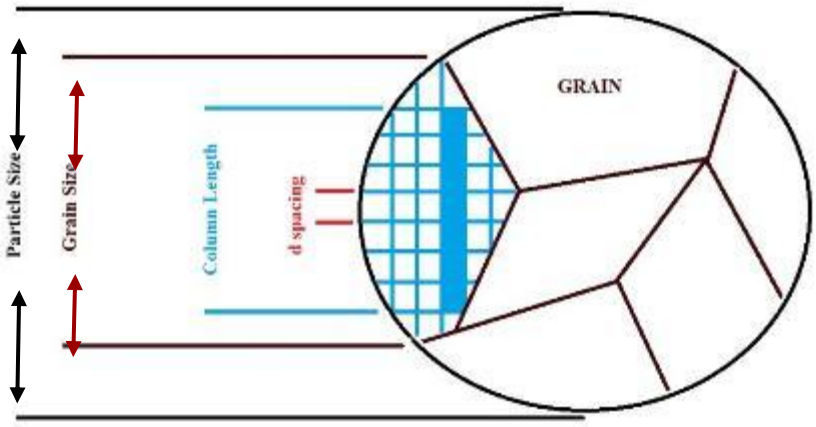

Figure 5.1 : Schematic illustration of particle, grain and crystallite size.

Table 5.1 : Comparison of crystallite size and strain rates of VC and WC reinforced metal matrixes according to different approaches.

	MA time (h)	FPA (nm)		Williamson – Hall C.S. (nm)	
		L	pV	FWHM	IB
Cu25VC	2	19.85	15.64	17.46	22.57
	4	22.90	18.04	10.11	12.83
	8	10.10	7.93	13.47	13.47
Ni25VC	2	22.90	19.65	22.90	30.97
	4	12.56	11.79	12.56	6.79
	8	11.50	10.80	11.50	20.30
Fe25VC	2	20.03	18.71	13.22	15.89
	4	14.10	13.24	10.23	7.25
	8	15.90	14.93	8.86	6.17
Cu25WC	2	29.63	25.78	22.44	26.90
	4	29.43	20.17	20.13	21.97
	8	16.99	12.28	14.63	17.0
Ni25WC	2	40.35	28.8	46.46	35.80
	4	23.80	22.2	13.92	17.02
	8	17.65	15.3	12.85	7.63
Fe25WC	2	13.35	10.42	13.21	15.80
	4	10.00	7.32	10.23	7.02
	8	7.60	7.67	8.86	7.63

Table 5.1 discloses the correlation of different approaches and models to determine the crystallite sizes of Cu, Fe and Ni during the presence of VC and WC. The results are in good agreement with different approaches. These calculations were compared to nano particle size measurements as given in Table 4.10 and 4.14 in previous

chapters. The calculations with the pseudo-Voigt function resulted lower than Lorentzian function. For most cases, the same phenomenon was observed by application of FWHM during W-H plot analysis. One can say that the difference between the approaches and functions is higher for WC reinforced powders than the VC ones. It is known when both Gaussian and Lorentzian peak types are observed, pseudo-Voigt function, as a result of its lattice type, Young modulus and density value, is more effective in analysing a system which is suitable for WC. Besides, it was seen that nano particle sizes obtained were approximately 100 nm. The minimum particle size values are found close to crystallite size calculations. Although fine particles were synthesized below 100 nm after leaching of metal matrixes, 52.73 for Cu25WC, 80.5 nm for Fe25WC and 28.1 nm for Ni25WC given in same tables, it cannot be said that there is a strong correlation between crystallite size and particle size. However, TEM bright and dark field micrographs confirmed that nano particles existed among the agglomerated and large particles as shown in Figure 5.2. The lighter areas indicate, WC (the heavier element), but the top view of image appears like agglomerated particle consisting of interpenetrated and overlapped fine and coarse particles belong to both phases, metal matrixes (Cu, Fe and Ni) and WC. Among them, WC particles were observed under 100 nm, even below 10 nm in the same time as shown in same figure. Polygonal/spheroidal shaped and equiaxed shaped particles in sizes varying between 20 nm to 200 nm are displayed. The ring patterns considered to be polycrystalline part of particles that exposed the metal matrix phases, were also illustrated (Figure 5.3). The ring patterns showed the characteristic planes (111), (200) and (220) of Cu; (110), (200) and (211) of Fe and (110), (200), (220) and (311) of Ni.

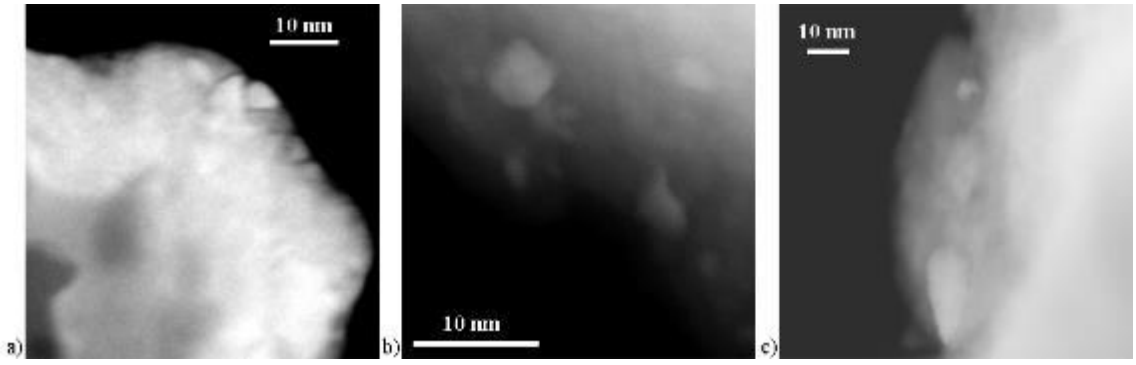

Figure 5.2 : Nano WC particles among 8h MA'ed a) Cu25WC, b) Fe25WC and c) Ni25WC composite powders.

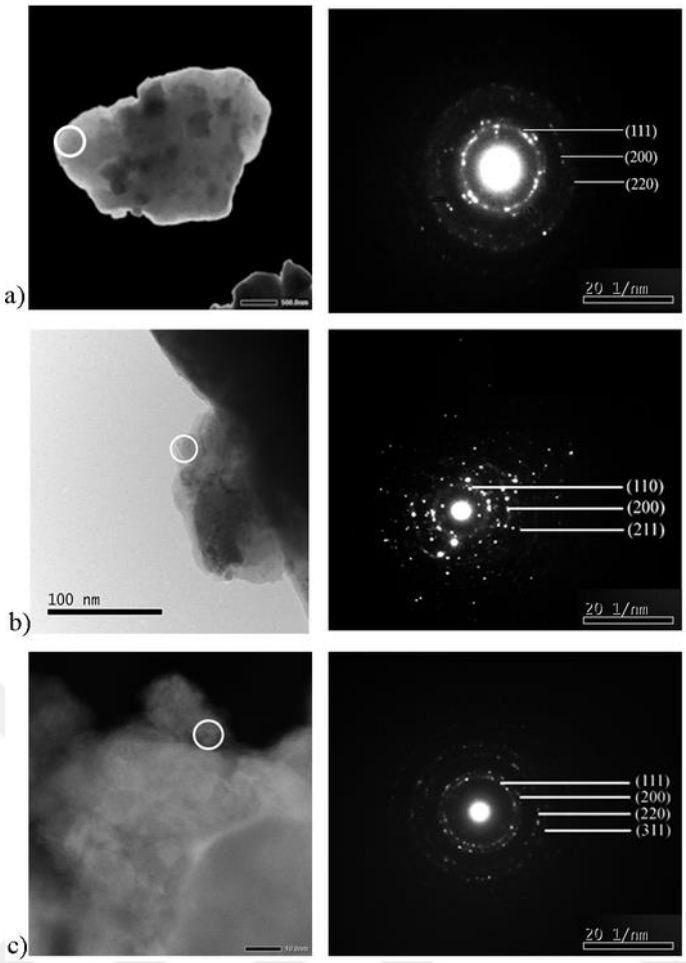

Figure 5.3 : a) Cu25WC particle and Cu ring pattern, b) Fe25WC particle and Fe ring pattern, c) Ni25WC particle and Ni ring pattern of composite powders after 8h MA.

In addition to TEM, SEM micrographs provided high-resolution images of fine particles at high magnification of samples (Figure 5.4).

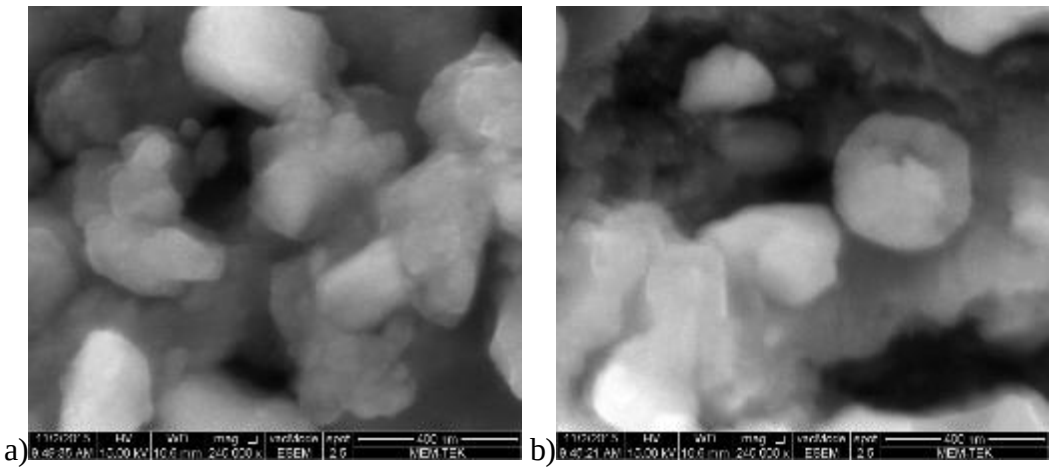

Figure 5.4 : SEM images of 8 h MA'ed a) Fe25WC and Ni25WC composite powders (x 240000).

Nano particles can be seen in the figures clearly. However, it is not easy to distinguish the particle's phases. Therefore, EDS mapping at high magnification was applied to specify which particle belong to which constituent and thus to comprehend the homogeneity at nano scales (Figure 5.5). It was discovered from the images that the homogeneity became quiet lower at those sizes. This was concluded as a result of nano particle agglomeration and condensation between relatively larger particles clogging the occurrence of more fracture and fragmentation. In order to see the density effect and distribution of brittle phase in metal matrix, VC distribution was observed in Cu and Ni matrixes by EDS mapping (Figure 5.6). Likewise, Cu matrix was substituted Fe in case any influence of matrix type. Despite having relatively more homogeneous distribution in Cu, the same situation was observed for all powder compositions after 8 h MA time. As mentioned before, the balance between fracture and cold welding seem to be established. This phenomenon was tried to be exposed by SEM fracture surfaces and XRD peak shiftings of brittle phases as given in Figure 5.7 and 5.8. The cleavage and slip planes and families of TaC, VC and WC were determined from the literature as (111), {100} and {1100}, respectively (Martin, 1980). Moreover, it was reported that the transition carbides fractured commonly on the B1 system {110} <110> (Toth, 1971). Toth has also inclined that these carbides (TaC and WC particularly) are a candidate to fracture without any creep. From the figures in which cracks indicate the on-going fracture mechanism during MA, cracks and fractures can be seen clearly. Hollows that can be observed obviously in the images can be an evidence of rupture. Peak shiftings of carbides revealed that hard-core solid solution is tried to be constituted and strongly related to carbide Young modulus and metal matrix lattice type.

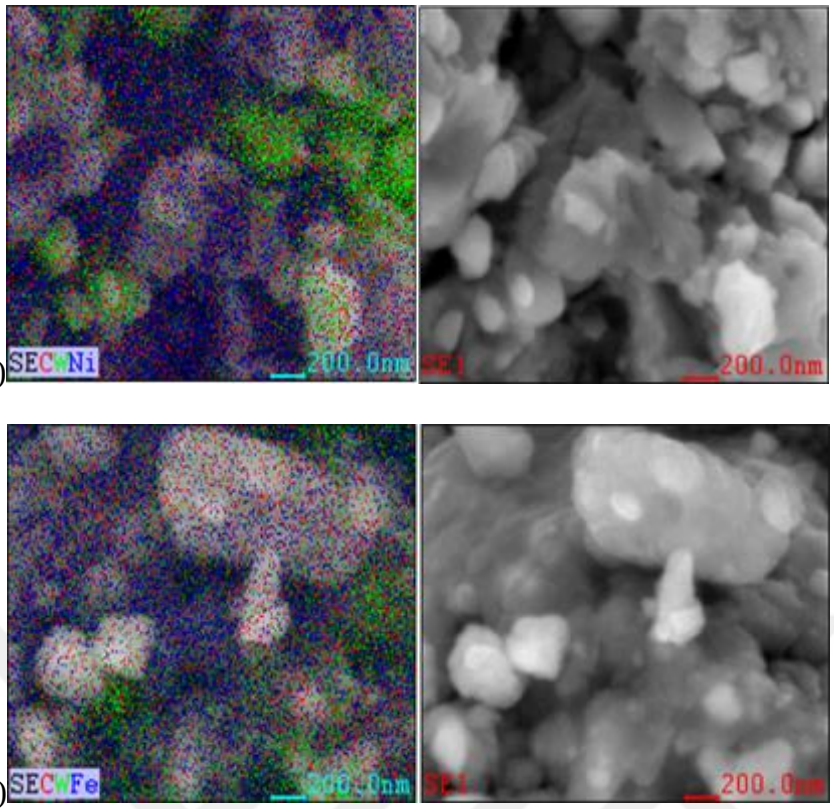

Figure 5.5 : EDS mapping of 8 h MA'ed a) Fe25WC and Ni25WC composite powders (x 120000).

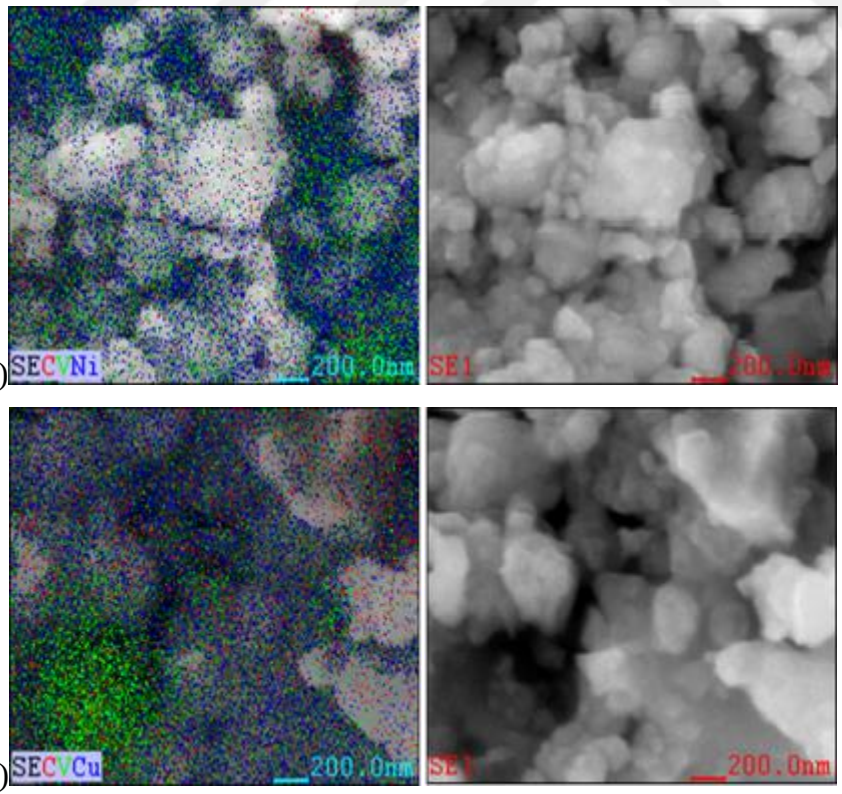

Figure 5.6 : EDS mapping of 8 h MA'ed a) Cu25VC and Ni25VC composite powders (x 120000).

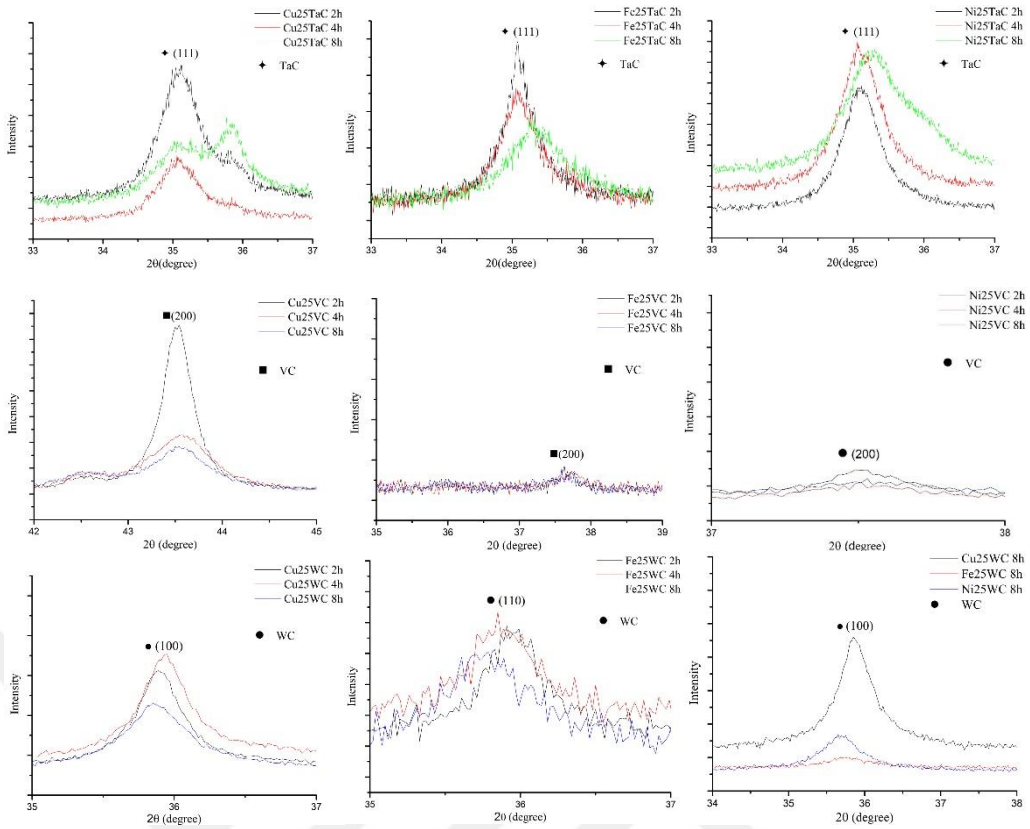

Figure 5.7 : Peak shiftings of brittle phase strongest peaks against MA time.

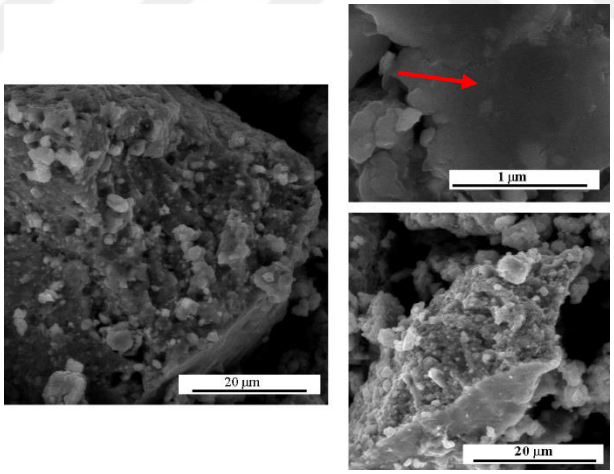

Figure 5.8 : Cracks, fracture, and rupture surfaces.

Figure 5.9 displays the SEM images of composite powders according to matrix type after 8h MA time at x 240 000 magnification.

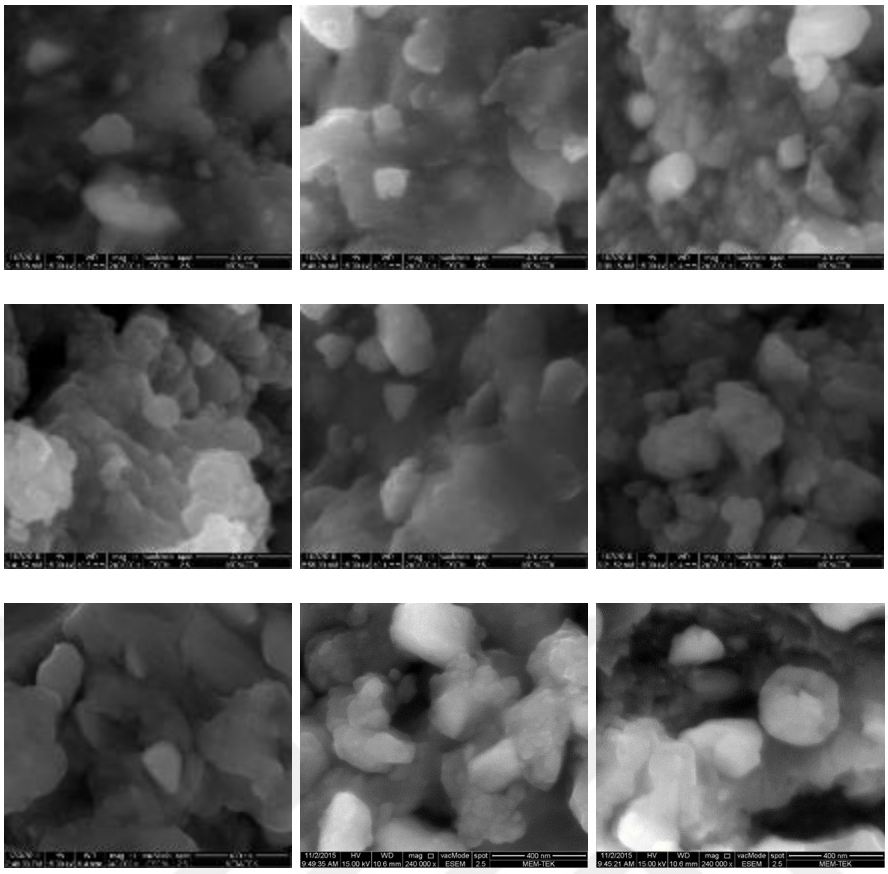

Figure 5.9 : SEM images of composite powders from right to left Cu, Fe and Ni matrixes; up to down TaC, VC and WC after 8h MA, respectively (x 240 000).

The SEM images and sizes are in accordance with nano and master particle sizer results. One can say that thermal conductivity and lattice type are strongly effective on MA. Having high number of slip planes, close packing planes, hexagonal and fcc structures have a great influence on fine particle production. Therefore, Cu matrixes are the most suitable for synthesizing WC particles, followed by Ni matrixes thanks to their fcc lattice structure. Both Cu and Ni were more suitable than TaC, VC and Fe. Microstructural photos of 8h MA'ed Cu25WC after leaching Cu, which reveals the nano particle presence, were given in Figure 5.10. As seen in the figures, nano particles are in existence among with larger particles.

Particularly, the fragmentation behaviour of WC in different matrixes was studied. It was seen that nanocrystalline WC particles can be produced through these metal matrixes. In this context, the initial and MA'ed crystallite size of WC phase was determined and initial WC phase was found as 134.6 nm. The reduction in crystallite size was observed with increasing MA durations. The smallest crystallite sizes were obtained as 16.96 nm, 36.60 nm and 24.73 nm for 8h MA'ed Cu25WC, Ni25WC and

Fe25WC, respectively. It was observed that the fragmentation of WC phase continues by MA time, simultaneously. In Figure 5.11 calculated WC crystallite sizes after MA in different metal matrixes and TEM micrograph of single WC particle detected in 8 h MA'ed Cu25WC composite powder are given. The change in crystallite size of WC phases can be seen in Figure 5.11a. In addition, nano sized particles were verified with microscopic studies. TEM image of 8 hrs mechanically alloyed WC particle in Cu matrix was given in Figure 5.11b as an example. As seen in the figure, hexagonal shape of single WC particle measured as 17.22 nm can be easily observed with distorted angles between lattice edges. The calculated crystallite size of WC was found agreeable with TEM results. In Bonache's study, the X-ray diffraction profile analysis revealed a WC phase refined to a crystallite size of 19 nm after 100 h milling at planetary ball mill (Bonache, 2011). Another research done by Silva showed that the crystallite size of WC reaches below 40 nm after 10 h cryogenic ball milling (Silva, 2010). Besides, Back and his colleagues reported that Co addition decreases the crystallite size of WC particles under 30 nm in same duration (Back, 2005). However, in this study, it was presented that WC crystallite size can be obtained under 20 nm for shorter milling durations with the presence of high rate of ductile matrix. Consequently, it can be said that XRD results confirm that our milling process has the possibility of synthesizing fine structured particles in shorter MA durations that can be considered as an advantage.

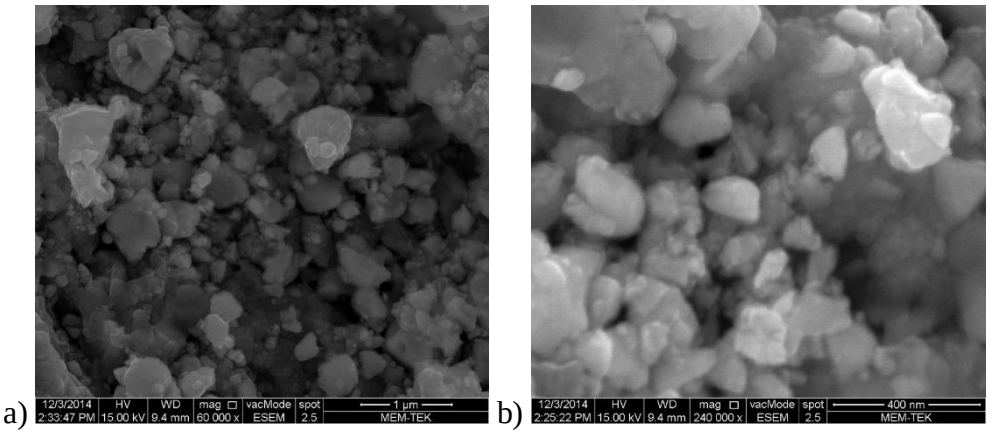

Figure 5.10 : SEM image of 8h MA'ed Cu25WC composite powder after leaching in H_2SO_4 at different magnifications a) x60 000 and b) x240 000.

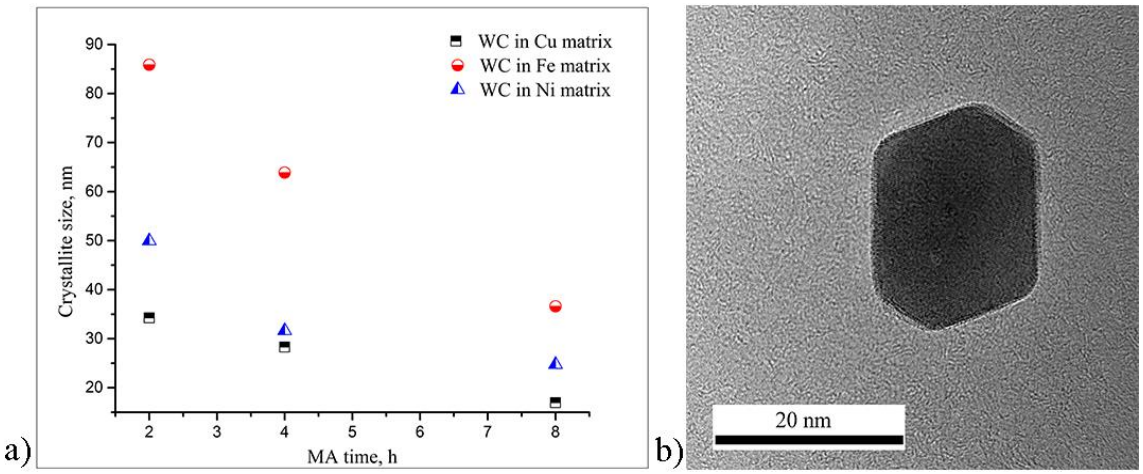

Figure 5.11 : a) Calculated WC crystallite sizes after mechanical alloying in different metal matrixes and b) TEM micrograph of single WC particle detected in 8 h MA'ed Cu25WC composite powder.

XRD study (given in Figure 5.12) was also performed on leached Cu to be sure of only WC production. Same phases were observed even after leaching. The diffractogram of 8h MA'd Cu25WC powders before leaching represents stronger broadening which can be a result of imperfections such as dislocations, vacancies, interstitials, substitutional and similar defects are to generate a distribution in the d-spacings of lattice planes. Furthermore, the XRD peaks of 8h MA'd Cu-WC composite powders after leaching are smooth and the intensities are lower than the powders before leaching.

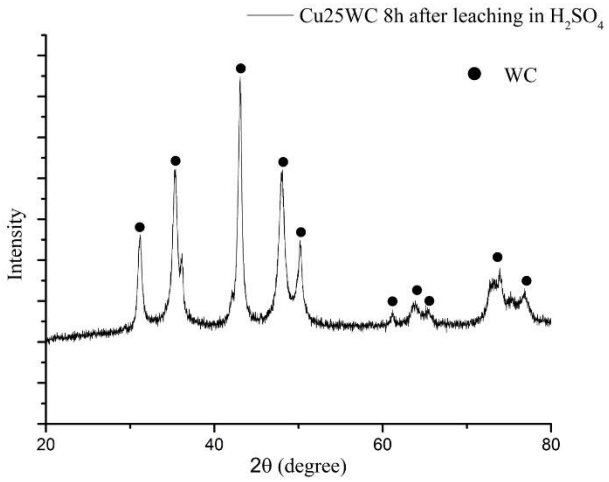

Figure 5.12 : XRD graph of WC particles after leaching of Cu from 8 h MA'ed Cu25WC composite powders.

6. CONCLUSIONS

The production of brittle particles in submicron/nano sizes and synthesis nanostructured composite powders within different ductile matrixes by mechanical alloying was aimed in this thesis. Within this scope, the fragmentation behaviour of carbide and metal powders were investigated. Different particle size and crystallite size approaches were applied to understand the appropriate characterization technique for further studies. The outputs of this dissertation can be listed as below:

- ✓ Production of nanostructured composite powders for different industries is possible by reinforcing high amount of carbide. The base metal's physical properties such as Young modulus and thermal conductivity are strongly effective on successful MA. Therefore, Cu was found to be most suitable material for production of nano sized particles. However, Ni was also a great candidate for production of nanostructured composite powder. Nano particles even under 20 nm were achieved to be synthesized for all powder compositions. The finer particles thought to be brittle phase were found as embedded onto bigger particles.
- ✓ Crystallite and particle sizes can be equalized for single crystals, likely. In addition, nano sizer measured the smallest sizes, which corresponds the crystallite sizes of some powder compositions. Williamson – Hall plot analysis was an effective way to ensure the crystallite size calculated by using software programs and to understand the deformation behaviour/type. Pseudo – Voigt profile analysis was found to determine anisotropic peak broadenings and peak asymmetries by considering both profile shapes. However, one can say that all results from various models are in converge.
- ✓ Although the relative homogenous composite powders were produced at least for macro level, non-homogeneous particle distribution was detected for nano levels at high magnifications. The density of carbide was strongly influential on the distribution.

- ✓ Not any new compounds were detected that constituted between carbide and metal phases. However, hard-core solid solution was considered to be occurred according to XRD peak shiftings and density changes.
- ✓ MA time for VC was found more effective than TaC and WC for all matrixes. It was observed that MA time was less effective for Fe matrix, which was concluded as a result of lattice type considering with elastic modulus. The peak intensities were similar against time. Almost the same phenomenon was seen for Ni matrix except VC presence that was considered effect of VC density. This was a remarkable effect of Young modulus according to results.
- ✓ As a result, production of Fe, Ni and Cu based composite powders having different types of carbides have been realized via MA for the direct or indirect utilization in different engineering applications as final product.

REFERENCES

Abe, H., Ishizaki, T., Kano, S., Li, F., Satoh, Y., Tanigawa, H., Hamaguchi, D., Nagase, T., and Yasuda, H. (2014). Mechanism of instability of carbides in Fe–TaC alloy under high energy electron irradiation at 673 K. *J. Nucl. Mater.*, *455*, 695–699.

Adams, D. M. (1981). *Inorganic Solids.* New York, NY: John Wiley & Sons.

Agrafiotis, C. C., Puszynski, J. A., and Hlavacek, V. (1991). Experimental study on the synthesis of titanium and tantalum nitrides in the self-propagating regime. *Combust. Sci. Technol., 76,* 187.

Aguzzoli C., Figueroa, C. A., Soares, G. V., and Baumvol, I. J. R. (2010). Physicochemical and structural characteristics of TiC and VC thin films deposited by DC reactive magnetron sputtering. *J. Mater. Sci., 45,* 4994-5001.

Ajayan, P. M., Schadler, L. S. and Braun, P. V. (2003). *Nanocomposite Science and Technology*, Wiley-VCH Verlag, Weinheim.

Aliofkhazraei, M. (2011). *Nanocoatings,* Springer Berlin Heidelberg.

Ashby M. F. (1992) *Materials Selection in Mechanical Design***,** Pergamon, Cambridge.

ASM Metals Reference Book. (1993). Materials Park, Ohio.

Athanassiadis, T., Lorenzelli, N., and de Novion, C. H. (1987). Diffraction studies of the order-disorder transformation in VSC_7. *Ann. Chim. France*, *12*, 129-142.

Back, S. H., Lee, G. H., and Kang, S. (2005). Effect of cryomilling on particle size and microstrain in a WC-Co alloy. *Mater. Trans., 46,* 105-110.

Bandow, S. and Saito, Y. (1993). Encapsulation of ZrC and V_4C_3 in graphite nanoballs via arc burning of metal carbides/graphite composites. *Jpn. J. Appl. Phys., 32,* 1677-1680.

Behrens, M., and Schlögl, R. (2012). X-Ray Diffraction and Small Angle X-Ray Scattering. In J. Védrine, M. Che (Eds.), *Characterization of Solid Materials and Heterogeneous Catalysts: From Structure to Surface Reactivity* (Vol. 2, pp. 609–653). Weinheim: Wiley-VCH**.**

Benesovsky F., Kieffer, R., and Ettmayer, P. (1981). Nitrides. In K. Othmer (Ed.) *Encyclopedia of Chemical Technology*, (3rd Ed., Vol. *15*, p.871) New York: John Wiley & Sons.

Benjamin, J. S., and Volin, T. E. (1974). The mechanism of mechanical alloying, *Metall. Trans.* ***5***, 1929.

Benjamin, J. S. (1988), The mechanical alloying process. *Mod. Dev. Powder Metall., 21,* 397–414.

Benjamin, J. S. (1992). Fundamentals of mechanical alloying. *Mater. Sci. Forum, 88,* 1-18.

Beyerlein, K. R., Snyder, R. L., Li, M., and Scardi, P. (2010). Application of the Debye function to systems of crystallites**,** *Philos. Mag., 90,* 3891–3905

Bohren C. F., and Huffman, D. R. (1998)**.** *Absorption and Scattering of Light by Small Particles.* Wiley-Interscience, New York.

Bonache, V., Salvador, M. D., Busquets, D., and Segovia E. F., (2011). Fabrication of ultrafine and nanocrystalline WC–Co mixtures by planetary milling and subsequent consolidations. *Powder Metall., 54,* 214-221.

Böhm, H. J., Eckschlager, A., and Han, W. (2002). Multi-inclusion unit cell models for metal matrix composites with randomly oriented discontinuous reinforcements. *Comp. Mater. Sci. 25,* 42-53.

Boselli, J., Pitcher, P. D., Gregson, P. J., Sinclair, I., (2001). Numerical modelling of particle distribution effects on fatigue in Al–SiC p composites. *Mater. Sci. Eng. A, 300,* 113.

Brewer, L. (1967). A most striking confirmation of the Engel metallic correlation. *Acta Metall., 15,* 553-556.

Buffat, P.H., and Borel, J.P. (1976). Size effect on the melting temperature of gold particles. *Phys. Rev. A, 13,* 2287.

Campbell, I. E., and Sherwood, E. M., (1967). *High-Temperature Materials and Technology*, John Wiley & Sons, New York.

Chawla, N. and Chawla, K. K. (2006). *Metal Matrix Composites*, Springer, New York.

Chao, M., Wang, W., Liang, E., Ouyang, D. (2008). Microstructure and wear resistance of TaC reinforced Ni-based coating by laser cladding. *Surf. Coat. Technol., 202,* 1918–1922.

Choa, Y. H., Bamba, N., Hayashi, H., Kondo, H., Sekino, T., and Niihara, K. (1999). Effect of pure-solvents without deflocculants for finer SiC particle dispersed MgO based composite. *J. Mater. Sci., 34,* 3789-3793.

Choa, Y. H., Nakahira, A., Niihara, K. (2000). Microstructure and mechanical properties of SiC-platelet reinforced Al_2O_3/SiC-particle hybrid composites. *J. Mater. Sci., 35,* 3143-3149.

Clavel, A. L., (1991). Tool coatings for the metal-working industry, *Thin Films, 91.*

Clyne, T. W., and Withers, P. J. (1993)**.** *Introduction to Metal Matrix Composites***,** Cambridge University Press, Cambridge.

Cotton, F. A., and Wilkinson, G. (1972). Advanced Inorganic Chemistry, Interscience Publishers, New York.

Cotton, F. A., and Wilkinson, G. (1980). Advanced Inorganic Chemistry, Interscience Publishers, New York.

Dahotre, N. B., Kadolkar, P., and Shah, S. (2001). Refractory ceramic coatings: processes, systems and wettability/adhesion**.** *Surf. Inter. Analysis***,** *31,* 659-672.

Dalfard, V. M. (2012). Effect of particle size of tungsten carbide on weight percent of carbide in Ni-WC nano-composite. *Int. J. Electrochem. Sci., 7***,** 3537-3542.

Davis, R. M., and Koch, C. C. (1987)**.** Mechanical alloying of brittle components: silicon and germanium. *Scripta Metall., 21,* 305–310.

Davis, R. F., (1993). Silicon carbide and diamond semiconductor thin films. *Am. Ceram. Sot. Bull., 72***,** 29.

de Novion, C. H., and Landesman, J. P. (1985). Order and disorder in transition metal carbides and nitrides**:** Experimental and theoretical aspects. *Pure Appl. Chem. 57,* 1391.

Dressler, S. (1991). Fully automatic plasma nitriding equipment in the automotive industry. *Indust. Heating, 58,* 38.

Dunbar, C., (1994). Surface Preparation for Continuously Applied Coatings. In *ASM Handbook, Surface Engineering* (9th ed., Vol. *5,* pp. 1392-1393). Materials Park, OH: .ASM International.

Ebbing, D. D. (1990). *General Chemistry*, Boston, MA: Houghton Mifflin Company.

Ekmar C. S. (1974). *U.S. Patent No. 3,832,221.* Washington, DC: U.S. Patent and Trademark Office.

Engel N. (1939). Some new viewpoints on the metallic bond. *Ingenioeren, M,* I0l.

Ettmayer, P., and Lengauer, W. (1994). Carbides: Transition metal solid state chemistry. In *Encyclopedia of Inorganic Chemistry* (p. 531). New York, NY: John Wiley & Sons.

Evans, R. C. (1979). *An Introduction to Crystal Chemistry***,** Cambridge, UK: Cambridge University Press.

Fang, Z. Z., Wang, X., Ryu, T., Hwang, K. S., and Sohn, H. Y. (2009). Synthesis, sintering, and mechanical properties of nanocrystalline cemented tungsten carbide – A review. *Int. J. Refract. Met. Hard Mater., 27,* 288–299.

Fecht, H. J. (2002). Nanostructured materials and composites prepared by solid state processing. In C.C. Koch (Ed.), *Nanostructured Materials: Processing, Properties and Potential Applications* (2nd ed., pp. 119-172), New York, NY: William Andrew Publishing.

Finseth, J. L. (1991). Overview of rover engine tests (Report File No. 313-002-91-059). NASA Final Report.

Fischer, J. J. and Haeberle, R. M. (1988). Commercial status of mechanically alloyed materials. *Mod. Dev. Powder Metall., 21,* 461–477.

Fogagnolo, J. B., Velasco, F., Robert, M. H., and Torralba, J. M. (2003). Effect of mechanical alloying on the morphology, microstructure and properties of aluminium matrix composite powders. *Mater. Sci. Eng. A, 342,* 131-143.

Gleiter, H. (1992). Materials with ultrafine microstructure: retrospectives and perspectives. *Nanostruct. Mater., 1,* 1–19.

Goff, A. (2003). *Modelling and synthesis of a piezoelectric ceramic-reinforced metal matrix composites*. (Master Thesis). Virginia Polytechnic Institute and State University, Blacksburg.

Goldschmidt, H. T. (1967). *Interstitial Alloys***.** New York, NY: Plenum Press**.**

Gonsalves, K. E., Rangarajan, S. P., Law, C. C., Garcia-Ruiz, A., and Chow, G. M. (1997). M50 nanostructured steel the chemical synthesis and characterization of powders and compacts. *Nanostruct. Mater., 9,* 169–172.

Gonzalez, G., Braham, C., Lebrun, J. L., Chastel, Y., Seiler, W., and Figueroa, I. A. (2012). Microstructure and texture of $Al_2Si_xS_n$ (x = 0, 4, 8 mass %) alloys processed by equal channel angular pressing. *Mater. Trans., 53,* 1234-1239.

Goodwin, T. J., Yoo, S. H., and Groza, J. R. (1997). Cementite-iron nanocomposite. *Nanostruct. Mater., 8***,** 559–566.

Greenwood, N. N. & Earnshaw, A. (1984). *Chemistry of the Elements.* Oxford, UK: Pergamon Press.

Greer, A. L. and Wilde, J. R. (2001). Novel Ni-TaC nanocrystalline cermets, *Mater. Sci. Forum, 360,* 261-266.

Gubanov, V. A., Ivanovsky, A. L., and Zhukov, V. P. (1994) Electronic *Structure of Refractory Carbides and Nitrides.* Cambridge, UK: Cambridge University Press.

Gusev, A. I., Rempel, A. A. & Magerl, A. J. (2001). *Disorder and Order in Strongly Nonstoichiometric Compounds: Transition Metal Carbides, Nitrides and Oxides.* Berlin, Germany: SpringerVerlag.

Gusev, A. I. (1998). Effects of the nanocrystalline state in solids. *Physics - Uspekhi***.** *41,* 49–76.

Gusev, A. I. & Rempel, A. A. (2004). *Nanocrystalline Materials*. Chippenham, UK: Cambridge International Science Publishing.

Hägg, G. (1931). Regularity in crystal structure in hydrides, borides, carbides, and nitrides of transition elements. *Z. Phys. Chem., 12***,** 33.

Haggerty, J. S. and Cannon, W. R. (1981). Sinterable powders from laser-driven reactions. In J.I. Steinfeld (Ed.), *Laser-Induced Chemical Processes* (pp. 165-241). New York, Plenum Press.

Halperin, W. (1986). Quantum size effects in metal particles. *Rev. Modern Phys., **58**,* 533-606.

Harris, C. C. (1967). On the limit of comminution. *Trans. Soc. Min. Engrs., 238,* 17.

Hasegawa N., Saito, M., Kataoka, N., and Fujimori, H. (1993). Soft magnetic properties of carbide-dispersed nanocrystalline films with high thermal stability. *J. Mater. Eng. Perform., 2,* 181.

Hauert, R. and Patscheider, J. (2000). From alloying to nanocomposites – Improved performance of hard coatings. *Adv. Eng. Mater., 2,* 247-59.

He, L. and Ma, E. (1996). Processing and microhardness of bulk Cu-Fe nanocomposites. *Nanostruct. Mater., 7,* 327–339.

Henglein, A. (1993). Physicochemical properties of small metal particles in solution: "microelectrode" reactions, chemisorption, composite metal particles, and the atom-to-metal transition. *J. Phys. Chem., 97,* 5457–5471.

Hintz, W., Antonyuk, S., Schubert, W., Ebenau, B., Haack, A. and Tomas, J. (2009). Determination of Physical Properties of Fine Particles, Nanoparticles and Particle Beds, In E. Tsotsas and A.S. Mujumdar (Eds.), *Modern Drying Technology* (Vol. *2,* p. 412). Weinheim: Wiley-VCH.

Ho, P., Buss, R. J. and Loehman, R. E. (1989). Glow discharge synthesis of silicon nitride precursor powders. *J. Mater. Res., 4,* 873**.**

Ho, C. Y., and El-Rahaiby, S. K. (1992). Assessment of the Status of Ceramic Matrix Composites Technology in the U.S. and Abroad. In 6th Annual Conference on Composites and Advanced Ceramic Materials Part 1, *Ceramic Engineering and Science Proceedings,* The American Ceramic Society, USA, January 7-10.

Hojo J., Oku, T., and Kato. A. (1978). Tungsten carbide powders produced by the vapor phase reaction of the WCl_6-CH_4-H_2 system. *J. Less-Common. Met., 59,* 85-95**.**

Hüttig, G.F., Fattinger, V. and Kohla, K. (1950). Preparation of metal carbides. *Powder Metall. Bull., 5,* 30-37**.**

Ida, T., Ando, M. and Toraya, H. (2000). Extended pseudo-Voigt function for approximating the Voigt profile, *J. Appl. Cryst., 33,* 1311–1316.

Ida, T. and Toraya, H. (2002).Deconvolution of the instrumental functions in powder X-ray diffractometry, *J. Appl. Crystallogr., 35,* 58-68.

Jain, M. K., Bhanuprasad, V. V., Kamat, S. V., Pandey, A. B., Varma, V. K., Bhat, B. V. R., and Mahajan, Y. R. (1993). Processing, microstructure and properties of 2124 Al-SiCp composites. *Int. J. Powder Metall., 29,* 267-275.

Jin X. H., Gao, L., Gui, L. H., and Guo, J. K. (2002). Microstructure and mechanical properties of SiC/ZTM nanocomposite prepared from mixtures of mullite gel, 2Y-TZP and SiC nanopowders. *J. Mater. Res., 12,* 1024–1029.

Eckert, J. (2002)**.** *Nanostructured Materials: Processing, Properties, and Applications***,** Norwich, NY: William Andrew Publishing.

Kainer, K. U. (1994). Keramische Partikel, Fasern und Kurzfasern für eine Verstärkung von metallischen Werkstoffen. In K.U.Kainer (Ed.), *Metallische Verbundwerkstoffe.* Oberursel, Germany: DGM Informationsgesellschaft.

Kainer, K. U. (2006) Basics of Metal Matrix Composites, In K.U.Kainer (Ed.), Metal *Matrix Composites: Custom-made Materials for Automotive and Aerospace Engineering* (Ch. 1, p. 330). Weinheim: Wiley-VCH Verlag.

Kamrani, S., Hesabi, Z. R., Riedel, R., and Reihani, S. M. S. (2011). Synthesis and characterization of Al–SiC nanocomposites produced by mechanical milling and sintering, *Adv. Compos. Mater., 20,* 13–27.

Kandemir, T., Kasatkin, I., Gigsdies, F., Zander, S., Kühl, S., Tovar, M., Schlögl, R., and Behrens, M. (2014). Microstructural and defect analysis of metal nanoparticles in functional catalysts by diffraction and electron microscopy: The Cu/ZnO catalyst for methanol synthesis. *Top. Catal., 57,* 188-206.

Kaufinann, R., and Meyer, O. (1983). Ion channeling in NbC_1- c: Determination of local atomic displacements around carbon vacancies. *Phys. Rev. B, 28,* 6216-6226.

Kieffer, R. and Benesovsky, F. (1965). *Hartmetalle.* Wien: Springer-Verlag.

Kieffer, R., Schwarzkopf, P. (1963). *Hartstoffe und Hartmetalle.* Wien: Springer-Verlag.

Kirino, F., Otomo, S., Koiso, N., and Yano, F. (1996). Effect of additional elements on the crystallization process in Fe-Ta-C thin films. *J. Jap. Inst. Metals, 60,* 519-528.

Kisly, P. S. (1986). The chemical bond strength and the hardness of high melting point compounds in science of hard materials. *Inst. Phys. Conf. Ser., 75,* 107-120.

Koch, C.C., Ovidko, I. A., Seal, S., and Veprek, S. (2007). *Structural Nanocrystalline Materials Fundamentals and Applications,* New York, Cambridge University Press.

Kosolapova, T. Y. (1971). *Carbides, Properties, Production, and Applications,* New York, Plenum Press.

Kubo, R. (1962). Electronic properties of metallic fine particles. *I. J. Phys. Soc. Jpn. 17,* 975-986.

Kumar, R, Joardar, J., Raman, R. K. S., Raja, V. S., Joshi, S. V., and Parida, S. (2016). Effect of chromium and aluminum addition on anisotropic and microstructural characteristics of ball milled nanocrystalline iron. *J. Alloys Compd. 671,* 164-169.

Kurlov, A. S., Gusev A. I. (2014). High-energy milling of nonstoichiometric carbides: Effect of nonstoichiometry on particle size of nanopowders, *J. Alloys Compd., 582,* 108–118.

Kurlov, A. S., Gusev, A. I. (2013). *Tungsten Carbides: Structure, Properties and Application in Hardmetals,* Heidelberg: Springer-Verlag.

Lascelles, K., Morgan, L. G., Nicholls, D., and Beyersmann, D. (2005). Nickel Compound. In *Ullmann's Encyclopedia of Industrial Chemistry*, Weinheim: Wiley-VCH.

Larsen-Basse, J. (1973). Wear of hard-metals in rock drilling: A survey of the literature. *Powder Metall., 16,* 1-32.

Lee, M., Home, J.G. and Tabor, D. (1979). The mechanisms of notch formation at the depth of cut line of ceramic tools machining nickel base superalloys. In K.C. Ludema, W.A. Glaeser and S.K. Rhee (Eds.), *Wear of Materials,* (pp. 460—469). New York, NY: ASME Publication.

Leunda, J., Soriano, C., Sanz, C., and García, N. V. (2011). Laser cladding of vanadium-carbide tool steels for die repair. *Phys. Procedia, 12,* 345–352

Lide, D. R. (1994). *Handbook of Chemistry and Physics*, 75th edition, London, UK: CRC Press.

Lipatnikov, V. N., Rempel, A. A., and Gusev, A. I. (1990). Effect of non-stoichiometry and ordering on the basal structural parameters of the monocarbides of niobium and tantalum. *Inorg. Mater., 26,* 2171-2175.

Lipatnikov, V. N., Lengauer, W., Ettmayer, P., Kei1, E., Groboth, G., and Kny, E. (1997). Effects of vacancy ordering on structure and properties of vanadium carbide. *J. Alloys Compd., 261,* 192-197.

Llorca-Isern, N. and Artieda-Guzmán, C. (2013). Metal-based composite powders. In I. Chang and Y. Zhao (Eds.), *Advances in Powder Metallurgy* (Ch. 9, pp. 241-272). Cambridge, Woodhead Publishing.

Lomaeva, S. F., Yazovskikh, K. A., Maratkanova, A. N., Volkov, V. A., Ulyanov, A. L., and Yelsukov, E. P. (2010). Fe–VC–Fe_3C nanocomposites produced by mechanical synthesis from various starting components. *Phys. Met. Metallogr., 109,* 534-546.

Lorenzelli, R., de Dieu1eveu1t, I. (1969). Existence d'une surstructure dans le carbure de thorium sous-stoechiometrique: $ThC_{o.76}$. *J. Nucl. Mater., 29,* 349-353.

Lu, K. (2012). *Nanoparticulate Materials: Synthesis, Characterization, and Processing*. New York, John Wiley & Sons.

Lucks, I., Lamparter, P., and Mittemeijer, E. J. (2004). An evaluation of methods of diffraction-line broadening analysis applied to ball-milled molybdenum. *J. Appl. Chrys., 37,* 300-311.

Lye, R. G., Hollox, G. E., and Venables, J. D. (1968). Bonding, structure, and mechanical behaviour of VC single crystals. In F.W. Vahldiek and S.A Mersol (Eds.), *Anisotropy in Single Crystal Refractory Compounds* (Vol. *1*, pp. 445-457). New York, Plenum Press.

Ma, Z. Y., Li, Y. L., Liang, Y., Zheng, F., Bi, J., and Tjong, S. C. (1996). Nanometric Si_3N_4 particulate reinforced aluminum composite. *Mater. Sci. Eng. A, 219,* 229-231.

Manotas-Albor, M., Vargas-Uscategui, A., Palma, R., Mosquera, E., (2014). In situ production of tantalum carbide nanodispersoids in a copper matrix by reactive milling and hot extrusion, *J. Alloys Compd.*, 598, 126–132.

Marchand, R., Laurent, Y., Guyader, J., L'Haridon, P., and Verdier, P. (1991). Nitrides and oxynitrides: Preparation, crystal chemistry and properties. *J. Europ. Ceram. Soc., 8*, 197-213.

Marques, M. T., Livramento, V., Correia, J. B., Almeida, A., and Vilar, R. (2007). Study of early stages of Cu–NbC nanocomposite synthesis. *J. Alloys Compd., 434–435*, 481–484.

Martin, J. W. (1980). *Micromechanisms in Particle-Hardened Alloys*. Cambridge: Cambridge University Press.

Martinez-Martinez, D. (2013). Nanocomposite Coatings**.** In Q. J. Wang and Y.W. Chung (Eds.), *Encyclopedia of Tribology*, New York, NY: Springer US.

McKenna, P. M. and Redmond, J. C. (1964). In Kirk-Othmer (Ed.) *Encyclopedia of Chemical Technology* (2nd edition, Vol. *4*, p. 75). New York, NY: Wiley.

McKenna, P. M. (1968). *U.S. Patent 3,379,503. Washington, DC: U.S.* Patent and Trademark Office.

Merzhanov, A. G., and Borovinskaya, J. P. (1975). A new class of combustion processes. *Combust. Sci. Technol., 10,* 195-201.

Merzhanov, A. G., Filonenko, A. K. and Borovinskaya, I. P. New phenomena in combustion of condensed systems. *Doklady Akademii Nauk SSSR, 208,* 892–894.

Metzger, T. H., Peisl, J., and Kaufinann, R. (1983). X-ray determination of local atomic displacements around carbon vacancies in NbC_{1-c} single crystals. *J. Phys. F: Metal Phys., 13*, 1103-1113.

Mittemeijer, E. J., and Welzel, U. (2012). *Modern Diffraction Methods*, Wienheim, Wiley-VCH.

Modine F. A., Major, R., Haywood, T., and Gruzalski, G. R. (1984). Optical properties of tantalum carbide from the infrared to the near ultraviolet. *Phys. Rev. B, 29*, 836-841.

Moffatt, W. G., (1986). *The Handbook of Binary Phase Diagrams***,** Amsterdam, NY: Genium Publishing.

Moisy-Maurice, V., Lorenzelli, N., de Novion, C. H., and Convert P. (1982). High temperature neutron diffraction study of the order-disorder transition in TiC_{I_x}. *Acta Metall., 30*, 1769-1779.

Moisy-Maurice, V., Lorenzelli, N., de Novion, C. H., and Convert P. (1981). Neutron Scattering Studies of the Defect Structures in TiC_{I_x} and NbC_{I_x}, In R. K. Viswanadham (Ed.) *Science of Hard Materials*, New York, NY: Plenum Press.

Morrell, R. (1987). Handbook of Properties of Technical and Engineering Ceramics. London, U.K.: National Physical Laboratory.

Munir, Z.A. & Holt, J.B. (1990). *Combustion and Plasma Synthesis of High Temperature Materials.* New York, NY: VCH Publishers.

Munir, Z.A. (1988). Synthesis of high temperature materials by self -propagating combustion methods. *Am. Ceram. Soc. Bull., 67,* 342-349.

Nakagawa, Y. (1958). Liquid immiscibility in copper-iron and copper-cobalt systems in the supercooled state, *Acta Metall., 6,* 704-711.

Nakahira, A., Murao, T., Takeda, S., Tajika, M., Sekino, T., Choa, Y. H., and Niihara, K., (1999). Effect of supercritical drying method on microstructure and properties of Al_2O_3 composites reinforced with ultrafine SiC particulate. *J. Am. Ceram. Soc., 107,* 460-464.

Narula, C. K., Allison, J. E., Bauer, D. R., and Gandhi, H. S. (1996)**.** Materials chemistry issues related to advanced materials applications in the automotive industry. *Chem. Mater., 18,* 984-1003.

Nishizawa, T., Ohnuma, I., and Ishida, K. (1997). Examination of the Zener relationship between grain size and particle dispersion**,** *Mater. Trans. JIM, 38,* 950-956.

Ohno, K., Tanaka, M., Takeda, J., and Kawazoe, Y. (2008). *Nano- and Micromaterials.* Heidelberg, Berlin: Springer-Verlag.

Oyama, S. T. & Kieffer, R. (1992)**.** Carbides. In: M.E. Howe-Grant (Ed.), *Kirk-Othmer Encyclopedia of Chemical Technology* (4th ed., p. 481). New York, NY: John Wiley & Sons.

Oyama, S. T. (1996). Introduction to the chemistry of transition metal carbides and nitrides. In S.T. Oyama (Ed.), *The Chemistry of Transition Metal Carbides and Nitrides* (Ch. 1, pp. 1-28) Bishopbriggs, Glasgow: Chapman & Hall.

Oyama, S. T. (2008). **Preparation** of Solid Catalysts. In: G. Ertl, H. Knozinger, F. Schüth, J. Weitkamp (Eds), *Handbook of Heterogeneous Catalysis* (2nd ed., Vol. *2,* pp. 49-138). Weinheim: Wiley-VCH Verlag VCH.

Oyama, S. T. & Kieffer, R. (1992). Carbides. In: M.E. Howe-Grant (Ed.), Kirk-Othmer Encyclopedia of Chemical Technology (4th ed., p. 841-848). New York, NY: John Wiley & Sons.

Öveçoğlu, M.L., (1987). *Development of a dispersion-strengthened Al-Fe-Ce alloy by mechanical alloying and related theoretical modeling of dislocations in composite materials* (PhD Thesis). Stanford University, Los Angeles.

Özkal, B., Upadhyaya, A., Öveçoğlu, M. L., and German, R. M. (2010). Comparative properties of 85W–15Cu powders prepared using mixing, milling and coating techniques. *Powder Metall., 53,* 236-243.

PalDey, S., and Deevi, S.C., (2003). Single layer and multilayer wear resistant coatings of (Ti, Al)N: a review. *Mater. Sci. Eng. A, 342,* 58–79.

Pati, S. P., and Das, D., (2014) Interfacial magnetic phenomena of mechanosynthesized Fe nanoparticles in MnO matrix, *Ceram. Int., 40,* 10343–10349.

Patscheider, J., Zehnder, T., and Diserens, M. (2001). Structure-performance relations in nanocomposite coatings. *Surf. Coat. Technol., 146,* 201–208.

Perenboom, J., Wyder, P., and Meier, F. (1981). Electronic properties of small metallic patricles. *Phys. Rep., 78,* 173-292.

Perez-Tijerina, E., Gracia-Pinilla, M., Mejia-Rosales, S., Ortiz-Mendez, U., Torres, A. A., and Jose-Yacaman M. (2008). Highly size-controlled synthesis of Au/Pd nanoparticles by inert-gas condensation. *Faraday Discuss, 138,* 353–362.

Pierson, H.O. (1992). *Handbook of Chemical Vapor Deposition (CVD): Principles, Technology, and Applications* (2nd ed.). Norwich, NY: William Andrew Publishing.

Pierson, H.O. (1996). *Handbook of Refractory Carbides & Nitrides: Properties, Characteristics, Processing and Applications.* Westwood, NJ: Noyes Publication.

Pitkethly, M. (2008). Nanotechnology: Past, present, and future. *Nano Today, **3**,* 6.

Prabhu, Y. T., Rao, K. V., Kumar, V. S. S., and Kumari, B. S. (2014). X-ray analysis by Williamson-Hall and Size-Strain Plot Methods of ZnO nanoparticles with fuel variation. *World J. Nano Sci. Eng., 4,* 21-28.

Prabhu, Y. T., Rao, K. V., Kumar, V. S. S., and Kumari, B. S. (2013). X-ray analysis of Fe doped ZnO nanoparticles by Williamson-Hall and Size-Strain Plot, *Inter. J. Eng. Adv.Technol., 2,* 2249-8958.

Prater, T. (2014)**.** Friction stir welding of metal matrix composites for use in aerospace structures, *Acta Astronaut., 93,* 366-373.

Pye, D. (1992). Distortion during nitriding. *Indust. Heating, 33.*

Ramesh, P. D., Vaidyanatha, B., Ganguli, M., and Rao, K. J. J. (1994). Synthesis of β-SiC powder by use of microwave radiation. *J. Mater Res, 9,* 2330 – 2340.

Rane, G. K., Apel, D., Welzel, U., and Mittemeijer, E. J. (2013). The microstructural evolution and thermal stability of nanocrystalline ball-milled Ni–15 at. % W powder. *J. Mater. Res., 28,* 873-886.

Reina, A., Jia, X., Ho, J., Nezich, D., Son, H., Bulovic, V., Dresselhaus, M. S., and Kong, J., (2009). Large area, few-layer graphene films on arbitrary substrates by chemical vapor deposition. *Nano Lett., 9,* 30-35.

Reniers, F., Detroye M., Kacim, S., Kons P., Maoujoud, M., Silberberg, E., El Begrani, S. M., Vandevelde, T., and Buess-Herman, C. (1996). Synthesis of Thin Films of Cr, Mo and W Carbides and Nitrides. In S.T. Oyama (Ed.), *The Chemistry of Transition Metal Carbides and Nitrides* (Ch. 14, pp. 274-290). Bishopbriggs, Glasgow: Chapman & Hall.

Rezaie, H. R., Shokuhfar, A., and Arianpour, F. (2013). Nanocomposite Materials from Theory to Application, In A. Öchsner and A. Shokuhfar (Eds.), *New Frontiers of Nanoparticles and Nanocomposite Materials* (Part 2, pp. 171-232). Heidelberg, Berlin: Springer-Verlag.

Rohde, S. L. (1994). Sputter Deposition. In *ASM Handbook, Surface Engineering* (9th ed., Vol. 5, pp. 1605-1625). Materials Park, OH: .ASM International.

Roman, O. V., Kirilyuk, L., and Chemousova, S., (1987) Gas-phase precipitation of tungsten carbide coatings. *Poroshk. Metall., 6,* 53-56.

Saito, Y., Okuda, M., Yoshikawa, T., Bandow, S., Yamamuro, S., Wakoh, K., Sumiyama, K., and Suzuki, K. (1994). Synthesis of $Sc_{15}C_{19}$ crystallites encapsulated in carbon nanocapsules by arc evaporation of Sc-C composite. Japan. *J. Appl. Phys., **33***,186-189.

Samsonov, G. V. (1964). *High-Temperature Materials*, New York, NY: Plenum Press**.**

Santhanam A. T., Tierney, P., and Hunt, J. L. (1990). *Metals Handbook, Properties and Selection* (10th edition, Vol. *2*, pp. 950—977). Materials Park, OH: .ASM International.

Santhanam, A. T. (1996). Application of transition metal carbides and nitrides in industrial tools, In S.T. Oyama (Ed.), *The Chemistry of Transition Metal Carbides and Nitrides* (Ch. 2, pp. 28-52). Bishopbriggs, Glasgow: Chapman & Hall.

Santhanam, A. T. (1992). Cemented Carbides. In M.E. Howe-Grant (Ed.), *Kirk Othmer Encyclopedia of Chemical Technology* (4th Edition, Vol. *4*, p. 848). New York, NY: John Wiley & Sons.

Savan, A., Boving, H. J., Fluehmann, F., and. Hintermann, H. E. (1993). Increased performance of bearings using TiC-coated balls. *J. de Phys., IV,* 943-948.

Scherrer, P. (1918). Nachrichten von der Gesellschaft der Wissenschaften zu Göttingen, *Mathematisch-Physikalische KlasseNachr. Ges. Wiss. Göttingen Sitzber*, 98.

Schey, J. A. (1987). *Introduction to Manufacturing Processes.* New York, NY: McGraw-Hill.

Schmauder, S. and Mishnaevsky, L. Jr. (2009). *Micromechanics and nanosimulation of metals and composites: Advanced Methods and Theoritical Concepts.* Heidelberg, Berlin: Springer Verlag.

Shokuhfar, A. & Mohebali, M. (2010). Nanostructured Materials. In J.M.P.Q. Delgado (Ed.), *Current Trends in Chemical Engineering*. Houston, USA: Studium Press.

Segurado, J. and Llorca, J. (2002). A numerical approximation to the elastic properties of sphere-reinforced composites. *J. Mech. Phys. Solids, 50* 2107-2121.

Sharma, N., Raj, T., and Jangra, K. K. (2016). Microstructural evaluation of NiTi-powder, steatite, and steel balls after different milling conditions. *Mater. Manuf. Processes, 31,* 628–632.

Silva, F. T. da, Nunes, M. A. M., Oliveira, R. M. V. de, Silva, G. G. da, Souza, C. P. de, and Gomes, U. U., (2010). Analysis of crystallite size and microdeformation crystal lattice the tungsten carbide milling in mill high energy. *Proceedings of Brazilian Congress on Engineering and Materials Science: 19th CBECIMAT.* São Paulo, Brazil.

Song, X. Y., Cao, W. Q., Ayers, M. R., and Hunt, A. J. (1995). Carbon Nanostructures in Silica Aerogel composites. *J. Mater.Res., 10,* 251-254.

Spearing, S. M. (2000). Materials issues in microelectromechanical systems (MEMS), *Acta Mater., 48,* 179-196.

Spriggs, G. E. and Bettie, D. J. (1975). Propertıes and end uses of cemented carbides, *Powder Metall., 18,* 53-70.

Storms, E. K. (1967). *The Refractory Carbides.* New York, NY: Academic Press.

Strudel, J.-L. (1983). Mechanical properties of multiphase alloys. In R.W. Cahn and P. Haasen (Eds.), *Physical Metallurgy* (3rd ed., Vol. 3, Ch. 25, pp. 1412–1481). Amsterdam: North-Holland Physics Publishing.

Suryanarayana, C., (2001). Mechanical alloying and milling. *Prog. Mater. Sci., 46,* 1-184.

Suryanarayana, C., Ivanov, E., and Tosoh S. M. D. (2013). Mechanochemical Synthesis of Nanocrystalline Metal Powders. In I. Chang and Y. Zhao (Eds.), *Advances in Powder Metallurgy* (Ch. 3, pp. 42-68). Cambridge, Woodhead Publishing.

Suryanarayana, C. & Norton, M. G. (1998). *X-Ray Diffraction: A Practical Approach*. New York, NY: Plenum Press.

Suzuki, M., Honda, H., Kobayashi, T., Wakabayashi, T., Yoshida, J., Takahashi, M. (1996) Development of a target directed magnetic resonance contrast agent using monoclonal antibody-conjugated magnetic nanoparticles. *Brain Tumor Pathol., 13,* 127–132.

Şelte, A., and Özkal, B. (2015). Infiltration behaviour of mechanical alloyed 75 wt% Cu - 25 wt% WC powders into porous WC compacts. *Arch. Metall. Mater., 60,* 1565-1568.

Thompson, P., Cox, D. E., and Hastings, J. B. (1987). Rietveld refinement of Debye–Scherrer synchrotron X-ray data from Al_2O_3. *J. Appl. Cryst., 20,* 79-83.

Tong, X.C. and Fang, H.S. (1998). Al-TiC composites in situ-processed by ingot metallurgy and rapid solidification technology: Part II. Mechanical behaviour. *Metall. Mater. Trans. A, 29,* 893-902.

Toth, L. E. (1971). *Transition Metal Carbides and Nitrides*. New York, NY: Academic Press).

Tsuchida, T. and Kakuta T. (2005). Synthesis of NbC and NbB2 by MA-SHS in air process. *J. Alloys Compd., 398,* 67–73.

Tulhoff, H., (1985). Carbides. In *Ullmann's Encyclopedia of Industrial Chemistry* (5th. ed., Vol. 15). Heidelberg, Berlin: Wiley-VCH Verlag.

Tung, D. K., Manh, D. H., Phong, L. T. H., Nam, P. H., Nam, D. N. H., Anh, N. T. N., Nong, H. T. T., Phan, M. H., and Phuc, N. X. (2016). Iron nanoparticles fabricated by high-energy ball milling for magnetic hyperthermia. *J. Electron. Mater., 45,* 2644-2650.

Van Acker, K., Vanhoyweghen, D., Persoons, R., and Vangrunderbeek, J. (2005). Influence of tungsten carbide particle size and distribution on the wear resistance of laser clad WC/Ni coatings. *Wear, 258,* 194-202.

Van Uitert, L. G. (1981). A comparison of melting point relations for metals, tetrahedral semiconductors, and metal carbides and nitrides with the rocksalt structure. *J. Appl. Phys., 52,* 5547.

Vaz, F., Rebouta, L., Goudeau, P., Pacaud, J., Garem, H., Riviere, J.P., Cavaleiro, A., and Alves, E. (2000). Characterization of $Ti_{1-x}Si_xN_y$ nanocomposite films. *Surf. Coat. Technol., 133,* 307–313.

Veprek, S., Veprek-Heijman, M.G.J., Karvankova, P., and Prochazka, J. (2005). Different approaches to superhard coatings and nanocomposites. *Thin Solid Films, 476,* 1–29.

Veprek, S., and Argon A.S., (2002). Towards the understanding of mechanical properties of super- and ultrahard nanocomposites. *J. Vac. Sci. Technol. B, 20,* 650–664.

Veprek, S., and Reiprich, S., (1995).A concept for the design of novel superhard coatings. *Thin Solid Films, 268,* 64–71

Vollath, D. (2013). *Nanomaterials: An Introduction to Synthesis, Properties and Application* (2nd ed.). Weinheim: Wiley-VCH Verlag.

Wang, J., Toby, B.H., Lee, P.L., Ribaud, L., Antao, S.M., Kurtz, C., Ramanathan, M., Von Dreele, R.B., and Beno, M.A. (2008). A dedicated powder diffraction beamline at the advanced photon source: Commissioning and early operational results. *Rev. Sci. Instrum.,79.* 085105.

Weast, R.C. (1981). *CRC Handbook of Chemistry and Physics* (6st edition). Boca Raton: CRC Press.

Wegner, K., Walker, B., Tsantilis, S., Pratsinis, S.E. (2002). Design of metal nanoparticle synthesis by vapor flow condensation. *Chem. Eng. Sci. 57,* 1753–1762.

Weng, L., Shen, Y., Fan, T., and Xu, J. (2015). A study of interface damage on mechanical properties of particle-reinforced composites. *J. Mater., 67,* 1413-1419.

Wilde, J. R., and Greer, A. L. (2001). A new thermally stable structural duplex Ni-TaC nanocomposite. *Mater. Sci. Eng. A, 304–306,* 932–936**.**

Yazdani, A., and Zakeri, A. (2015). An insight into formation of nanostructured coatings on metallic substrates by planetary ball milling. *Powder Technol., 278,* 196–203.

Yoshimura, M., Ohji, T., Sando, M., Choa, Y.H., Sekino, T., Niihara, K. (1999). Synthesis of nanograined ZrO_2-based composites by chemical processing and pulse electric current sintering. *Mater. Lett., 38,* 18-21.

Yusoff, M., Othman, R., and Hussain, Z. (2011). Mechanical alloying and sintering of nanostructured tungsten carbide-reinforced copper composite and its characterization. *Mater. Des., 32,* 3293–3298.

Zhong, M. and Liu, W. (2007). Laser surface cladding: The state of the art and challenges. *J. Mater. Process. Technol., 182,* 297.

Zhurakovskii, E. A., and Vasilenko, N. N. (1974). The State of the Carbon Atom in Transition Metal Carbides. In G.V. Sansanov (Ed.), Refractory *Carbides.* New York: Consultant Bureau.

CURRICULUM VITAE

Name Surname **:** Aydın Şelte

Place and Date of Birth **:** İstanbul, 16.03.1985

E-Mail **:** aydinselte@gmail.com

EDUCATION **:**

- **B.Sc.** **:** 2009, Yıldız Technical University, Faculty of Chemical and Metallurgical Engineering, Metallurgy and Materials Engineering
- **M.Sc.** **:** 2012, İstanbul Technical University, Faculty of Chemical and Metallurgical Engineering, Metallurgy and Materials Engineering

PROFESSIONAL EXPERIENCE AND REWARDS:

- 2016-today Research & Development Engineer at Uddeholms AB
- 2014-2016 Project Assistant at ISTANBUL Technical University Particulate Materials Laboratory
- 2016 Student Fellowship, SCTE2016 Conference Fellowship Committee
- 2012-2014 Technical Service Manager at Böhler-Uddeholm A.Ş.
- 2011 Project Assistant at Institute for Materials Applications in Mechanical Engineering at RWTH AACHEN University
- 2010-2011 Research & Development Engineer at Bilsa Kalıp&Kaizen MIM A.Ş.
- 2009-2010 Project Assistant at YILDIZ Technical University

PUBLICATIONS, PRESENTATIONS AND PATENTS ON THE THESIS:

- **Şelte A. and Özkal B.** (2019). Crystallite size and strain calculations of hard particle reinforced composite powders (Cu/Ni/Fe-WC) synthesized via mechanical alloying. *Proceedings of the Estonian Academy of Sciences*, 68 (1), 66-78.

- **Şelte A. and Özkal B.** (2017). Formation of Nanostructured Ni-TaC and Fe-TaC Composite Powders via Mechanical Alloying, *Solid State Phenomena*, 257, 179-182.
- **Şelte A. and Özkal B.** 2017: Characterization of VC reinforced Cu, Fe and Ni composite powders produced via mechanical alloying, Proceedings of International Conference on Materials Science & Engineering (BraMat 2017), March 13-16, 2017 Brasov, Romania.
- **Şelte A. and Özkal B.** 2016: Mechanical Alloying of 25 wt. % WC particle reinforced Cu, Ni and Fe based composite powders and their characterization, 2nd International Advanced and Functional Materials Technologies (AFMAT), October 20-22, 2016 Antalya, Turkey.
- **Şelte A. and Özkal B.** 2016: Effects of Mechanical Alloying Time and Annealing Temperature on the Physical Properties of Al - WC Composite Powders, 13th International Congress Machines, Technologies, Materials, September 14-17, 2016 Varna, Bulgaria.
- **Şelte A. and Özkal B.** 2015: Production and Characterization of Al - WC Composite Powders via Mechanical Alloying, 12th International Congress Machines, Technologies, Materials, Varna, Bulgaria, September 16-19, 2015 Varna, Bulgaria.

OTHER PUBLICATIONS, PRESENTATIONS AND PATENTS:

Thesis

- **Şelte A.** (2012)**.** The Effects of Mechanical Alloying Method on Densification of the WC – Cu System which is Produced by Infiltration Technique, Master Thesis (in Turkish), Istanbul Technical University, Istanbul, Turkey.
- **Şelte A.** (2009). The Design of Structure and Property of Non – Metal Materials, Bachelor thesis (in Turkish), Yıldız Technical University, Istanbul, Turkey,

Papers in Refereed Journals (SCI, SCI Expanded, SSCI and AHCI Indexed)

- **Şelte, A., Özkal, B., Arslan, K., Ülker, S. and Hatman, A.** (2018). The Effects of Nitriding Conditions on the Wear Properties of P/M Steels Having Different V, Cr and Mo Alloy Contents, *Metal Science and Heat Treatment*, 59 (11-12), 729-734.
- **Şelte A. and Özkal B.** (2015). Infiltration Behaviour of Mechanical Alloyed 75 wt.% Cu-25 wt.% WC Powders into Porous WC Compacts, *Archives of Metallurgy and Materials*, 60 (2), 1565 – 1568.
- **Şelte, A., Güler, K. A. and Marşoğlu, M**. (2012). The Evaluation of Waste Papers for the Ceramic Industry. *MP Materials Testing-Materials and Components Technology and Application*, 54 (2), 126-129.

Papers in Refereed Journals

- **Şelte A. and Özkal B.** (2016). Effects of Mechanical Alloying Time and Annealing Temperature on the Physical Properties of Al -WC Composite Powders, *Machines, Technologies, Materials*, 10, 15-17.
- **Şelte A. and Özkal B.** (2015). Production and Characterization of Al - WC Composite Powders via Mechanical Alloying, *Machines, Technologies, Materials*, 12, 34-37.
- **Şelte, A., Arslan, K., Ülker, S. and Hatman, A.** (2013). Comparison of Different Thermochemical Treatments on Surface Properties of Impax Supreme Tool Steel, *Journal of Materials Science and Engineering A*, 3 (12), 732-737.
- **Şelte A. (2013).** Yüksek Performanslı Toz Metalürjik Takım Çeliklerinde Kırılma Prosesi, *Maschinen Markt/Makina Magazin Dergisi* (in Turkish), 202, 91-94.

Papers in Other Journals

- **Arslan, K. and Şelte, A.** (2013). Takım Çeliklerinde Sıfıraltı Isıl İşlem Mekanizması, *Metalurji* (in Turkish), 167, 37 – 40.
- **Şelte A.** (2010). Metal Enjeksiyon Kalıplama Teknolojisi, *Metalurji* (in Turkish), 159, 14 – 20.

Papers in Peer-Reviewed Conference Proceedings

- **Şelte A. and Özkal B.** 2017: Characterization of VC reinforced Cu, Fe and Ni composite powders produced via mechanical alloying, Proceedings of International Conference on Materials Science & Engineering (BraMat 2017), March 13-16, 2017 Brasov, Romania.
- **Şelte A. and Özkal B.** 2016: Mechanical Alloying of 25 wt. % WC particle reinforced Cu, Ni and Fe based composite powders and their characterization, 2nd International Advanced and Functional Materials Technologies (AFMAT), October 20-22, 2016 Antalya, Turkey.
- **Şelte A. and Özkal B.** 2016: Effects of Mechanical Alloying Time and Annealing Temperature on the Physical Properties of Al - WC Composite Powders, 13th International Congress Machines, Technologies, Materials, September 14-17, 2016 Varna, Bulgaria.
- **Şelte A. and Özkal B.** 2016: Formation of Nanostructured Ni-TaC and Fe-TaC Composite Powders via Mechanical Alloying, 20th Solid Compounds and Transition Elements (SCTE), April 11-15, 2016, Zaragoza, Spain.
- **Şelte A. and Özkal B.** 2015: Production and Characterization of Al - WC Composite Powders via Mechanical Alloying, 12th International Congress Machines, Technologies, Materials, Varna, Bulgaria, September 16-19, 2015 Varna, Bulgaria.

- **Şelte, A., Özkal, B., Arslan, K., Gezici, I., Ülker, S. and Hatman, A.** 2014: The Effects of Nitriding Conditions on the Wear Properties of Powder Metallurgical Steels Consisting of Different Vanadium and Chromium, 17th International Metallurgy & Materials Congress (IMMC), September 11-13, 2014, Istanbul, Turkey.
- **Şelte, A., Özkal, B., Arslan, K., Gezici, I., Ülker, S. and Hatman, A.** 2014: The Effects of Vanadium and Chromium Content on the Microstructure of Powder Metallurgical Steels after Nitriding Process, 2nd International Surface Treatment Symposium, June 25-27, 2014, Istanbul, Turkey.
- **Şelte A**. **et all.** 2013: The Effects of Different Heat Treatment Parameters on the ductility of hot work tool steel with the 2.3% Mo Content, 4th Heat Treatment Symposium, October 24-25, 2013, Istanbul, Turkey.
- **Şelte A. and Özkal B.** 2012: Infiltration Behaviour of Mechanical Alloyed 75 wt.% Cu-25 wt.% WC Powders into Porous WC Compacts, 12th International Symposium on Novel and Nano Materials (ISNNM), August 26-30, 2012, Istanbul, Turkey.
- **Şelte A. and Özkal B. 2012:** Mechanical Alloying of 75 wt. % Cu - 25 wt. % WC Powder Composition and its Powder State Characterization, 16th International Metallurgy & Materials Congress (IMMC), September 13-15, 2012, Istanbul, Turkey.